creative commons
COMMONS DEED

저작자표시-비영리-변경금지 2.0 대한민국

이용자는 아래의 조건을 따르는 경우에 한하여 자유롭게

- 이 저작물을 복제, 배포, 전송, 전시, 공연 및 방송할 수 있습니다.

다음과 같은 조건을 따라야 합니다:

저작자표시. 귀하는 원저작자를 표시하여야 합니다.

비영리. 귀하는 이 저작물을 영리 목적으로 이용할 수 없습니다.

변경금지. 귀하는 이 저작물을 개작, 변형 또는 가공할 수 없습니다.

- 귀하는, 이 저작물의 재이용이나 배포의 경우, 이 저작물에 적용된 이용허락조건을 명확하게 나타내어야 합니다.
- 저작권자로부터 별도의 허가를 받으면 이러한 조건들은 적용되지 않습니다.

저작권법에 따른 이용자의 권리는 위의 내용에 의하여 영향을 받지 않습니다.

이것은 이용허락규약(Legal Code)을 이해하기 쉽게 요약한 것입니다.

Disclaimer

dCollection

공학박사 학위논문

Single Station-based Precise Positioning System using Multi-Antenna Arrangement

다중 안테나 배치를 통한
단일 스테이션 기반 정밀 위치결정 시스템

2018 년 8 월

서울대학교 대학원

기계항공공학부

김 오 종

Single Station-based Precise Positioning System using Multi-Antenna Arrangement

다중 안테나 배치를 통한
단일 스테이션 기반 정밀 위치결정 시스템

지도 교수 기 창 돈

이 논문을 공학박사 학위논문으로 제출함
2018 년 4 월

서울대학교 대학원
기계항공공학부
김 오 종

김오종의 공학박사 학위논문을 인준함
2018 년 6 월

위 원 장 강 유 단 (인)

부위원장 기 창 돈 (인)

위 원 박 찬 국 (인)

위 원 박 병 운 (인)

위 원 권 의 호 (인)

Single Station-based Precise Positioning System using Multi-Antenna Arrangement

Advisor: Prof. Changdon Kee

Submitting a Ph.D. Dissertation of
Public Administration

April 2018

Graduate School of Engineering
Seoul National University
Department of Mechanical and Aerospace Engineering

O-Jong Kim

Confirming the Ph.D. Dissertation written by
O-Jong Kim
June 2018

Chair	Youdan Kim	(Seal)
Vice Chair	Changdon Kee	(Seal)
Examiner	Chan Gook Park	(Seal)
Examiner	Byungwoon Park	(Seal)
Examiner	Euiho Kim	(Seal)

ABSTRACT

Single Station-based Precise Positioning System using Multi-Antenna Arrangement

O-Jong KIM
School of Mechanical and Aerospace Engineering
The Graduate School
Seoul National University

A single station-based positioning system is designed for an alternative navigation system for environments in which satellite-based navigation systems are unavailable. Additional multiple pseudolite antennas broadcasting one-way continuous signals are installed together with conventional Distance Measuring Equipment (DME). This single station based system makes it possible for time-synchronization among different signals, and 3D positioning using only one station is also possible. As DME works without any changes to the current operation, compatibility to current DME systems is preserved. As two types of signals, one-way signals from pseudolite and two-way signals from DME, are used, the aircraft traffic capacity of DME can also be improved.

Positioning from one station generally offers only poor geometrical features, poor Dilution of Precision (DOP). To address this issue, carrier-phase measurements with noise levels in the mm-level range are utilized. However, relying on carrier-phase

measurements causes the problem of integer cycle ambiguity, an unknown integer-term multiplied by the wavelength. To mitigate the cycle ambiguity issue, the Mosaic concept is utilized to limit the number of cycle ambiguity candidates geometrically for the efficient resolution of the cycle ambiguity issue.

This dissertation also includes research on the optimized antenna arrangement of the single station-based positioning system considering the two aspects of positioning accuracy and the cycle ambiguity resolution performance over the Area of Interest (AOI). In terms of the cycle ambiguity resolution, this paper presents a new technique, Ambiguity Net Technique, which assesses whether or not the antenna arrangement is favorable for easy and fast ambiguity resolution. The Ambiguity Net Technique counts the crossing points of the drawn measurement trajectories of each cycle ambiguity candidate of each antenna in the image domain. In terms of positioning accuracy, the worst DOP value according to the AOI is the performance index to be minimized.

A strategy for the antenna arrangement considering the two factors of the positioning accuracy and the cycle ambiguity resolution performance, in the AOI is also presented. With this strategy, not only the relative arrangement of the antennas but also the number of antennas and the distances between antennas are minimized, guaranteeing good ambiguity resolution performance and meeting the accuracy requirements.

Simulation-based analyses are conducted to verify the methods and strategy presented in this dissertation. The positioning accuracy and performance to mitigate the cycle ambiguity resolution issue from a generated antenna arrangement by means of the optimization of the DOP performance index and the Ambiguity Net Technique are verified. In addition, the results of antenna arrangements cases are compared and analyzed.

Keywords: APNT, Mosaic, DME, Ambiguity Resolution, Ambiguity Net, Weighted DOP, Antenna Arrangement

Student Number: 2013-30191

TABLE OF CONTENTS

Chapter 1. Introduction 1

1.1 Motivation and Purpose 1

1.2 Literature Survey 4

1.3 Outline of the Dissertation 7

1.4 Contributions 9

Chapter 2. Background 10

2.1 Alternate Positioning Navigation and Timing (APNT) 10

2.1.1. NextGen and APNT 10

2.1.2. APNT Requirements (Navigation Accuracy) 12

2.2 Distance Measuring Equipment (DME) 13

2.3 VOR/DME system 14

2.4 Multilateration (MLAT) 17

Chapter 3. A Single Station-based Positioning System (Mosaic/DME System) 19

3.1 Mosaic Concept 19

3.2 Mosaic/DME System 22

3.2.1. System Configuration 22

3.2.2. Positioning Algorithm 25

3.2.3. Potential Solutions 28

3.2.4. Special Features 30

3.3 Positioning Accuracy Analysis 31

3.3.1. Measurement Error 32
3.3.2. Weighted DOP 34
3.3.3. Accuracy Simulation 39
3.4 Ambiguity Resolution 43
3.4.1. Features of Cycle Ambiguity 43
3.4.2. Strategy of Ambiguity Resolution 44
Chapter 4. Multi-Antenna Arrangement Method for 2D Environment 47
4.1 Area of Interest (AOI) 48
4.2 Antenna Arrangement for Positioning Accuracy 49
4.3 Antenna Arrangement for Ambiguity Resolution 54
4.3.1. Ambiguity Net Image 54
4.3.2. Pixel Bound Analysis 61
4.3.3. Ambiguity Net Technique 65
4.3.4. Tendency Simulation 71
4.4 Antenna Arrangement considering Positioning Accuracy and Cycle Ambiguity Resolution Performance 73
4.4.1. Antenna Arrangement Method 73
4.4.2. Robust Antenna Arrangement to Antenna Position Error 77
4.4.3. Bound Size Analysis for Ambiguity Net Technique 80
Chapter 5. Strategy of Multi-Antenna Arrangement 83
5.1 Strategy Background 83
5.2 Antenna Arrangement Strategy 85
5.3 Simulation Results for 2-D environment 91
5.3.1. AOI: ±30° bound 92

5.3.2. AOI: ±60° bound 97
5.3.3. AOI: all area (-180° ~ 180°) 101
Chapter 6. Multi-Antenna Arrangement for 3D Environment . 106
6.1 Area of Interest (AOI)..... 107
6.2 Antenna Arrangement for Positioning Accuracy..... 108
6.3 Antenna Arrangement for Ambiguity Resolution..... 108
6.4 Simulation Results..... 115
6.4.1. Simulation Settings 115
6.4.2. Ambiguity Resolution Results 120
6.4.3. Positioning Accuracy Results 125
Chapter 7. Conclusions 128
7.1 Conclusions..... 128
7.2 Suggestions for Future Work..... 129
Chapter 8. Reference 131
Appendix A: Analysis about Linear Assumption of Hyperbolic Asymptotes 136
Appendix B: Probabilistic Analysis of Zero-ANCP 141

LIST OF FIGURES

Figure 1-1 Conceptual design of single station-based positioning system 3
Figure 2-1 A Picture of VOR/DME station [34] 15
Figure 2-2 Airspace Class B and Mode-C Veil [35] 16
Figure 2-3 Conceptual design of Mosaic system for surveillance 18
Figure 3-1 Geometric description using two pseudolites (PL) 19
Figure 3-2 Asymmetric pyramid array of pseudolite 24
Figure 3-3 Potential solutions of Mosaic/DME in 2-dimenstional case 29
Figure 3-4 Potential solutions of Mosaic/DME in 3-dimenstional case 30
Figure 3-5 WDOP according to relative azimuth and elevation angles with DME error size of 185 m (1σ) *(top: WHDOP, bottom: WVDOP)* 37
Figure 3-6 WDOP according to relative azimuth and elevation angles with DME error size of 34 m (1σ) (top: WHDOP, bottom: WVDOP) 38
Figure 3-7 Simulation results of the relationship between distance and horizontal accuracy 40
Figure 3-8 Simulation results of the relationship between distance and vertical accuracy 40
Figure 3-9 Horizontal accuracy through the boundary of airspace class B 42
Figure 3-10 Ambiguity resolution scenario of Mosaic/DME 46
Figure 4-1 AOI and antenna arrangement settings considered in this chapter 48
Figure 4-2 Inverse rotation for the calculation of ANDOP 50
Figure 4-3 Maximum ANDOP according to α_2 and α_3 when AOI is ±30° 52
Figure 4-4 Maximum ANDOP according to α_2 and α_3 when AOI is ±60° 53

Figure 4-5 Hyperbola and asymptote 55
Figure 4-6 Asymptotes by each cycle ambiguity (four candidate case)..... 55
Figure 4-7 All asymptotic lines by cycle ambiguity when four antennas are considered (left: general case, right: existence of hazardous candidate 'black rectangular')..... 57
Figure 4-8 Ambiguity Net Image drawn with one antenna baseline..... 58
Figure 4-9 Ambiguity Net Image drawn with three antenna baselines (three layers) when α_1 =90°, α_2 =30° and α_3 = -30° from Figure 4-1..... 60
Figure 4-10 Pixel bound according to the slope angle of asymptote..... 63
Figure 4-11 Bound residuals caused by the pixel resolution..... 64
Figure 4-12 Ambiguity Net Image and boundary checks at each layer (dashed rectangle is the boundary)..... 66
Figure 4-13 Ambiguity Net Image considering AOI of ±60° (black filled circle: crossing points through all layers)..... 68
Figure 4-14 Average number of crossing points (AOI of ±30°) 70
Figure 4-15 Average number of crossing points (AOI of ±60°) 71
Figure 4-16 Simulation results about the relation between ANCP and the ambiguity resolution performance..... 72
Figure 4-17 Search process using optimization method when AOI is ±30° 75
Figure 4-18 Search process using optimization method when AOI is ±60° 76
Figure 4-19 ANCP contours according to α_2 and α_3..... 78
Figure 4-20 Enlarged ANCP contours around white-rectangle of Figure 4-19 79
Figure 4-21 ANCP contour around white-rectangle of Figure 4-19 with $3\sigma_{\Delta\phi}$ bound ... 81
Figure 5-1 Antenna arrangement strategy (method A)..... 86
Figure 5-2 Antenna arrangement strategy (method B)..... 88
Figure 5-3 Method B-based searching process when AOI is ±30° (contours: ANCP).. 89
Figure 5-4 Method B-based searching process when AOI is ±30° (contours: ANDOP) 90

Figure 5-5 Antenna arrangement cases for AOI of ±30° (top-left: case 1, top-right: case 2, bottom-left: case 3)..... 94
Figure 5-6 Histogram of required epochs for ambiguity resolution (AOI ±30°: case 1) 96
Figure 5-7 Histogram of required epochs for ambiguity resolution (AOI ±30°: case 3) 96
Figure 5-8 Antenna arrangement cases for AOI of ±60° (top-left: the form of antenna arrangement, top-right: case 1, top-left: case 2, bottom-right: case 3)..... 98
Figure 5-9 Histogram of required epochs for ambiguity resolution (AOI ±60°: case 2) 100
Figure 5-10 Histogram of required epochs for ambiguity resolution (AOI ±60°: case 3) 100
Figure 5-11 Antenna arrangement cases for all area (top-left: case 1, top-right: case 2, bottom-left: case 3)..... 103
Figure 5-12 Histogram of required epochs for ambiguity resolution (AOI ±180°: case 1) 104
Figure 5-13 Histogram of required epochs for ambiguity resolution (AOI ±180°: case 2) 104
Figure 5-14 Histogram of required epochs for ambiguity resolution (AOI ±180°: case 3) 105
Figure 6-1 Antenna formation of regular rectangular pyramid 106
Figure 6-2 Circular hyperboloid (left), asymptotic circular cones (right) and asymptotic circles on the surfaces (yellow rings) [59, 60] 109
Figure 6-3 Asymptotic circles by each cycle ambiguity candidates when user position (circle) is on the azimuth of 30° and elevation of 10° (left: position domain, right: azimuth-elevation angles domain)..... 110
Figure 6-4 Ambiguity Net Image when the elevation angle of user is fixed..... 112

Figure 6-5 Ambiguity Net Image when the azimuth angle of user is fixed 112
Figure 6-6 Pixel bounds according to elevation angle when antenna baseline is on z-axis 114
Figure 6-7 Bound residuals caused by pixel resolution when antenna baseline is on z-axis 114
Figure 6-8 Grid for 3-D Ambiguity Net Technique with elevation step angle of 5° (left: Cartesian coordinate system, right: spherical coordinate system) 116
Figure 6-9 Antenna arrangement cases (3-D simulation) (top-left: case 1, bottom-left: case 2, bottom-right: case 16)..... 118
Figure 6-10 AOI for 3-D simulations (left-top: top view, left-bottom: front view, right: isometric view)..... 119
Figure 6-11 Tendency between ANCP and cycle ambiguity resolution performances 122
Figure 6-12 Histogram of required epochs for ambiguity resolution (3-D: case 1)... 123
Figure 6-13 Histogram of required epochs for ambiguity resolution (3-D: case 2)... 124
Figure 6-14 Histogram of required epochs for ambiguity resolution (3-D: case 16). 124
Figure 6-15 Grid points for positioning accuracy simulations 126

LIST OF TABLES

Table 2-1 Required NSE for APNT 13
Table 2-2 VOR/DME/TACAN Standard Service Volumes (SSV) [33] 14
Table 3-1 Example of antenna arrangement of Mosaic/DME 25
Table 3-2 Simulation Settings 32
Table 3-3 Statistical error of measurements (if λ = 27.5cm) 33
Table 4-1 Upper and lower pixel bounds in Figure 4-12 67
Table 4-2 Ambiguity resolution performance of searched antenna arrangement 76
Table 4-3 Ambiguity resolution performance of four cases of Figure 4-20 79
Table 4-4 Ambiguity resolution performance for case 1 and 5 of Figure 4-21 81
Table 5-1 Strategy process for the AOI of ±30° 93
Table 5-2 Cases of antenna arrangements to be compared (AOI of ±30°) 94
Table 5-3 Monte-Carlo results of ambiguity resolution (AOI of ±30°) 95
Table 5-4 Strategy process for the AOI of ±60° 97
Table 5-5 Cases of antenna arrangements to be compared (AOI of ±60°) 98
Table 5-6 Monte-Carlo results of ambiguity resolution (AOI of ±60°) 99
Table 5-7 Strategy process without bound (all area) 101
Table 5-8 Cases of antenna arrangements to be compared (all area) 102
Table 5-9 Monte-Carlo results of ambiguity resolution (all area) 102
Table 6-1 Azimuth and elevation angles for regular rectangular pyramid (az : azimuth, el: elevation) 106
Table 6-2 Antenna arrangement cases (No. of antenna: 5, baseline length: 4.38λ) ... 117
Table 6-3 WDOP and ANCP for each case (3-D simulation) 120

Table 6-4 Monte-Carlo results of ambiguity resolution (3-D simulation) 121
Table 6-5 Monte-Carlo results of positioning accuracy (3-D simulation) 126
Table A-1 Maximum $\Delta\psi$ with different ranges 140

Chapter 1. Introduction

1.1 Motivation and Purpose

A single station-based positioning system has been designed for an alternative navigation system considering environments in which satellite-based navigation systems are unavailable as well as a primary navigation system.

One good application of a single station-based positioning system is an indoor navigation system. Inside of a building or structure, Global Navigation Satellite System (GNSS) signals cannot reach users, owing to the inherently low intensity of these signals. Therefore, an independent navigation system is necessary for indoor applications. A single station-based positioning system, termed as the Mosaic project, has been suggested for use as a navigation system for indoor environments [1]. The key feature of the indoor Mosaic concept is that it is an integer-cycle ambiguity-free approach even given its use of carrier-phase measurements [2].

Another application of the Mosaic concept is an alternate navigation system for air transport. In the Next Generation Air Transportation System (NextGen), GNSS plays the main roles of positioning, navigation, and surveillance of aviation users. However, GNSS is vulnerable to certain types of radio frequency interference, such as jamming or spoofing, as well as unexpected events, such as GNSS failures or degradation. Therefore, the Alternative Positioning, Navigation and Timing (APNT) solution is often relied upon as a backup system for GNSS to provide safe and continuous flight. Current terrestrial based navigation systems, such as the Distance Measuring Equipment (DME) system,

Very High Frequency Omni-directional Radio (VOR) system, and non-directional beacons or their combinations do not provide sufficient levels of performance as required by APNT [3]. Moreover, they are not compatible with Performance Based Navigation (PBN) for area navigation (RNAV) and the Required Navigation Performance (RNP).

The single station-based positioning concept presented in this dissertation can serve as an upcoming terrestrial-based solution to replace legacy navigation systems. The most significant characteristic is that it can provide three-dimensional positioning, including the altitude of the aircraft using only a single station. This can be achieved using a single DME station with multiple pseudolite transmitters, which are inherently time-synchronized as conceptually described in Figure 1-1. DME operates using round-trip signals, and multiple pseudolites, in addition to this station, transmit one-way continuous signals. The range measurements from the DME station and carrier phase measurements from the multiple pseudolites allow the aircraft to establish positions that satisfy the APNT accuracy requirement. In this dissertation, applications are focused on APNT, as APNT provides the required performance for terrestrial based navigation in the near future.

The basic Mosaic concept is an integer-cycle ambiguity-free concept using carrier-phase measurements with a limited antenna baseline of half of the wavelength [1, 2, 4]. However, half of the signal's wavelength is generally very small, at a few centimeters, causing poor geometry for positioning and poor Dilution of Precision (DOP) characteristics. Therefore, it is not suitable for aircraft applications, whose operation range is up to 100 nmi. Hence, longer distances between antennas are required for sufficient positioning accuracy. However, distances longer than half of the wavelength creates uncertainty via the integer cycle ambiguity problem, which must be solved inevitably for proper positioning.

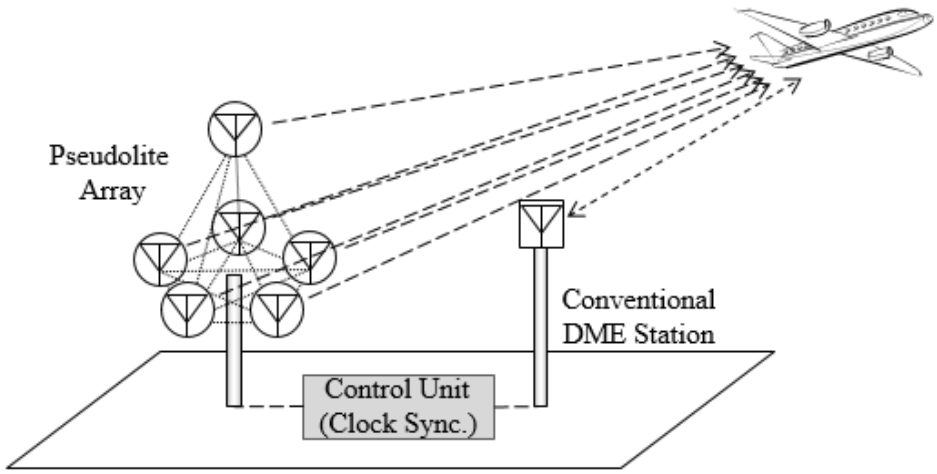

Figure 1-1 Conceptual design of single station-based positioning system

When the Mosaic concept is applied to the cycle ambiguity problem of a single station-based system with multiple pseudolite antennas, it bounds the range of the cycle ambiguity candidate geometrically and makes the ambiguity resolution efficient. Considering the factors of safety and integrity, however, the system must be capable of providing assurance with regard to the cycle ambiguity resolution. In previous work, the formation of multiple antennas was found to affect the ambiguity resolution performance; it is clear that a symmetric formation is more adverse than an asymmetric formation of antennas [5]. Hence, the focus of this dissertation is to search an antenna arrangement which offers useful features with which to solve the cycle ambiguity problem.

The formation of the antenna arrangement also affects the positioning accuracy as different arrangements mean different relative geometries of the measurement between the station and the user. A strategy which finds the antenna arrangement, therefore, should

consider not only the cycle ambiguity performance but also the positioning accuracy.

Another factor to consider during the antenna arrangement process is the Area of Interest (AOI). Some stations do not need to consider omnidirectional coverage around a station, when the air route or airspace is partially distributed. In these cases, only the air route or airspace is considered as the AOI. Moreover, the optimization process for the antenna arrangement is performed in this target area. Considering the AOI contributes to the effective of the antenna arrangement process and the concise system configuration, as it means that a small number of pseudolite antennas can satisfy the required positioning accuracy and ambiguity resolution performance targets.

Therefore, the primary purpose of this dissertation is to derive and verify a novel antenna arrangement strategy for a single station-based positioning system considering both the positioning accuracy and ambiguity resolution performance.

Throughout the dissertation, this system is referred to as Mosaic/DME for convenience, as it is in earlier studies [6, 7]. The word Mosaic generally has two meanings when discussed in the context of this system. The first meaning defines a method that considers the cycle ambiguity problem of carrier phase measurements for positioning, and the second pertains to a geometrical array of pseudolite antennas to apply with the former. Therefore, Mosaic/DME can be defined as a DME station with a certain form of a pseudolite antenna array, and its cycle ambiguity problem is addressed Mosaic approach.

1.2 Literature Survey

The APNT working group presented their study in 2010 [3]. This document describes the

purpose, mission statement, background, current APNT infrastructure, APNT assumptions, APNT Analysis Objectives, and the three APNT alternatives of DME/DME Network Optimization, Passive Wide-area Multilateration (MLAT), and Pseudolite-based MLAT. In 2012, the FAA published the Concept of Operations for NextGen APNT containing information such as current operations and capabilities, the APNT concept of operations, and operational scenarios [8]. The new system, presented in this dissertation, mainly refers to these documents, as they present the upcoming standards and requirements for terrestrial-based navigation systems.

Various studies have been conducted to find APNT solutions. One approach seeks to improve the performance of the current DME system and to provide navigation with more than two DME stations [9, 10]. A capacity study of DME systems was also conducted with regard to future air traffic [11]. Moreover, enhanced DME which uses the concept of the DME carrier phase, can significantly improve the performance of DME according to recent experimental evaluations [12, 13]. Another APNT approach involves the use of passive ranging, with broadcasting one-way signals. Examples include pseudolites that use DME signals and Automatic Dependent Surveillance Broadcast (ADS-B) signals [14, 15]. A coverage analysis of a pseudolite ground network has also been performed [16]. Multilateration (MLAT), which uses ADS-B signals for surveillance, was also studied as a candidate for APNT [17]. As time synchronization between terrestrial stations even without GNSS is an issue for a multiple station-based positioning system, research on time-sync alternatives to GNSS has been conducted [18, 19].

The first Mosaic work, focusing on indoor applications, was a patent. After its registration in Republic of Korea [1], it was also registered in the United States and China [20, 21]. This development is also pending in Europe [22]. A simulation-based study on the effects

by error sources in relation to the indoor Mosaic approach has also been performed [2].

A Mosaic system for APNT, known as Mosaic/DME, was presented in 2012 [6]. Subsequently, an asymmetric antenna arrangement with improved ambiguity resolution performance was presented [5]. A study of error sources, such as the multipath, tropospheric delay and antenna misalignment forms, was also presented [23], as was in-depth research on a Mosaic/DME system which took into consideration of various error sources. This study examined positioning accuracy and presented an ambiguity resolution strategy and tested it with a simulation [24].

The concept of a single DME station with multiple antennas has been presented [25]. This system is known as the DME-based Landing System (DLS), which uses an array of multiple DME antennas for the additional purpose of direction finding. The DLS employs two horizontal linear arrays of antennas on the ground for the azimuth and a vertical arrangement of directive antennas for elevation. This configuration performs three-dimensional positioning, which includes the altitude of the aircraft. The DLS can also provide navigation services not only for terminal areas but also for en-route airspace. Furthermore, a deeper study of the angle of arrival estimation was conducted to analyze the theoretical and experimental performance capabilities, error sources including multipath, and hardware implementation issues [26].

The system proposed here differs from the DLS in terms of the operational principles. While the DLS employs the conventional phased array principle for angle detection, the proposed system employs an approach similar to Carrier Phase Differential GPS (CDGPS) which uses the Least Square Ambiguity Search Technique (LSAST) for ambiguity resolution and the Weighted Least Square (WLS) solution for three-dimensional positioning. The DLS uses two-way round trip DME signals, and only the

DME station, not the aircraft, can estimate the aircraft's direction. Therefore, extra data should be transferred to the aircraft to inform the pilot of the direction. On the other hand, the proposed system uses two types of signals: one-way continuous and two-way conventional DME signals. These allow the aircraft to calculate its position by itself. In addition, as the proposed system uses two types of signals, it has the potential to improve aircraft capacity levels and it requires fewer antennas compared to the DLS.

1.3 Outline of the Dissertation

This dissertation presents a study of a single station-based precise positioning system, Mosaic/DME, focusing on its antenna arrangement for positioning accuracy and cycle ambiguity resolution.

After the introduction in the first chapter, the second chapter describes the background including APNT with its requirements and ground-based navigation systems. Ground-based navigation systems, such as VOR/DME and MLAT are concisely described and compared to the Mosaic/DME system.

In the third chapter, the details of the Mosaic/DME system are described, mainly the conceptual design, positioning algorithm, cycle ambiguity problem, and special features. For an accuracy analysis, the Weighted Dilution of Precision (WDOP) concept is applied and the proper WDOP for this system is defined. Subsequently, the strategy for the resolution of the cycle ambiguity problem, an unavoidable issue in a carrier phase-based positioning system, is described. The contents of this chapter are based on an earlier study [24].

In the fourth chapter, antenna arrangement methods considering the issue of positioning accuracy and cycle ambiguity resolution performance in the AOI are described in a two-dimensional environment. The performance index for positioning accuracy used in a 2-D environment is Angular DOP (ANDOP), which is minimized in the AOI, and the Ambiguity Net Technique used to determine antenna arrangements which ensure the fast and robust ambiguity resolutions is described. Results and analyses based on simulations of the cycle ambiguity resolution are conducted to compare the derived results with a non-optimized antenna arrangement.

In the fifth chapter, the strategy used to find an antenna arrangement which meets specific requirements is discussed. This strategy determines the antenna arrangement, specifically the number of antennas and the distance between the antennas to meet the target requirements. In this dissertation, the target for positioning accuracy is the APNT requirement. Simulations are also conducted and the results are compared with other antenna arrangements to display the improved positioning accuracy and the cycle ambiguity resolution performance.

The antenna arrangement process for use in a 2-D environment is extended to 3-D environments in the sixth chapter. The Weighted Horizontal DOP (WHDOP) is used for proper performance index targeting APNT requirement, and the extended Ambiguity Net Technique for 3D is applied and analyzed based on simulations.

Finally, the conclusions, including a summary and future suggestions, are provided.

1.4 Contributions

The first contribution of this dissertation is that it proposes a new concept of a positioning system, a single station-based positioning system with multiple pseudolite antennas. The system configuration and special features, the positioning algorithm, an accuracy analysis using the weighted DOP, and the strategy for the cycle ambiguity resolution are described and discussed. Monte-Carlo simulations are also conducted to investigate the properties of positioning accuracy considering various error sources, in this case thermal-noise, tropospheric delay and multipath.

The next contribution is that the study presents a strategy for a multi-antenna arrangement considering both the positioning accuracy and the ambiguity resolution performance within the AOI. In earlier studies, it was empirically demonstrated that an asymmetric formation of pseudolite antennas can offer a rapid ambiguity resolution. In this dissertation, the Ambiguity Net Technique can be used to investigate the ambiguity resolution performance and can probabilistically determine whether or not a certain antenna arrangement is favorable for robust and fast ambiguity resolutions. Assurance of the cycle ambiguity resolution is very important, as cycle ambiguity resolution is essential for carrier phase-based positioning, and an incorrect cycle ambiguity resolution can cause serious positioning offset. The AOI is also considered as part of an effective antenna arrangement process for a concise system configuration to optimize the target area.

Chapter 2. Background

2.1 Alternate Positioning Navigation and Timing (APNT)

2.1.1. NextGen and APNT

Next Generation Air Transport System (NextGen) is an air traffic modernization program being developed by Federal Aviation Administration (FAA) for future aircraft transportations. According to FAA, “NextGen is a comprehensive overhaul of our National Airspace System to make air travel more convenient and dependable, while ensuring your flight is as safe, secure and hassle-free as possible” [27]. In NextGen program, Global Navigation Satellite System (GNSS)-based system generally performs the main role for positioning, navigation and surveillance. However, GNSS-based system is very vulnerable to Radio Frequency Interference (RFI) such as jamming and spoofing. With regard to RFI or any other GNSS unavailable situations, Alternate Positioning Navigation and Timing (APNT) system becomes an essential issue to maintain the safety of air service and reduce GNSS unavailable economic impacts.

APNT is non-GNSS architecture for aviation users to operate when GNSS services are unavailable, so this system should be not satellite-based (or space-based) but terrestrial-based system. In 2025, it is predicted that air traffic is 2-3 times more than current level in United States [3], which means that the capacity, how many aircraft can use APNT system at the same time, and efficiency, how many aircraft can operate in a limited airspace, cannot be overlooked. The second factor ‘efficiency’ has a strong relationship with accuracy. If the navigation system provides better accuracy, the safe distance

between aircrafts can be narrower, meaning that more aircraft can operate in a limited space. Cost-effectiveness, include avionics and ground station upgrading costs, is also an important factor for APNT. In addition, APNT is also required to have a compatibility with conventional aircraft navigation system, such as GNSS, Distance Measuring Equipment (DME), VHF Omni-Directional Ranging (VOR) or Non-Directional Beacon (NDB).

Conventional terrestrial aircraft navigation systems are VOR, DME, and NDB for civil application and Tactical Air Navigation (TACAN) for military use. And these systems are generally combined for positioning, such as VOR/DME, DME/DME, VOR/TACAN and DME/DME/Inertial. However, legacy APNT systems, mentioned above, are not compatible with Performance-based Navigation (PBN) operations for Area Navigation (RNAV) and Required Navigation Performance (RNP), preparing for future aircraft traffic levels [3].

APNT working group, therefore, is searching for the solution of backup navigation system. One option is to create a new signal optimized for APNT requirements. But this can cause severe disadvantages, for example, high cost for the updates of user and station equipment, difficulty to avoid interference with existing signals, and compatibility with existing navigation system. Another option is to utilize existing signals. If the performance of this option is enough for APNT requirements, this option is preferred, as it can solve the problems of high cost and signal interference with existing infrastructure [15].

2.1.2. APNT Requirements (Navigation Accuracy)

The APNT Concept of Operations (CONOPS) by the FAA describes the performance requirements of the APNT as follows [8]:

- APNT must provide RNAV or RNP 2 en-route,
- between RNAV or RNP 1.0 to 0.3 for terminal Class B and C airspace,
- Lateral navigation (LNAV) or RNP 0.3 for approaches,
- RNAV or RNP 1 for missed approach, where economically beneficial or required for safety.

In general, the navigation accuracy, RNV or RNP, means the horizontal 95% of Total System Error (TSE) in units of nautical miles. TSE is the statistical sum of the Flight Technical Error (FTE) and Navigation System Error (NSE). Therefore, the required NSE can be described as Equation (2-1):

$$NSE^2 = TSE^2 - FTE^2 \tag{2-1}$$

According to RTCA DO-208 [28], the general FTE can be defined through three types: 0.5nmi for Manual (MA), 0.25nmi for Flight Detector (FD), and 0.125nmi for Autopilot (AP). Subsequently, the required NSE can be calculated as shown in Table 2-1.

In the feasibility study of the Mosaic/DME system, the required navigation accuracy of the APNT is mainly concerned.

Table 2-1 Required NSE for APNT

RNAV/RNP (TSE)	FTE	Required NSE (95%)
2 nmi	FD 0.25 nmi	1.98 nmi (3674.9 m)
2 nmi	MA 0.5 nmi	1.94 nmi (3586.4 m)
1 nmi	FD 0.25 nmi	0.97 nmi (1793.2 m)
1 nmi	MA 0.5 nmi	0.87 nmi (1603.9 m)
0.3 nmi	AP 0.125 nmi	0.27 nmi (505.1 m)
0.3 nmi	FD 0.25 nmi	0.17 nmi (307.1 m)

2.2 Distance Measuring Equipment (DME)

The DME is an international standard of the two-way pulse-ranging system for air service. It operates within a range of 960-1215MHz. The aircraft interrogator transmits pulses on one of 126 channels, spaced 1MHz apart in a range of 1025-1150MHz, while the ground station receives these pulses and transmits them back to the aircraft after a 50μsec delay on frequencies above or below 63MHz. Each DME station is designed to have a capacity of at least 50 aircraft at a time and typically contains roughly 100 [29]. According to the FAA-E-2996, the performance specification of DME, the total system error of DME shall not exceed ±370m (0.2nmi) [30].

The DME has been widely utilized for the APNT solution because this system has already been widely spread all over the world and has a great potential for attaining high levels of accuracy [31, 32]. The Mosaic/DME also uses the DME as its base system.

According to '2010 FEDERAL RADIONAVIGATION PLAN', DME service volumes are described in Table 2-2 that maximum range is up to 130NM (~240km) [33].

Table 2-2 VOR/DME/TACAN Standard Service Volumes (SSV) [33]

SSV CLASS	ALTITUDE AND RANGE BOUNDARIES
T (Terminal)	From 1,000ft AGL up to and including 12,000ft AGL at radial distances out to 25NM
L (Low Altitude)	From 1,000ft AGL up to and including 18,000ft AGL at radial distances out to 40NM
H (High Altitude)	From 1,000ft AGL up to and including 14,500ft AGL at radial distances out to 40NM. From 14,500 AGL up to and including 60,000ft at radial distances out to 100NM. From 18,000ft AGL up to and including 45,000ft AGL at radial distances out to 130NM.

2.3 VOR/DME system

VOR are assigned frequencies in the 108 to 117.795 MHz (VHF) frequency band, separated by 50 kHz. VOR transmits two 30Hz modulations resulting in a relative electrical phase angle equal to the azimuth angle of the receiving aircraft providing the azimuth information from station to aircraft. And performance of VOR is about ±1.4° of 2-sigma [33], which means that it becomes inaccurate as the aircraft is farther from VOR station. A single station combined VOR with DME can also provide short-range navigation [29]. It is possible for the aircraft to provide 2D-positioning using VOR and

DME together providing azimuth angle and distance respectively. VOR/DME station has the form as in Figure 2-1.

In case of terminal class B, however, the distance from airport is up to 30NM, Mode-C veil as in Figure 2-2. At this area, positioning accuracy in the angular direction using VOR/DME is about 0.7M (<95%) greater than APNT requirement 0.3NM (<95%). VOR/DME station has a limitation in traffic capacity, because DME uses two-way active signals for measuring distances. Hence, it can provide the range measurement to one aircraft at a time, not simultaneously. All these consequences that legacy VOR/DME is not suitable as a solution for future air transport.

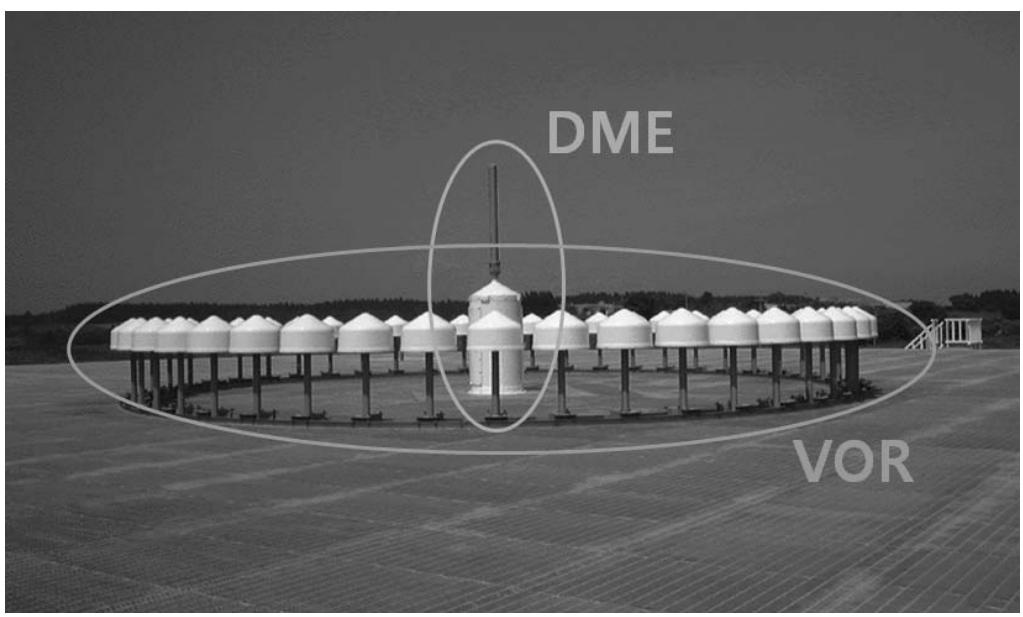

Figure 2-1 A Picture of VOR/DME station [34]

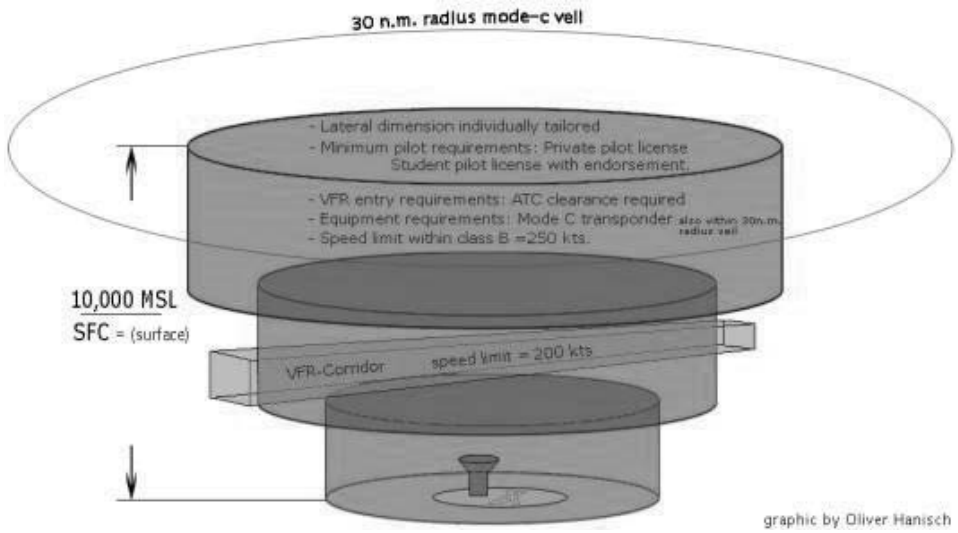

Figure 2-2 Airspace Class B and Mode-C Veil [35]

In terms of system configuration, the Mosaic/DME system is similar with VOR/DME, as both uses DME for the round-trip distance measurement and phase differences between multiple antennas of VOR or Mosaic pseudolites are used for the direction finding.

In operational principles, the Mosaic/DME system is different from VOR/DME. While VOR employs the conventional phased array principles for angle detection, the proposed system employs the approach using the single-differenced carrier phase measurement for Time Difference of Arrival (TDOA) for positioning similar with Carrier Phase Differential GPS (CDGPS), and it uses the Least Square Ambiguity Search Technique (LSAST) for ambiguity resolution process and the Weighted Least Square (WLS) solution for positioning. Therefore, the Mosaic/DME system can provide precise positioning accuracy even for 3D positioning including altitude with fewer antennas

compared to VOR/DME.

2.4 Multilateration (MLAT)

MLAT is generally used for the surveillance based on TDOA measurements relaying on more than two stations. For air transport applications, after the aircraft broadcast a signal, multiple stations receives the signal at each location, and the master station calculates the position of the aircraft using TDOA measurements. If MLAT is utilized for the navigation of aviation user, the calculated positions need to be informed to the user through a certain link, such as Traffic Information-Broadcast [17].

Active MLAT utilizes the interrogation between station and user for a round-trip distance measurement, calculated at station using Mode-A/C/S of Secondary Surveillance Radar (SSR). On the other hand, passive MLAT does not utilize interrogation, instead the aircraft only broadcast the signal continuously, such as Automatic Dependent Surveillance-Broadcast (ADS-B). MLAT and ADS-B have already been integrated using Mode-S Extended Squitter (1090ES) and Universal Access Transceiver (UAT) [36]. In the future, passive MLAT will be preferred because ADS-B will be a main surveillance beyond 2020 [37]. For APNT studies, Wide Area MLAT (WAM) including Passive Wide Area MLAT (P-WAM) is the main concern [17, 36-38].

Mosaic system is also applicable for MLAT for surveillance. Conceptually, a single station with multiple antennas receives a signal from the aircraft, and the station calculate the position of aircraft using phase differences of received signals between antennas as described in Figure 2-3. If an interrogator such as Mode-S is available, the characteristics of the system is very similar to Mosaic/DME except the direction of signal is the opposite.

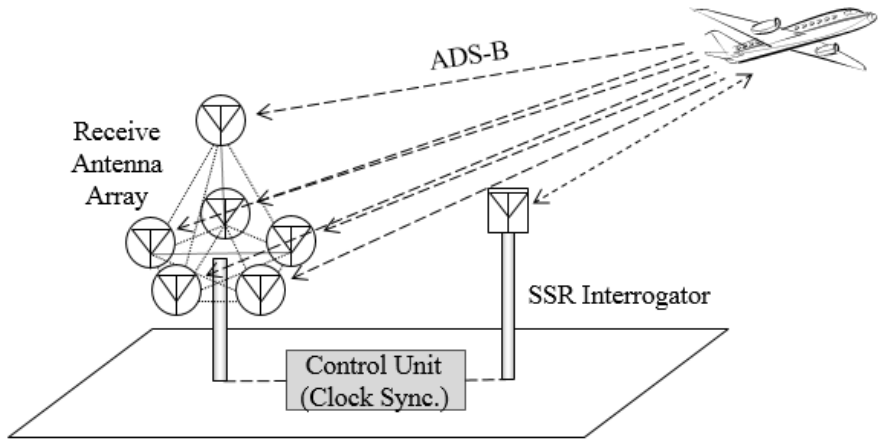

Figure 2-3 Conceptual design of Mosaic system for surveillance

However, this dissertation has a focus on the navigation, the subject of positioning is user. Hence, the application of Mosaic to MLAT, not only for the WAM and P-WAM but Local Area MLAT is remained for future works.

Chapter 3. A Single Station-based Positioning System (Mosaic/DME System)

3.1 Mosaic Concept

The operation of the Mosaic/DME should utilize the carrier phase measurements to satisfy the required accuracy levels of the Alternate Positioning Navigation and Timing (APNT). As the positioning algorithm of this system is based on the Least Square Ambiguity Search Technique (LSAST), which is used in Carrier Phase Differential GPS (CDGPS), it is essential to solve the cycle ambiguity problem of the carrier phase measurements. The Mosaic concept is used for this purpose, as it bounds the integer of the cycle ambiguity geometrically.

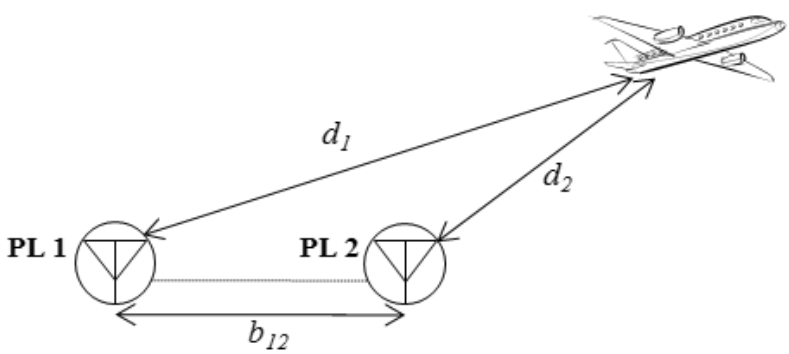

Figure 3-1 Geometric description using two pseudolites (PL)

The carrier phase measurement model can be described as shown below [39]:

$$\phi_j = d_j + N_j\lambda + B - b + t_j + m_j + \varepsilon_j \quad (3\text{-}1)$$

where, ϕ is the measured carrier phase, d is the distance between the pseudolite and the receiver of the aircraft as shown in Figure 3-1, N is the integer cycle ambiguity, λ is the wavelength of the carrier signal, B is the receiver clock offset, b is the station clock offset, t is tropospheric delay, m is the multipath error, ε is other noise, and subscript j represents the measurement from the j-th pseudolite. In Figure 3-1, as the measurements are received from pseudolite number 1 and 2, the measurements are denoted as ϕ_1 and ϕ_2, respectively.

For single-differenced carrier phase measurements, Equation (3-1) can be rewritten using pseudolites 1 and 2 as Equation (3-2).

$$\Delta\phi_{12} \equiv \phi_1 - \phi_2 = \Delta d_{12} + \Delta N_{12}\lambda + \Delta\varepsilon'_{12} \quad (3\text{-}2)$$

The receiver clock offset is eliminated because of the single difference process, and the station clock offset could be neglected because each pseudolite shares one clock source for time synchronization. And the tropospheric and multipath errors are combined with ε for ε'.

Once Equation (3-2) is divided by wavelength (λ) and rounded, the integer ambiguity can be described as follows:

$$\Delta N_{12} = round\left(\frac{\Delta\phi_{12}}{\lambda}\right) - round\left(\frac{\Delta d_{12} + \Delta\varepsilon'_{12}}{\lambda}\right). \quad (3\text{-}3)$$

In Figure 3-1, b_{12} denotes the distance between the pseudolites and is always greater than Δd_{12}. b_{12} can be expressed using a certain integer M and p $(0 \leq p < 0.5)$ as shown in Equation

(3-4).

$$b_{12} \le (M + p) \cdot \lambda \tag{3-4}$$

If Δd_{12} is positive, then the following is satisfied:

$$round\left(\frac{\Delta d_{12} + \Delta \varepsilon'_{12}}{\lambda} \right) \le round\left(\frac{(M + p)\lambda + \Delta \varepsilon'_{12}}{\lambda} \right) = M + round\left(p + \frac{\Delta \varepsilon'_{12}}{\lambda} \right). \tag{3-5}$$

The last round-term of Equation (3-5) is required to be set to zero with an appropriate value of p. If the error term ($\Delta \varepsilon'_{12}$) is greater, then p should be made smaller to make the round term zero. And the M is the minimum integer that is required to satisfy Equation (3-4) with the given antenna spacing (b_{12}). If Equation (3-5) is combined with Equation (3-3), then the lower bound of the cycle ambiguity is as follows:

$$\Delta N_{12} \ge round\left(\frac{\Delta \phi_{12}}{\lambda} \right) - M \tag{3-6}$$

.

With consideration of the negative case of Δd_{12}, the upper and lower bounds are as shown below:

$$-M + round\left(\frac{\Delta \phi_{12}}{\lambda} \right) \le \Delta N_{12} \le M + round\left(\frac{\Delta \phi_{12}}{\lambda} \right) \tag{3-7}$$

.

Equation (3-7) describes the geometrical bound of the cycle ambiguity between pseudolites 1 and 2. This process collects the cycle integer candidates of which only one is true.

According to above concept, it is natural that a greater antenna spacing (b_{12}) yields better performance, but it also increases the number of candidates, resulting in difficulty in the process of ambiguity resolution. On the other hand, the cycle ambiguity will not exist for a small enough antenna spacing—it should be smaller than 0.5λ—with M of 0. It could be utilized for indoor navigation in small spaces [2], but will not be appropriate for air services.

3.2 Mosaic/DME System

3.2.1. System Configuration

The Mosaic/DME is based on a single DME station with multiple pseudolite transmitters. Its conceptual design is depicted in Figure 1-1. The Mosaic array is installed a few meters apart from the DME station to avoid direct interference, but they are a wired sharing controller unit.

In general, more than four pseudolites can provide the positioning results by themselves. But this system operates using a single station with m-level antenna baseline for tens or hundreds of km-level distance. Hence, the positioning results are spread through the radial direction because of the bad geometric performance. Without DME, the Mosaic system seems to provide only the relative direction, elevation and azimuth angles, from the station to the aircraft. Therefore, DME is required to limit the distance for positioning.

One of the important features of the Mosaic/DME is that all signals from the DME and the multiple pseudolites are inherently time synchronized, as it shares a clock source. This is the strength of the single station based positioning concept.

In this dissertation, the system configuration is simplified with assumptions. Pseudolite Mosaic array is installed together with the DME station. The DME operates using two-way round-trip signals to measure the distance between the station and aircraft, which is identical to the conventional DME work. Additional Mosaic antennas broadcast one-way continuous signals to provide carrier phase measurements. It is carefully assumed that additional pseudolites occupy another DME operational channel. All pseudolites in every station occupy the same frequency, but each uses a different Pseudo Random Number (PRN) to distinguish from others using Code Division Multiple Access (CDMA), such as GNSS. Hence, it is expected that only one frequency can be shared by all Mosaic/DME stations. To minimize the effects to DME channels, the bandwidth of the Mosaic signal is recommended to limit the most of transmitted energy within one DME channel width (1MHz) regulating code chipping rate. For instance, a Universal Access Transceiver also modulates its signal to keep the transmitted energy in one DME channel [14, 15]. And the onboard receiver (DME interrogator) processes the DME signal and is also required to have phase tracking for the carrier phase measurements attained from the pseudolite signals.

In general, it is not allowed to transmit the CDMA signals in DME operational channels without changing spectrum allocation. But the operational frequency of Mosaic does not have to limit in DME channels. As this paper cannot cover the operation using non-DME frequency, more in-depth study of the operational frequency remains for future work.

Signals from the Mosaic may contain data that uses additional modulation with contents regarding station information, antenna positions, health status or other necessary information.

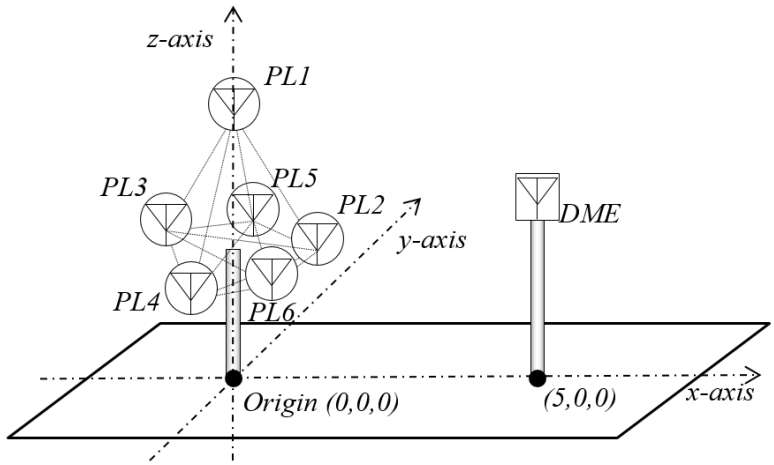

Figure 3-2 Asymmetric pyramid array of pseudolite

In this chapter, the asymmetric pyramid is considered for the fast ambiguity resolution. This is because the axial symmetry of the pyramid leads to the geometrical singularity degrading the performance of the ambiguity resolution [5]. The shape of the antenna array used in this chapter is as shown below in Figure 3-2.

Table 3-1 describes an example of the antenna positions of the pseudolites and the DME. The origin of the coordinate frame is located at ground point on which the center pole of the Mosaic arrays stands as shown in Figure 3-2. Its formation is described in Table 3-1. All analysis and simulations performed in this chapter consider six different pseudolite antennas and coordinates as shown in Table 3-1. The six pseudolites are set experimentally using various simulations.

As this system operates using a single station with m-level antenna spacing, it naturally yields a low level of geometrical performance for a distant aircraft, which may be order

of tens or hundreds of km away. However, the poor geometry of the system is overcome through the use of the carrier phase measurement, which has mm-level errors. The method of using these carrier phase measurements for positioning is referred to as Mosaic.

Table 3-1 Example of antenna arrangement of Mosaic/DME

	X-position (m)	Y-position (m)	Z-position (m)
PL1	0	0	3.73
PL2	1.63	0.04	1.42
PL3	-1.34	0.93	2
PL4	-1.08	-1.22	1.42
PL5	0.38	1.58	1.42
PL6	0.54	-1.54	2
DME	5	0	2

3.2.2. Positioning Algorithm

Positioning of the Mosaic/DME is based on the Weighted Least Square (WLS) method with consideration of two different measurements: one is the carrier phase and the other is range. Their different error levels of measurements are also considered as described in Kim et al. [2]. Because the Mosaic/DME demands ambiguity resolution, it employs the Least Square Ambiguity Search Technique (LSAST) to decrease the number of candidates for the better ambiguity resolution efficiency [40].

In this paper, the WLS method is performed for every epoch to locate the aircraft. It is assumed that the positioning is calculated by the onboard receiver. The carrier phase measurement can be described as shown below using Equation (3-2):

$$\Delta\phi_{ij} = \Delta d_{ij} + \Delta N_{ij}\lambda + \Delta\varepsilon'_{ij} = (\overline{R}_i - \overline{R}_u)\cdot\hat{e}_i - (\overline{R}_j - \overline{R}_u)\cdot\hat{e}_j + \Delta N_{ij}\lambda + \Delta\varepsilon'_{ij}, \quad (3\text{-}8)$$

$$\Delta\phi_{ij} - \overline{R}_i\cdot\hat{e}_i + \overline{R}_j\cdot\hat{e}_j - \Delta N_{ij}\lambda = (\hat{e}_j - \hat{e}_i)\cdot\overline{R}_u + \Delta\varepsilon'_{ij}. \quad (3\text{-}9)$$

where, $\overline{R}_i$ and $\overline{R}_j$ are i-th and j-th pseudolite antenna's positions, respectively, and $\overline{R}_u$ is the aircraft's (user) position. $\hat{e}_i$ denotes the line-of-sight unit vector from the user to the i-th pseudolite antenna. The range measurement of the DME can be simply described as shown in Equations (3-10) and (3-11).

$$r = d + v = (\overline{R}_r - \overline{R}_u)\cdot\hat{e}_r + \varepsilon'_r \quad (3\text{-}10)$$

$$r - \overline{R}_r\cdot\hat{e}_r = -\hat{e}_r\cdot\overline{R}_u + \varepsilon'_r \quad (3\text{-}11)$$

where, r is the range measurement between the DME and aircraft, $\overline{R}_r$ is the position of the DME antenna, $\hat{e}_r$ is the line-of-sight unit vector from the user to the DME, and ε'_r is the error of the DME range measurement.

Measurement equations are as shown below:

$$\overline{z} \equiv \begin{bmatrix} \Delta\phi_{12} - \overline{R}_1\cdot\hat{e}_1 + \overline{R}_2\cdot\hat{e}_2 - \Delta N_{12}\lambda \\ \Delta\phi_{13} - \overline{R}_1\cdot\hat{e}_1 + \overline{R}_3\cdot\hat{e}_3 - \Delta N_{13}\lambda \\ \Delta\phi_{14} - \overline{R}_1\cdot\hat{e}_1 + \overline{R}_4\cdot\hat{e}_4 - \Delta N_{14}\lambda \\ \Delta\phi_{15} - \overline{R}_1\cdot\hat{e}_1 + \overline{R}_5\cdot\hat{e}_5 - \Delta N_{15}\lambda \\ \Delta\phi_{16} - \overline{R}_1\cdot\hat{e}_1 + \overline{R}_6\cdot\hat{e}_6 - \Delta N_{16}\lambda \\ r - \overline{R}_r\cdot\hat{e}_r \end{bmatrix}, \quad (3\text{-}12)$$

$$H \equiv \begin{bmatrix} \hat{e}_2 - \hat{e}_1 & \hat{e}_3 - \hat{e}_1 & \hat{e}_4 - \hat{e}_1 & \hat{e}_5 - \hat{e}_1 & \hat{e}_6 - \hat{e}_1 & -\hat{e}_r \end{bmatrix}^T, \quad (3\text{-}13)$$

$$\overline{v} \equiv \begin{bmatrix} \Delta\varepsilon'_{12} & \Delta\varepsilon'_{13} & \Delta\varepsilon'_{14} & \Delta\varepsilon'_{15} & \Delta\varepsilon'_{16} & \varepsilon'_r \end{bmatrix}^T, \quad (3\text{-}14)$$

$$\bar{z} = H \cdot \bar{R}_u + \bar{v} \quad . \tag{3-15}$$

For the weighting of measurements, the single differenced covariance matrix is defined as Equation (3-16).

$$V \equiv \mathrm{cov}\left[\bar{v}\right] = \begin{bmatrix} 2\sigma_\phi^2 & \sigma_\phi^2 & \sigma_\phi^2 & \sigma_\phi^2 & \sigma_\phi^2 & 0 \\ \sigma_\phi^2 & 2\sigma_\phi^2 & \sigma_\phi^2 & \sigma_\phi^2 & \sigma_\phi^2 & 0 \\ \sigma_\phi^2 & \sigma_\phi^2 & 2\sigma_\phi^2 & \sigma_\phi^2 & \sigma_\phi^2 & 0 \\ \sigma_\phi^2 & \sigma_\phi^2 & \sigma_\phi^2 & 2\sigma_\phi^2 & \sigma_\phi^2 & 0 \\ \sigma_\phi^2 & \sigma_\phi^2 & \sigma_\phi^2 & \sigma_\phi^2 & 2\sigma_\phi^2 & 0 \\ 0 & 0 & 0 & 0 & 0 & \sigma_r^2 \end{bmatrix} \tag{3-16}$$

where, σ_ϕ^2 is the Gaussian-assumed variance of the pseudolite carrier phase error, and σ_r^2 is the Gaussian variance of the DME range error. It is assumed that all carrier phase measurements have the same levels of errors. As a result, the position can be calculated as:

$$\bar{R}_u = (H^T V^{-1} H)^{-1} H^T V^{-1} \bar{z} \quad . \tag{3-17}$$

Equation (3-17) is the general WLS equation.

As the LSAST is applied to this equation, the measurements are divided into two groups: the primary and secondary groups. The primary group includes the measurements of the pseudolites 1 to 4 and the DME, while the secondary group includes pseudolites 5 and 6. The cycle ambiguity of the secondary group is calculated directly using the result of the primary group as shown below:

$$\Delta N_{1k} = \text{round}\left(\frac{\Delta\phi_{1k} - \overline{R}_1 \cdot \hat{e}_1 + \overline{R}_k \cdot \hat{e}_k + (\hat{e}_1 - \hat{e}_k) \cdot \hat{R}_{u,p}}{\lambda} \right). \quad (3\text{-}18)$$

where, k is 5 or 6, and $\hat{R}_{u,p}$ is the position calculated via only the primary group. Using the LSAST, the process needs to solve the cycle ambiguities only in the primary group (ΔN_{12}, ΔN_{13}, *and* ΔN_{14}). For example, if the value of M of Equation (3-7) is 3, then there are 7 integers from -3 to +3 for each single differenced measurement. As a result, there are a total of 7^3 potential solutions with LSAST, and 7^5 without LSAST. The details are referenced to [40].

3.2.3. Potential Solutions

Because of the cycle ambiguity of the carrier phase, there are many potential solutions of which only one is true. As the Mosaic/DME is the system that combines the two types of measurements, its potential solutions have different features compared to the CDGPS. These features can be easily displayed via a 2D case simple simulation. The simulation shown in Figure 3-3 is performed using a known true solution so that it can be displayed with other potential solutions which reflect changes in integer ambiguities.

In this simulation, the antenna spacing of the two pseudolite is measured to be 3.4λ, M is 3, and p is 0.4. As M is set as 3, there are a total of 7 potential solutions corresponding to the 7 integers from -3 to +3, according to Equation (3-7). Among the circled candidate solutions in Figure 3-3, the true solution is marked as a star. An interesting finding from the figure is that the potential solutions are spread on the semi-circle of the DME bound. This is because the measurement from the DME to the user is fixed using the real range

measurement. Therefore, the change of integer ambiguity leads to the difference in directions only.

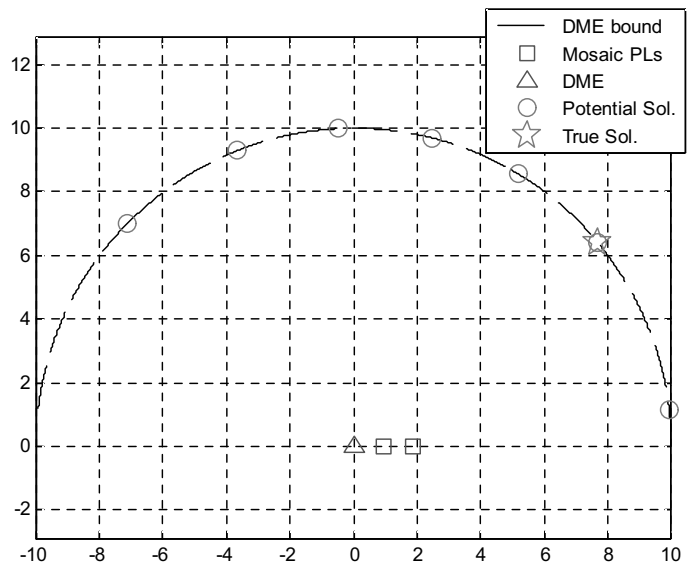

Figure 3-3 Potential solutions of Mosaic/DME in 2-dimenstional case

If this simulation is extended to the 3D case, the potential solutions are spread on the surface of sphere as shown in Figure 3-4. In Figure 3-4, five pseudolites are considered with an antenna spacing of 3.4λ at the origin (0,0,0). All potential solutions have the same distance to the DME station, which is identical to the 2D case, and the solutions are distant from each other. These tendencies are quite different from the CDGPS case, and are quite important for the easy ambiguity resolution. Details of the ambiguity resolution are described in the ambiguity resolution section.

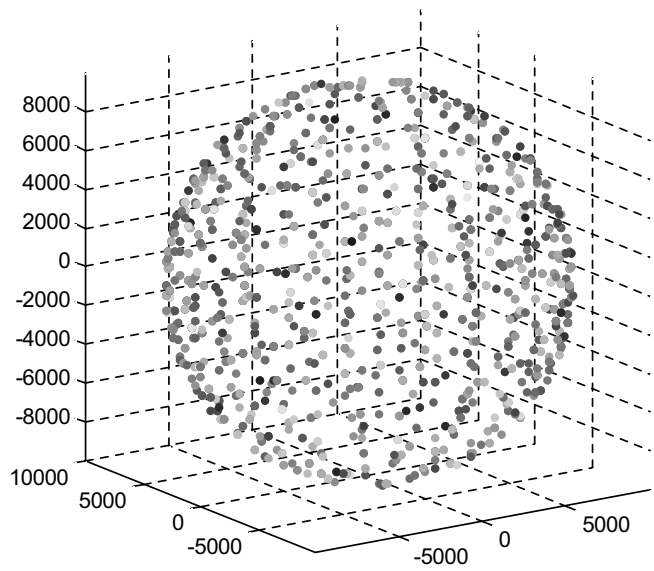

Figure 3-4 Potential solutions of Mosaic/DME in 3-dimenstional case

3.2.4. Special Features

Because of the specific form and characteristics of the Mosaic/DME system, some features need to be described. As this system uses the DME as its base system, and new signals from the pseudolites are designed to avoid the installed DME frequency, the Mosaic/DME has full compatibility with the conventional DME operation.

As the Mosaic/DME computes the 3-dimensional positioning using only one station, the synchronization of the clocks between the stations in different regions is not necessary.

This system meets navigation accuracy requirements even with a single station. It yields

a higher level of performance if two or more stations are available.

Although the integrity and capacity studies should be treated thoughtfully, it is not sufficiently performed in this paper. They remain for future work. However, they can be conceptually described as follows:

If more than two stations are available, it has an integrity advantage because each station can individually provide positioning solutions.

It is expected that the capacity of the Mosaic/DME is better than that of the conventional DME if a highly stable oscillator is available. This is because the two types of signals, two-way round-trip and one-way continuous, are used. Once time synchronization between the Mosaic/DME and aircraft is performed, the one-way signals can be regarded as the real range. Therefore, it requires fewer round-trip range measurements, ultimately increasing the capacity of the DME.

3.3 Positioning Accuracy Analysis

The purpose of this section is to investigate the accuracy of the Mosaic/DME system and whether this system can satisfy the navigation accuracy requirement of the APNT or not. This investigation is performed through an analysis using the Weighted Dilution of Precision (WDOP) concept and the Monte-Carlo simulations.

The simulation settings used in this chapter are described in Table 3-2. The carrier frequency is set at the middle of the DME operational frequency as a representative. The antenna baseline is determined as Equation (3-4) with the parameters of M of 10 and p of

0.25. And the parameter M is determined empirically to satisfy the required accuracy of APNT.

Table 3-2 Simulation Settings

Carrier Frequency	Wavelength (λ)	Antenna Spacing	No. of Potential Solutions
1088.5 MHz	27.54 cm	2.823m (M=10, p=0.25)	9261

3.3.1. Measurement Error

The statistical errors of the DME ranging and the carrier phase measurement are listed in Table 3-3. For the DME's error size, two different values are considered. One is the specified performance of the current DME, which includes all error sources following the FAA-E-2996 [30]. The other is the error budget determined by the APNT team for the future DME performance upgrades [32].

A brief study on the effects of the error sources on Mosaic system has already been performed [23]. But it is inappropriate to apply directly to the investigation of generalized performance, because some specific environments and conditions were assumed for the former works. Therefore, the statistical errors of the carrier phase measurement are applied based on the results of GPS attitude determination by Cohen [41-43]. The attitude determination using GPS has common features with Mosaic/DME system, such as meter-level antenna baselines, CDMA signals, and utilizing differential carrier phase measurements. The main differences are the direction of signal and the operational frequency, GPS L1 (1575.42MHz) and Mosaic (1088.5MHz). Therefore, the measurements of GPS attitude determination is regarded as the proper source to

understand the errors of Mosaic with the considerations of their differences.

Table 3-3 Statistical error of measurements (if $\lambda = 27.5$cm)

	Error Sources	Standard Deviation (σ)	RMS
DME error	FAA-E-2996	185.2m	-
	APNT team	34m	-
Carrier phase error	Multipath (differential)	-	7.2mm
	Troposphere	Model	
	Carrier-to-noise ratio	2.8mm	-
	Equipment-specific errors	1mm	-

According to the multipath errors of the GPS attitude determination, it was practically experienced that the differential multipath error is not over 5mm RMS even in difficult multipath environments [42, 43]. And the multipath difference by different antenna baselines from 50cm to 10m can be neglected [42]. The signals of Mosaic system have the opposite direction of the attitude determination system. However, the multipath effect does not depends on the direction of the signal but the satellite-reflector-antenna geometry when considering the ray-tracing approach [44]. As the operational frequencies are different, the proportional scaling, considering the wavelengths of two systems, is applied based on the multipath mathematical model [41, 44, 45]. For Monte-Carlo simulations, the differential multipath error is generated as a bandlimited random process whose RMS is 7.2mm [42, 45].

Tropospheric error is modelled and added to the Monte-Carlo simulations using the Wide

Area Augmentation System (WAAS) model [46]. For the implementation of the WAAS model, latitude of 35deg, and day of year of 100 are considered. Following the experimental results of GPS attitude determination, the measurement noise by carrier-to-noise ratio is less than 1mm (1σ), but, conservatively, the noise of the 1% of the wavelength (2.8mm) is applied for standard deviation [41, 47]. Other error sources, such as cross talk, line bias, and inter-channel bias, are smaller than 1mm (1σ) if they are well designed and calibrated [41].

The total statistical sum of errors of the carrier phase measurement and the DME standard derivation are applied when forming a weighting matrix V of Equation (3-16).

3.3.2. Weighted DOP

The WDOP is the improved description of the Dilution of Precision (DOP) when considering the error levels of each measurement. The WDOP was derived for the GNSS quality measure with the different weightings of each satellite [48]. For the GNSS studies, the weightings are calculated based on the Signal to Noise Ratio (SNR) of the signals [49] or the elevation angles of the satellite [50]. Both cases improved the performance levels of the DOP with proper weightings.

In the Mosaic/DME, the conventional DOP cannot sufficiently provide the measure of geometry. This is because the two types of measurements, ranging from the DME and carrier phases from the pseudolites, are simultaneously considered as shown in Equations (3-12)~(3-15). Because the two measurements have different scales in error magnitudes, the WDOP is essentially required for the Mosaic/DME.

The definition of the WDOP follows Sairo et al. [48]. However, the Mosaic/DME uses the single differenced measurement of the observation matrix as shown in Equation (3-13). Therefore, the definitions of the observation matrix (H) and measurement covariance matrix (V) are different compared to those of Sairo et al. [48]. The result of Equation (3-20) from the covariance matrix of position error, which is defined as Equation (3-19), represents the Weighted Position DOP (WPDOP). And the Weighted Horizontal DOP (WHDOP) and the Weighted Vertical DOP (WVDOP) are shown as Equations (3-21) and (3-22), respectively. In these equations, D_{ij} denotes the element of the i-th row and j-th column in matrix D.

$$D \equiv \mathrm{cov}(\bar{R}_u) = (H^T V^{-1} H)^{-1} \tag{3-19}$$

$$WPDOP = \sqrt{trace(D)} \tag{3-20}$$

$$WHDOP \equiv \sqrt{D_{11} + D_{22}} \tag{3-21}$$

$$WVDOP = \sqrt{D_{33}} \tag{3-22}$$

Matrices used in Equation (3-19) are already defined in Equations (3-13) and (3-16). The weightings of the measurements consider only the type of measurements as shown in Equation (3-16).

The WDOP of the Mosaic/DME is calculated for analyses of the navigation accuracy. Three analyses are considered for the accuracy studies: First is the accuracy around the Mosaic/DME station. In this case, the distance from the station to the aircraft is fixed, but the relative azimuth and elevation angles from the station are varied. The second case is the relationship between the accuracy and distance from the station to aircraft. The last case is the verification of the required performance levels in the airspace Class B area, which requires the highest measure of accuracy, RNAV or RNP 0.3.

For the WDOP calculation, the positions of the pseudolite and the DME antennas are as shown in Table 3-1, basic settings are shown in Table 3-2, and measurements errors are in Table 3-3.

With consideration of the geometrical characteristics of this system, it is better to explain the system performance in terms of radial and angular axes. However, because the APNT requirement establishes the horizontal performance, the system performances are mainly displayed in horizontal and vertical sides.

Figure 3-5 and Figure 3-6 show the WHDOP and WVDOP of the Mosaic/DME according to its relative azimuth and elevation angles with different DME error levels. The distance from the station to the aircraft is fixed at 10km (about 5.4nmi). And the axes of elevation and azimuth angles in figures are different for clear recognition.

These figures help identify the tendencies of accuracy according to the relative azimuth and elevation angles around station. With the changes in elevation angle, the Mosaic/DME yields significant difference in WDOP values for both horizontal and vertical cases. As the elevation angle increases, the WHDOP is decreased, while the WVDOP is increased. This is the result of combining two different types of measurements; the DME range is the primary contributor of vertical positioning in high elevation angles, while it is also the main cause of the horizontal error in low elevation angles. It is difficult to clearly distinguish the effect of the carrier phase measurements according to elevation angle, but its tendency is the reverse of the one of the DME ranges.

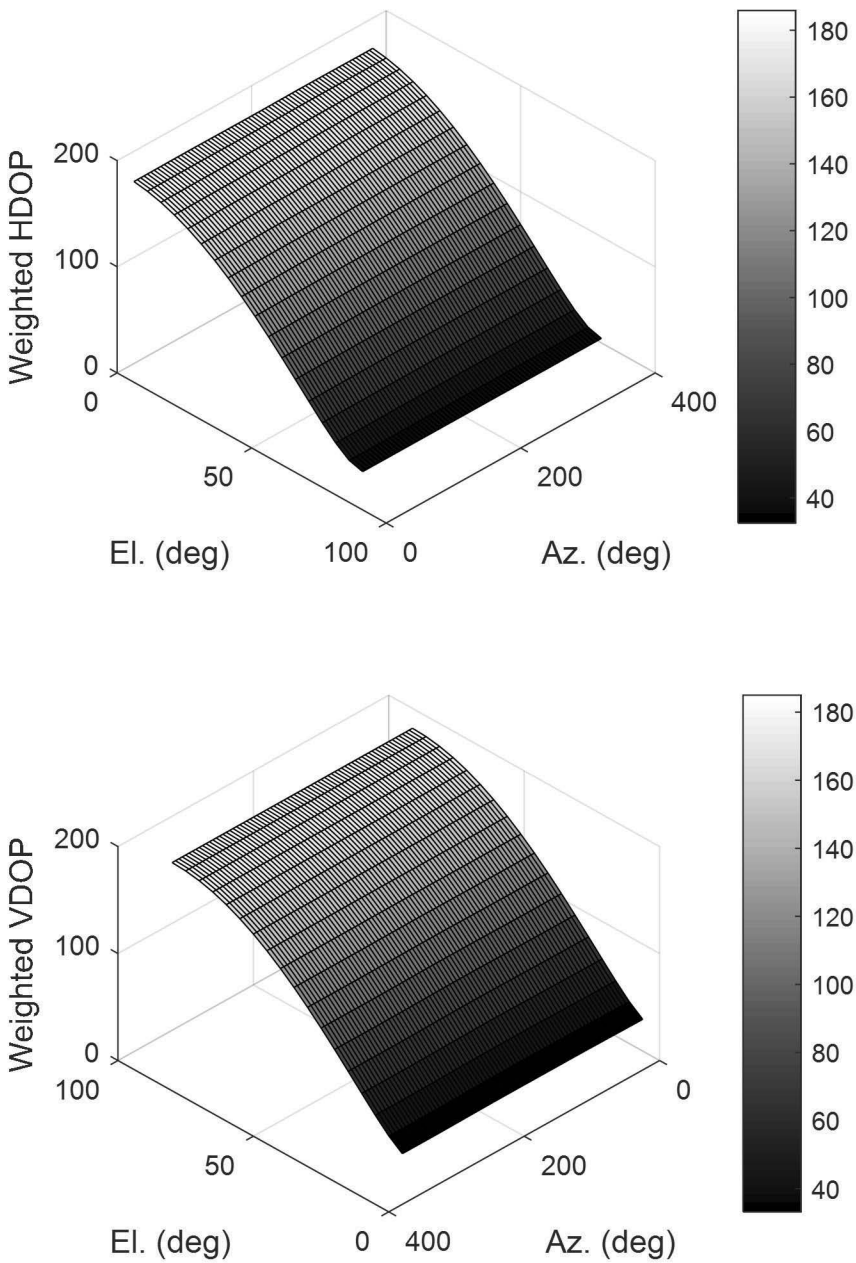

Figure 3-5 WDOP according to relative azimuth and elevation angles with DME error size of 185 m (1σ) *(top: WHDOP, bottom: WVDOP)*

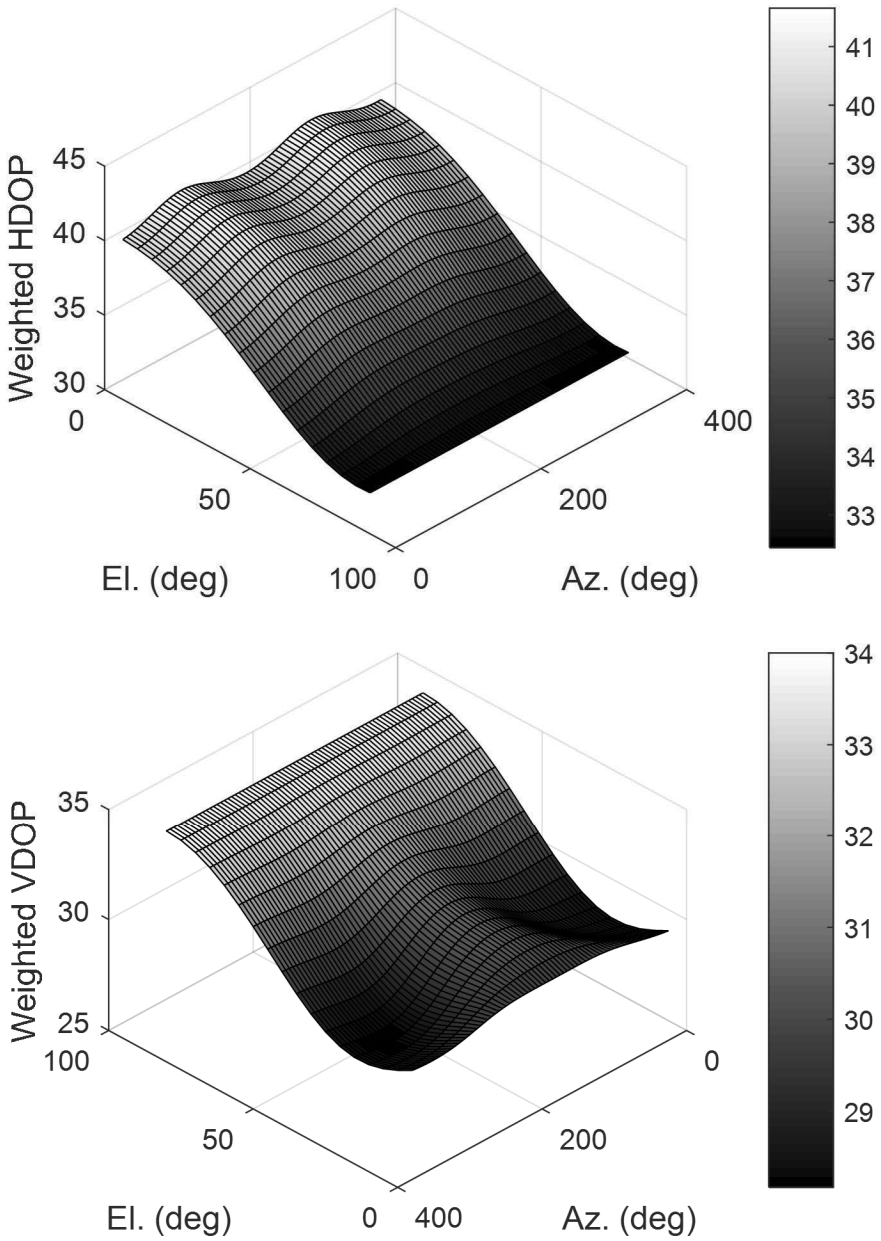

Figure 3-6 WDOP according to relative azimuth and elevation angles with DME error size of 34 m (1σ) (top: WHDOP, bottom: WVDOP)

The WDOP results that depend on the distance from the station to aircraft and the airspace class B area are described together with the Monte-Carlo simulations shown in Figure 3-7, Figure 3-8, and Figure 3-9.

3.3.3. Accuracy Simulation

The navigation accuracy of the Mosaic/DME is investigated using Monte-Carlo simulations. The horizontal Distance Root Mean Square (DRMS) and vertical RMS are statistically calculated via the 1,000 executions. And results are displayed along with the WDOP values.

The basic simulation settings are described in Table 3-1, Table 3-2, and Table 3-3. For the error model of the DME range measurement, both two values from the FRP and APNT team, shown in in Table 3-3, are considered.

During the simulations, it is assumed that cycle ambiguity problem is perfectly solved, which enables the investigation of the pure navigation accuracy.

The first simulation focuses on the investigation of the relationship between distance from the station to the aircraft and navigation accuracy. The distance is from 1km to 240km (approximately 0.54nmi to 130nmi), and its guideline is through the 3 degree glide path.

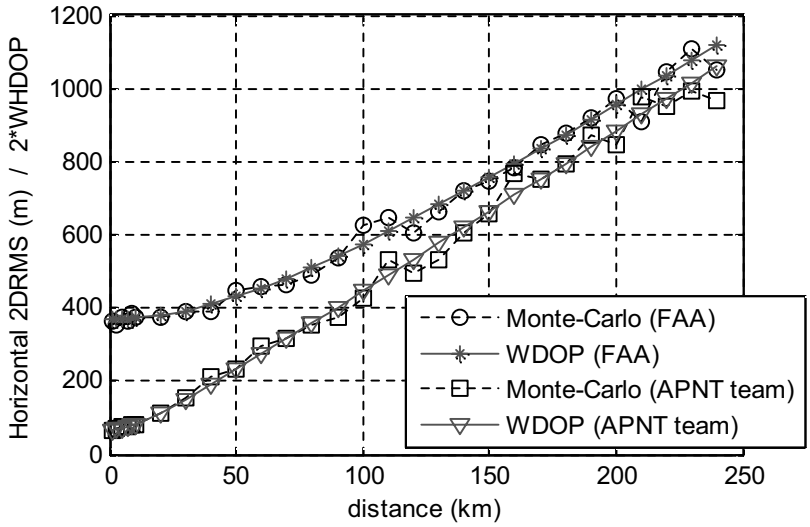

Figure 3-7 Simulation results of the relationship between distance and horizontal accuracy

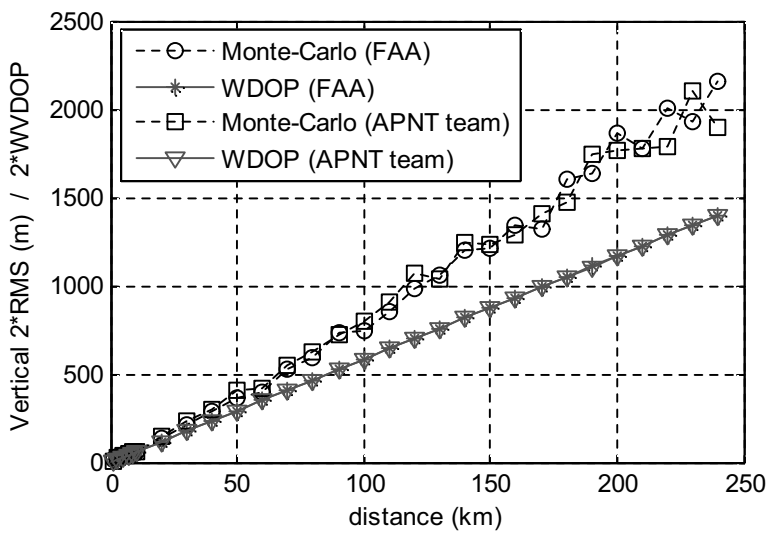

Figure 3-8 Simulation results of the relationship between distance and vertical accuracy

Figure 3-7 and Figure 3-8 describe the simulation results of the Monte-Carlo in 95% probability of the error magnitude and twice the WDOP in both the DME error of FAA (185m) and APNT team (34m). In overall, the tendency shows the positive linear relationship between performance and distance.

The APNT en-route performance requirement is RNAV or RNP 2. In considerations of FTE of FD and MA, the required NSE is 3.7km (1.98nmi) and 3.6km (1.94nmi) respectively as shown in Table 1. The horizontal error slope displays that the accuracy performance of the Mosaic/DME is sufficient, even for the RNAV/RNP 1.

In the horizontal result shown in Figure 3-7, the WDOP and Monte-Carlo results have almost the same tendency in both the DME error cases. Furthermore, the DME error of 34m indicates higher levels of performance near the station. However, the difference between them becomes smaller as the distance is increased. This state can be easily explained conceptually; the portion of the DME error in horizontal performance becomes smaller as the error caused by the Mosaic pseudolites becomes larger for a greater distance from the station to the user. In the vertical case, on the other hand, there is no difference between the two DME error magnitudes, and the Monte-Carlo result displays a steep slope of linearity compared to that of the WDOP. This is because of the tropospheric delay, which is not considered in the WDOP. As tropospheric delay increases the bias of the vertical position error, the RMS error is increased, as shown in Figure 3-8. The features that combine the two different measurements make the tropospheric effect solely influence the vertical position error.

To verify the required performance for airspace class B and C, the simulation of only class B area is performed. Since class B is larger than class C, satisfying the class B accuracy of the RNP or RNAV 0.3 to 1.0 shows that this level of accuracy is sufficient

for class C as well. In reality, the size of the class B area is different from that of each airport. This is because the environment and traffic patterns are considered when designing the class area. However, the general airspace class B has an outer boundary of 30nmi (55.56km) in radius, 10,000ft (3.05 km) in height, and a shape of an inverted wedding cake. Therefore, if the simulations of this outer boundary satisfy the requirements of the APNT, the inner area of this boundary, which includes both class B and C, automatically satisfies the requirement.

In simulations, it is assumed that the Mosaic/DME station is located near the airport, and the general airspace class B is formed around this station. The horizontal accuracy performance through the outer boundary of class B area is displayed in Figure 3-9.

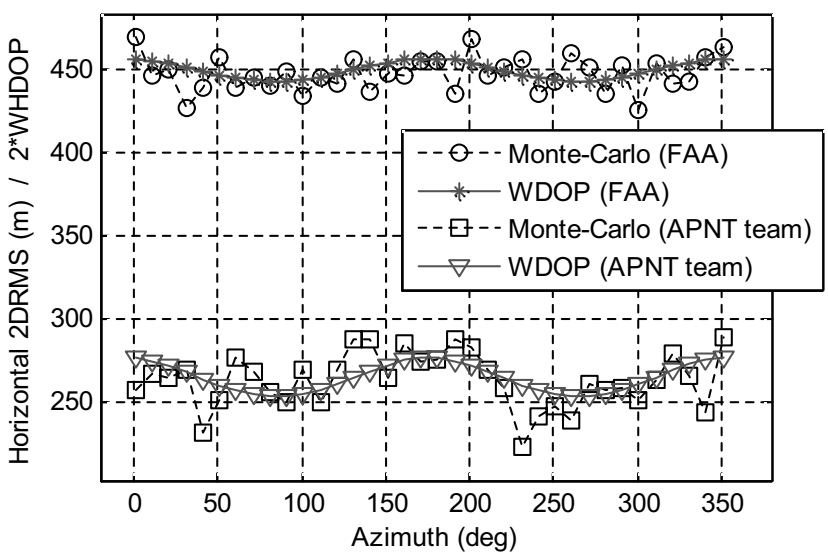

Figure 3-9 Horizontal accuracy through the boundary of airspace class B

The required NSE for RNP or RNAV 0.3 with FTE FD is 307.1m (0.17nmi), and the one for FTE AP is 505.1m (0.27nmi). The graphs in Figure 3-9 describe that the future horizontal accuracy using the DME error magnitude, 34m from the APNT team, can satisfy the required performance of the FTEs, FD (307.1m) and AP (505.1m). On the other hand, the performance of the FRP DME error is not high enough for the FTE FD case (307.1m). However, when FTE AP is considered, it can satisfy the requirement of TSE 0.3nmi.

3.4 Ambiguity Resolution

Ambiguity resolution can be defined as the process of selecting the true solution from potential candidates which are generated due to the integer cycle ambiguity. In another feasibility study of the Mosaic/DME system, the performance of the ambiguity resolution is essentially found to function as a navigation system. In this section, the strategy for the ambiguity resolution is described, and the verification of ambiguity resolution will be described in later chapters together with the antenna arrangement optimized for fast and robust cycle ambiguity resolution.

3.4.1. Features of Cycle Ambiguity

Cycle ambiguity of the Mosaic/DME is different from that of the conventional CDGPS. The first difference is the spacing between potential solutions. In CDGPS the gap between solutions can be generally measured in centimeter levels (or inch levels). On the other hand, because the potential solutions of the Mosaic/DME are spread out as shown

in Figure 3-4, they are kilometer-level (or nmi-level) apart if the range from the station to aircraft is tens or hundreds of kilometers (or nautical miles). The other difference is that, in the Mosaic/DME, the true position is geometrically guaranteed from the potential candidates as derived in Equation (3-7). These properties help the ambiguity resolution of the Mosaic/DME to be fast and easy.

3.4.2. Strategy of Ambiguity Resolution

The ambiguity resolution of the Mosaic/DME is required to be performed, whether the GNSS is available or not. In the former case, ambiguity can be easily fixed because the GNSS level accuracy can point to the true position from the candidates.

As an APNT solution, the Mosaic/DME is still required to solve the ambiguity problem even when GNSS is unavailable. If the user has knowledge of the previous position, the ambiguity resolution of Mosaic/DME can be established relatively easily. Once ambiguity is fixed, it is possible to keep tracking it without the use of the ambiguity resolution process until the cycle slip occurs. If the cycle slip occurs when the GNSS is unavailable, the Mosaic/DME system needs to resolve the cycle ambiguity problem. If the last position before the cycle slip is known, then this position can easily be applied to the ambiguity resolution. If the ambiguity problem requires a solution without the last position, then there are different solutions that can be separated into two cases: the ambiguity resolution using external aids or the ambiguity resolution using only the aircraft and the Mosaic/DME. For the former case, if external systems, such as VOR, DME, MLAT, altimeter or other sensors, are available, the ambiguity resolution can be performed accurately and rapidly. When the onboard is used, the potential solutions are

geometrically strained because the altimeter bounds the altitude of the aircraft. As the potential solutions are wide spread on the sphere whose radius is the DME range, which is the distance from station to aircraft, the altimeter eliminates the large number of false potential solutions increasing the performance of ambiguity resolution considerably [24].

Without these external aids, the cycle ambiguity can be solved using only the measurements from Mosaic/DME station. This scenario of the ambiguity resolution is described in Figure 3-10. And this dissertation focuses on the worst case ambiguity resolution, where only the Mosaic/DME is available (grey box in Figure 3-10).

The LSAST ambiguity resolution method is concerned with reducing the number of potential solutions [40]. The next step is the statistical test of the residuals using the threshold test and ratio test. The residuals of the measurements can be expressed using the Weighted Square Sum of Error (WSSE) defined as below:

$$\delta\bar{z} \equiv \hat{z} - \bar{z} = H \cdot \hat{R}_u - \bar{z} \tag{3-23}$$

$$P \equiv H(H^T V^{-1} H)^{-1} H^T V^{-1} \tag{3-24}$$

$$WSSE : \Omega \equiv \delta\bar{z}^T V^{-1} \delta\bar{z} = \bar{z} V^{-1} (I - P)\bar{z} \tag{3-25}$$

The threshold test compares the WSSE of each potential solution with the threshold of the chi-square distribution to eliminate the false candidates [51]. And the base concept of the ratio test underlines that the ratio of two chi-square distributions has a f-distribution [51]. Hence, the ratio of the two WSSEs, whose denominator is the minimum WSSE in the potential solutions, is compared with a certain threshold, which is generated using the f-distribution. Each threshold value of the two tests is calculated with the appropriate level of probability and degrees of freedom.

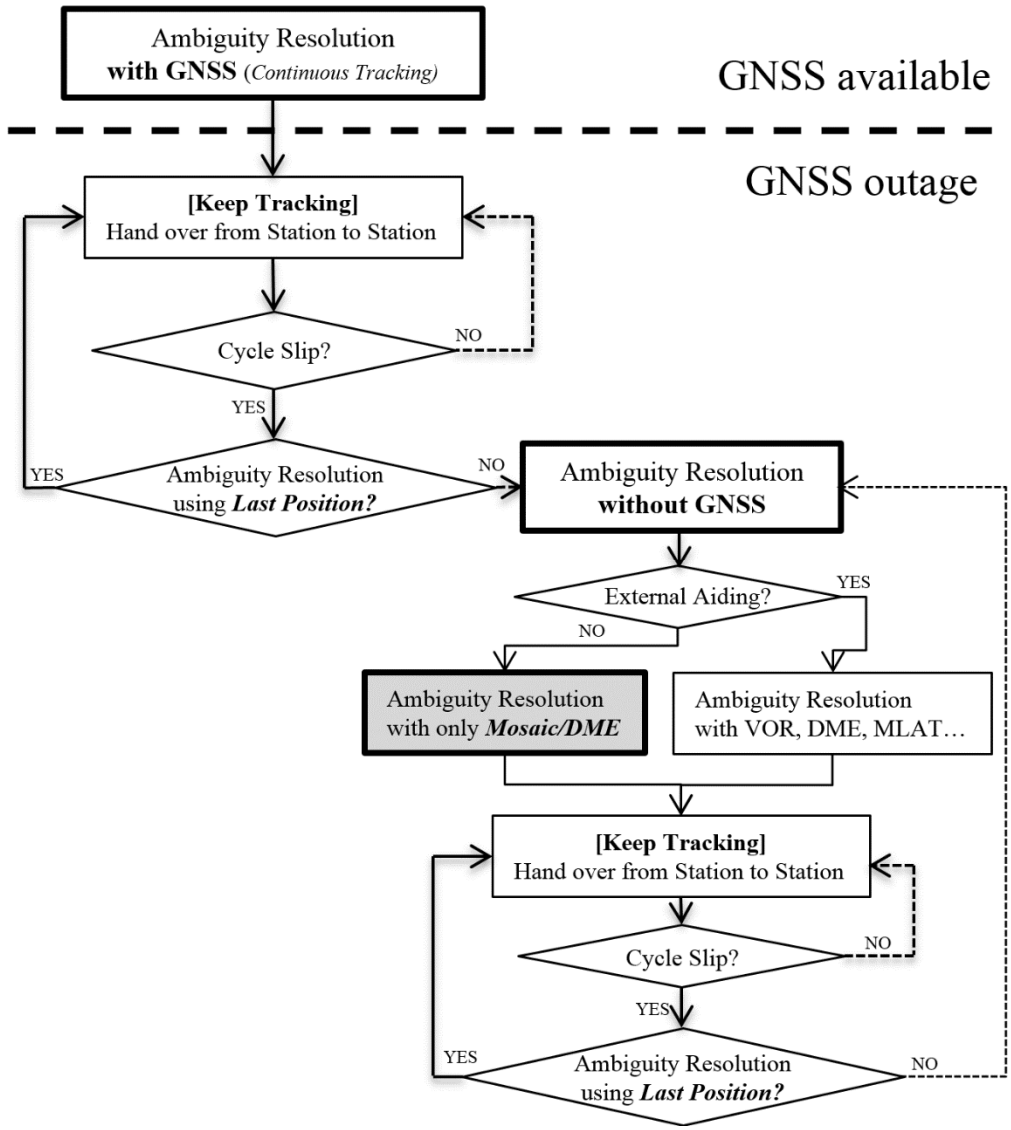

Figure 3-10 Ambiguity resolution scenario of Mosaic/DME

The verification of the strategy of ambiguity resolution will be described in later chapters considering the antenna arrangement optimized for fast and robust ambiguity resolution.

Chapter 4. Multi-Antenna Arrangement Method for 2D Environment

A formation of multiple pseudolite antennas at station affects the positioning accuracy of user changing the geometry from station to user, and it is empirically found that the cycle ambiguity resolution performance is also affected by the antenna formation.

In this chapter, methods of antenna arrangement to maximize the positioning accuracy and the cycle ambiguity resolution performance for a 2-dimensional environment considering the Area of Interest (AOI) are described. This chapter has a focus on the derivation of antenna arrangement process for a 2D environment to display conceptually. Even though, it is the step for a 3-dimensional environment which will be described in Chapter 6, but it is also useful for marine application where the altitude difference between the station and user is negligible.

In a 2D environment, the minimum number of pseudolite antennas for the cycle ambiguity resolution is four, because three carrier-phase measurements and one distance measurement are required for 2-D positioning eliminating clock bias between station and receiver, and at least one additional measurement is essential for residual tests of ambiguity resolution process. Hence, the station with four pseudolite antennas and one Distance Measurement Equipment (DME) is considered in this chapter.

The antenna arrangement process considers two perspectives: the positioning accuracy and the cycle ambiguity resolution performance. This chapter describes each perspectives separately, and the method considering both perspectives is also described. In addition,

the Monte-Carlo simulation results resolving the cycle ambiguity are described and analyzed.

4.1 Area of Interest (AOI)

For the antenna arrangement process, two areas around the station, AOI and Non-Interested Area (NIA) are defined. When the Mosaic/DME system is considered, AOI is the main air routes around the station. It is easily figured out if the locations of VOR/DME stations and lines of air-routes on the air chart are considered. In a 2D environment, the NIA is the area except AOI, and it is disregarded during the antenna arrangement process.

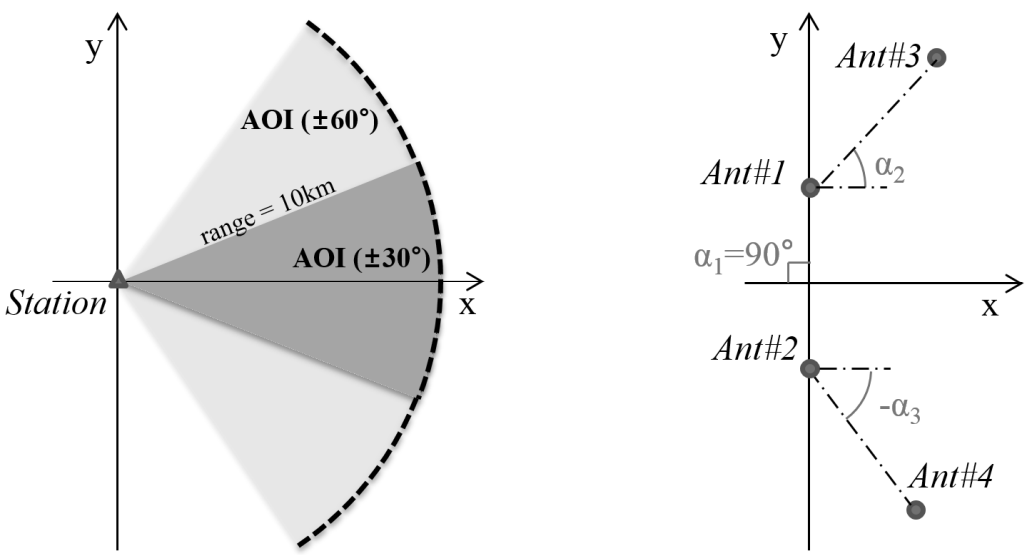

Figure 4-1 AOI and antenna arrangement settings considered in this chapter

AOI and NIA are defined with the angular bounds on the polar coordinated system. The station is located at the origin of the coordinated system, and the AOI is defined using angle parameters as on the left of Figure 4-1. The AOI bound in radial direction is fixed, because, in the aspect of positioning accuracy, the range from station to user only causes to the scaling of positioning error and the characteristics are mainly affected by angular direction as described in section Chapter 33.3. The characteristics of cycle ambiguity resolution are also mainly depend on angular direction, which will be described in section Chapter 44.3.

In this chapter, two cases of AOI bounds are considered as on the left of Figure 4-1: ±30° and ±60°. And only two baseline angles out of four-antenna arrangement are independent variables (α_2 and α_3) and one has a fixed value (α_1=90°) to simplify and visualize the process. Two baseline angles, α_2 and α_3 are defined as on the right figure of Figure 4-1. In addition, it is assumed that lengths of all antenna baselines are equal.

4.2 Antenna Arrangement for Positioning Accuracy

The formation of antenna arrangement affects the characteristics of positioning accuracy. This property differs along the angle in the polar coordinate system as already described in Figure 3-5, Figure 3-6 and Figure 3-9, if the Mosaic/DME station is located at the origin of the coordinates. In addition, the properties of positioning accuracy are maintained along the radial direction. The distance from station to user makes a proportional increase of errors as described in Figure 3-7 and Figure 3-8.

The performance index of the antenna arrangement process to optimize for positioning accuracy, considered in this dissertation, is the worst accuracy in AOI. The purpose is to

maximize the accuracy at the worst location, in other words, minimize the DOP at the worst location. This kind of approach is suitable if a certain level of accuracy is required all over the AOI, such as APNT requirement of RNP or RNAV 0.3.

DOP which is used for the performance index of a 2D environment is Angular DOP (ANDOP). Because of the distance measurement relying on DME round-trip signals, the 2-dimensional error ellipse of Mosaic/DME has two axes of radial and angular directions. The error bound to radial direction is fixed relying on the quality of DME measurement. Hence, the formation of pseudolite antennas only affects the error of angular direction. Therefore, considering ANDOP is enough for the performance index of the antenna arrangement process.

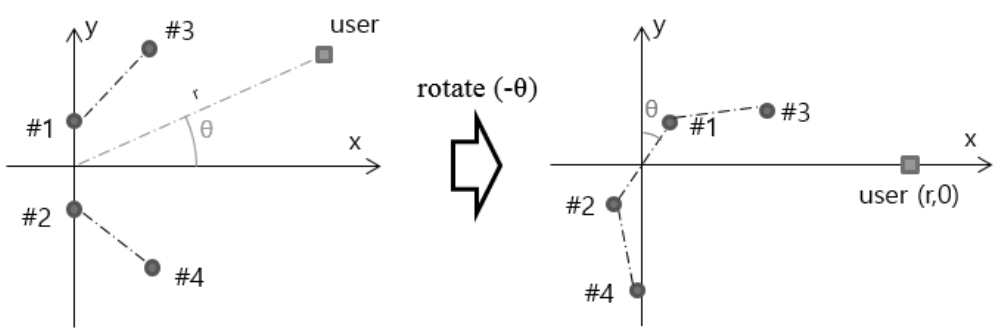

Figure 4-2 Inverse rotation for the calculation of ANDOP

For the calculation of ANDOP, the formal approach is to calculate the eigenvalues of error ellipse, then two eigenvalues represent the error bounds of radial and angular directions if the distance from station to user is long enough. In this dissertation, however,

the intuitive approach to calculate the ANDOP is used. The formation of antenna arrangement and the user position performs an inverse rotation by user's angle, then the user position is on x-axis as in Figure 4-2.

Subsequently, the non-diagonal term of error ellipse is almost zero, and the error-term in x-axis means the error size of radial direction, the value in y-axis can be represented as the angular direction.

Error ellipse matrix, *D*, is defined as in Equation (3-19). Four antennas case in a 2D environment with antenna baselines as in Figure 4-2 has H-matrix and V-matrix as Equations (4-1) and (4-2):

$$H \equiv \begin{bmatrix} \hat{e}_2 - \hat{e}_1 \\ \hat{e}_3 - \hat{e}_1 \\ \hat{e}_4 - \hat{e}_2 \end{bmatrix} \tag{4-1}$$

$$V \equiv \begin{bmatrix} 2 & 1 & -1 \\ 1 & 2 & 0 \\ -1 & 0 & 2 \end{bmatrix} \tag{4-2}$$

where, $\hat{e}_i$ denotes the line-of-sight unit vector from the user at *(r, 0)* to the i-th pseudolite antenna after -θ rotation.

As the user position is on the x-axis, YDOP can be regarded as ANDOP as in Equation (4-3). Hence, ANDOP can be defined as Equation (4-4).

$$D \equiv (H^T V^{-1} H)^{-1} = \begin{pmatrix} D_{11} & D_{12} \\ D_{21} & D_{22} \end{pmatrix} \approx \begin{pmatrix} D_{11} & 0 \\ 0 & D_{22} \end{pmatrix} \tag{4-3}$$

$$ANDOP \equiv \sqrt{D_{22}} \tag{4-4}$$

Calculated maximum ANDOPs all over the AOI according to α_2 and α_3 are in Figure 4-3 and Figure 4-4: ±30° and ±60° cases, where all antenna baselines are 67.3cm (~2.5λ) and the range from station to user is 10km.

The purpose of the optimization is to maximize the accuracy at the worst location, in other words, minimize the ANDOP at the worst location. Hence, if the antenna arrangement of Figure 4-1 is considered, the optimization problem is defined as Equation (4-5) to find α_2 and α_3.

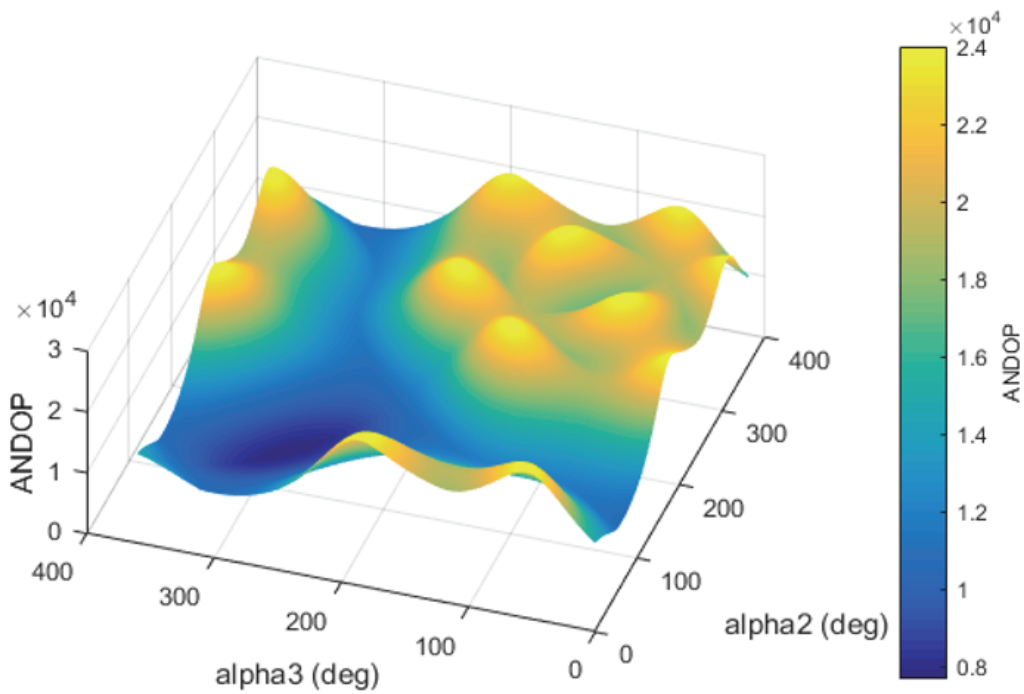

Figure 4-3 Maximum ANDOP according to α_2 and α_3 when AOI is ±30°

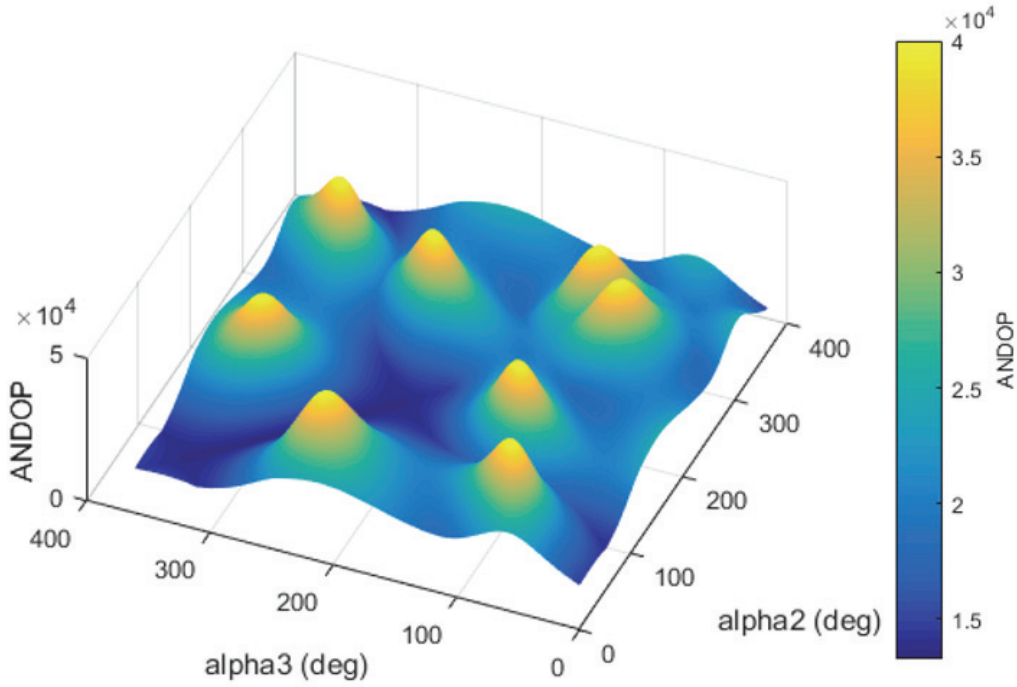

Figure 4-4 Maximum ANDOP according to α_2 and α_3 when AOI is ±60°

$$\begin{aligned}\{\alpha_2,\alpha_3\} &= \arg\min_{0<\alpha_2,\alpha_3<2\pi}\left[\max_{\theta \text{ in } AOI}\left(ANDOP(\alpha_2,\alpha_3,\theta)\right)\right] \\ &= \arg\min_{0<\alpha_2,\alpha_3<2\pi}\left[\max_{\theta \text{ in } AOI}\left(\sqrt{D_{22}(\alpha_2,\alpha_3,\theta)}\right)\right]\end{aligned} \tag{4-5}$$

In Figure 4-3 and Figure 4-4, the optimized antenna arrangement *(α_2, α_3)* to minimize the worst ANDOP are (90°, 270°) and (95.6°, 264.4°) for AOI ±30° and ±60° cases respectively, when the resolution for searching the antenna arrangement is 0.2°.

4.3 Antenna Arrangement for Ambiguity Resolution

4.3.1. Ambiguity Net Image

A general approach of ambiguity resolution is to eliminate the false candidate until the last candidate which is the true one is remained by means of the magnitude of measurement residuals [51]. Mosaic/DME system also uses the residual tests to solve the cycle ambiguity problem as described in section 3.4.

One of key feature for fast and robust ambiguity resolution is that the false candidate of potential solutions have large residuals that is distinct from the true candidate. The Ambiguity Net Technique has been derived focusing on this feature that it is able to assess the existence of hazardous false candidate with small residuals at a certain antenna formation.

The Ambiguity Net Technique draws the curves of each single-differenced carrier-phase measurements of each ambiguity candidate in the image domain, and the pixels dotted by curves of each antenna baselines are processed to investigate the possibility of hazardous false candidates. This technique is utilized to find an antenna formation without hazardous false candidate guaranteeing fast and robust ambiguity resolution.

For the positioning and ambiguity resolution of Mosaic/DME system, single-differenced carrier-phase measurements from pseudolites are used. A single-differenced measurement draws a hyperbolic curve, because the difference (single-differenced carrier-phase measurement) of the distances to two fixed points (locations of two antennas) is constant. If the distance from antenna to user is long enough, hyperbolic curves can be regarded as linear lines, asymptotes as in Figure 4-5. An analysis about this

assumption is depicted in Appendix A.

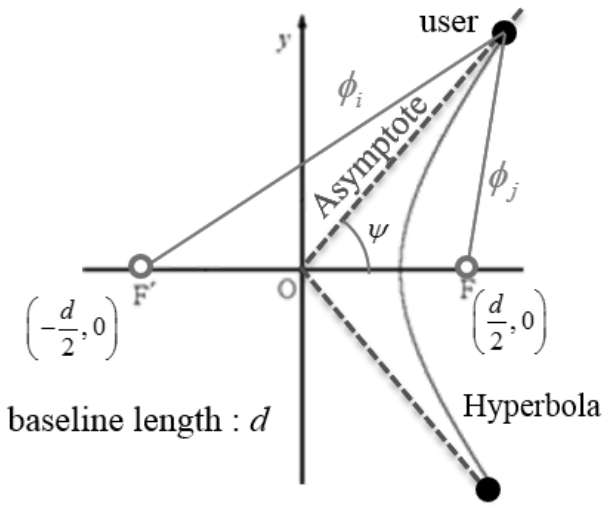

Figure 4-5 Hyperbola and asymptote

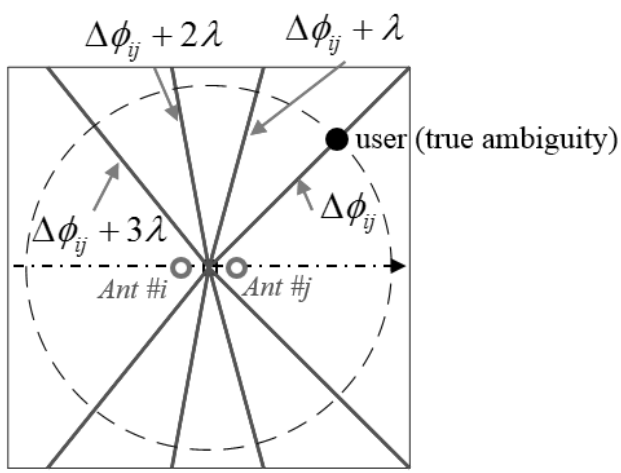

Figure 4-6 Asymptotes by each cycle ambiguity (four candidate case)

The cycle ambiguity of single-differenced carrier-phase measurements makes each asymptote with different slope angles as described in Figure 4-6. This relation can be derived relying on the equations of hyperbola and asymptote.

When single-differenced carrier-phase is used as defined in Equation (3-8), the slope angle of asymptote ψ of user position can be described as in Equation (4-6) which can be derived using the formula of hyperbola asymptote; where, d is the antenna baseline length. As the Equation (3-8) includes the cycle ambiguity integer-term, the slope angle of each asymptote by each cycle ambiguity can be derived as in (4-7), where M is the cycle ambiguity integer satisfying the condition of $|p \pm M\lambda| < d$ which is bounded by the Mosaic concept, λ is the wavelength of carrier signal, and p is defined as in Equation (4-8) satisfying the condition of $-0.5\lambda \le p \le 0.5\lambda$.

$$\tan\psi = \pm\sqrt{\left(\frac{d}{\Delta\phi_{ij}}\right)^2 - 1} \tag{4-6}$$

$$\tan\psi_M = \pm\sqrt{\left(\frac{d}{p \pm M\lambda}\right)^2 - 1} \tag{4-7}$$

$$p \equiv \Delta\phi_{ij} - \lambda \cdot round\left(\frac{\Delta\phi_{ij}}{\lambda}\right) \tag{4-8}$$

The slope angle ψ_M of each candidate of cycle ambiguity integer M can be derived from Equation (4-7) to Equation (4-9) considering its condition.

$$\psi_M = \begin{cases} \arctan\left(\pm\sqrt{\left(\dfrac{d}{p \pm M\lambda} \right)^2 - 1} \right), & if\ (p \pm M\lambda > 0) \\ \pi - \arctan\left(\pm\sqrt{\left(\dfrac{d}{p \pm M\lambda} \right)^2 - 1} \right), & if\ (p \pm M\lambda < 0) \\ \pm\dfrac{\pi}{2}, & if\ (p \pm M\lambda = 0) \end{cases} \quad \text{(4-9)}$$

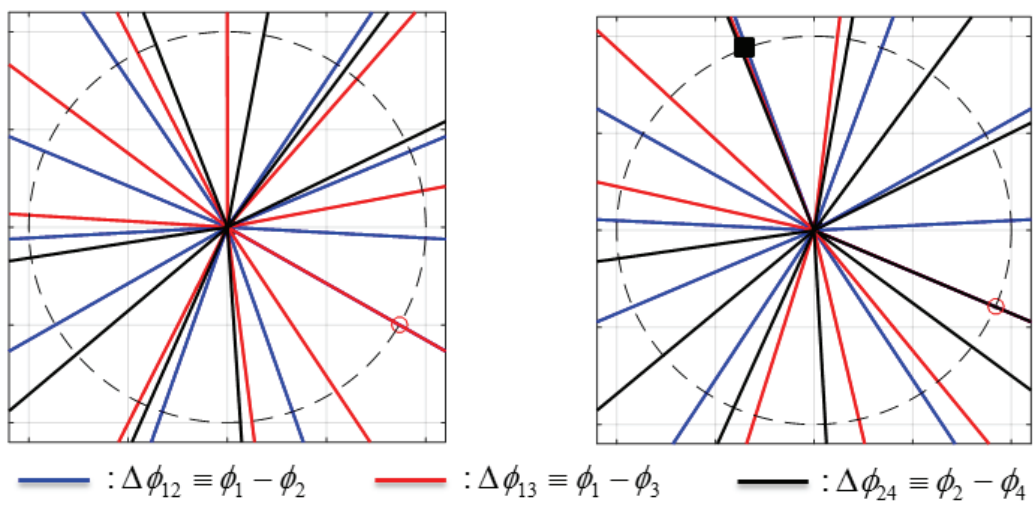

Figure 4-7 All asymptotic lines by cycle ambiguity when four antennas are considered (left: general case, right: existence of hazardous candidate 'black rectangular')

These asymptotic lines can be utilized to search the hazardous false candidates. According to the left of Figure 4-7, the position of true integer (small red circle) overlaps asymptotic lines of all antenna baselines; blue, red and black lines are overlapped but red

and black lines are appeared on the left and the right of Figure 4-7, respectively. Other false candidates have angular gaps representing the residuals of measurements. On the other hand, the hazardous false candidate (black rectangle), on the right of Figure 4-7, has all overlaps or near asymptotic lines, difficult to make a distinction from true cycle ambiguity.

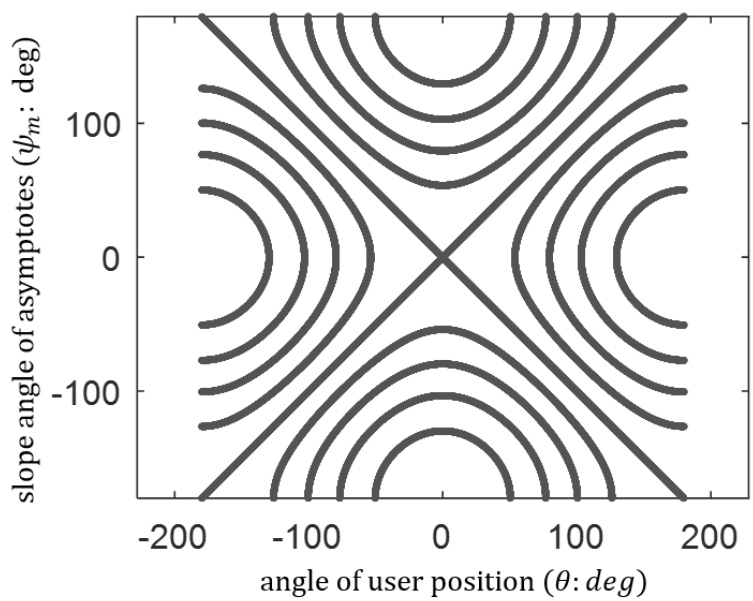

Figure 4-8 Ambiguity Net Image drawn with one antenna baseline

The relation between the asymptotes of single-differenced carrier-phase and the hazardous false candidate all over the AOI can be represented on 2-dimensional image, Ambiguity Net Image. In this image, x-axis represents the angle of user position, and y-axis represents the angle of slope by each cycle ambiguity belong to the angle of user

position. These trajectories have equations using trigonometric functions as Equation (4-10) derived from Equation (4-7), where θ is the angle of user position. The Ambiguity Net Image displayed using Equation (4-10) is as in Figure 4-8 when the antenna baseline is on the x-axis with the slope angle of 0° and its length is about 2.5λ.

$$\cos(\psi_M) - \cos(\theta) = \frac{M}{d}\lambda \tag{4-10}$$

Slope angles of two or more single-differenced carrier-phases can be drawn on the image together. In addition, trajectories of single-differenced carrier-phase have a variation according to the slope angle of antenna baselines, α_k of Figure 4-1, as in Equation (4-11). The Ambiguity Net Image with four pseudolite antennas (three antenna baselines) is described in Figure 4-9.

$$\cos(\psi_M - \alpha_k) - \cos(\theta - \alpha_k) = \frac{M}{d}\lambda \tag{4-11}$$

One Ambiguity Net Image can represent all single-differenced carrier-phase trajectories by each cycle ambiguity using multi-layers of each antenna baseline at a certain antenna formation. And these trajectories represent the continuous changes of the slope angles of asymptotes according to the slope angle of user.

Ambiguity Net Image can be represented as in Equation (4-12) according to the pixel size.

$$ANI^k(u,s) = \begin{cases} 1 & dot\ by\ k\text{-}th\ antenna\ baseline\ at\ pixel\ of\ (u,s) \\ 0 & otherwise \end{cases} \tag{4-12}$$

In Equation (4-12), *ANI* represents *Ambiguity Net Image*, *k* is an index of antenna baseline

and also an index of layer of the image, u is the pixel address on x-axis where $1 \le u \le U$ and $u \in \mathbb{N}$, and s is the pixel address of y-axis where $1 \le s \le S$ and $s \in \mathbb{N}$. S and U are the end of pixel indexes of x-axis and y-axis respectively.

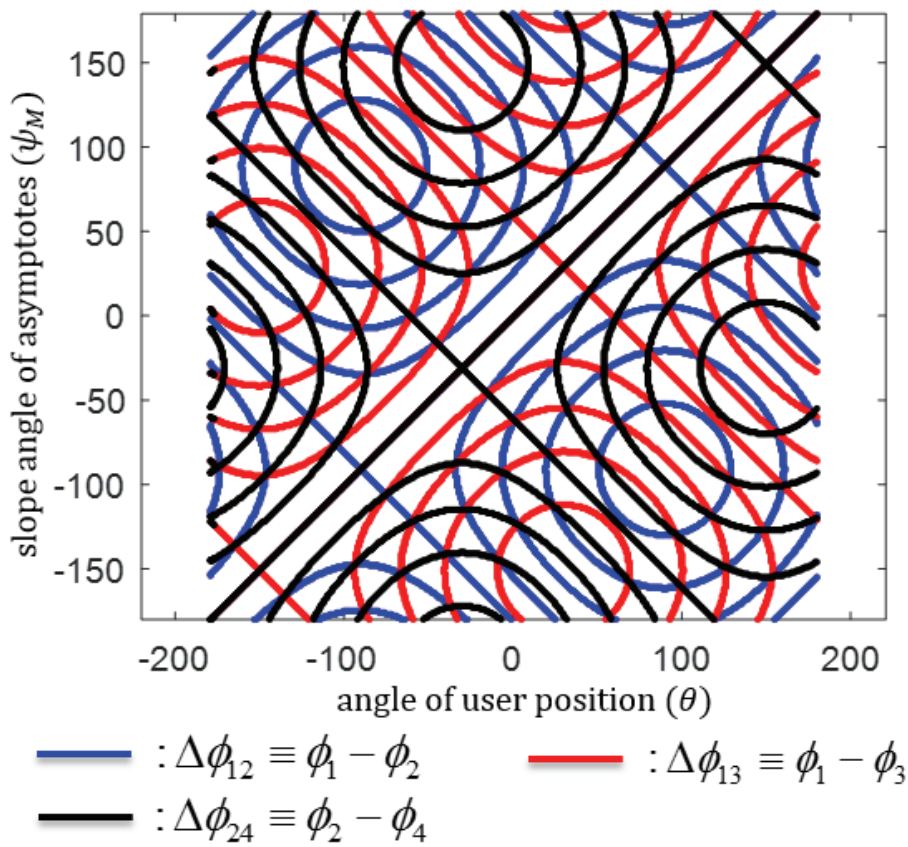

Figure 4-9 Ambiguity Net Image drawn with three antenna baselines (three layers) when α_1 =90°, α_2 =30° and α_3 = -30° from Figure 4-1

For the case of Figure 4-9, there are three layers by three antenna baselines; the blue

curves are dotted on the layer of $ANI^1(u,s)$, and red and black curves are on $ANI^2(u,s)$ and $ANI^3(u,s)$ respectively.

If the pixel step size is 0.2°, the number of pixels on x-axis or y-axis (U or S) is 1800, as each axis has a range from -179.8° to 180°. The total number of pixel at this image is $1800^2 = 3240000$.

Crossing points of all measurements (blue, red and black curves) on the image represents the candidate with residuals of almost zero. The line of '$y=x$' represents the true cycle ambiguity, and the crossing points not on '$y=x$' are hazardous false candidates. Therefore, the total number of crossing points not on '$y=x$' line can be an indicator that a certain antenna arrangement is favorable for easy and fast ambiguity resolution. If the number of crossing points is zero, this antenna formation has no hazardous false candidate, that is to say, all false solution have large magnitude of residuals to be eliminated easy and fast during the ambiguity resolution process.

Counting the crossing points of drawn curves is conducted in pixels of the image domain as in Figure 4-9. A certain criterion is required to distinguish all curves at each layers are crossed or not. In this dissertation, the criterion is applied in the pixel unit on Ambiguity Net Image, but it is derived from the measurement domain.

4.3.2. Pixel Bound Analysis

The assessment of crossing points considers if there are dots on all layers of ANI^k around a certain pixel boundary. If all layers of ANI^k for all k have at least a dot within a certain level of radius around the pixel index of (u, s), then (u, s) is a crossing point. It

makes sense that the criteria, a certain level of radius, is derived from the statistical error levels of measurements. Therefore, the converting process from measurement domain to pixel domain through angular domain is necessary.

The measurement variations make different size of angular variations according to the slope angle originated from the principal axis of hyperbola. From Equation (4-6), Equation (4-13), (4-14) and (4-15) are derived.

$$\psi = \pm \arccos\left(\frac{\Delta\phi_{ij}}{d} \right) \tag{4-13}$$

$$\Delta\phi_{ij} = d \cdot \cos(\psi) \tag{4-14}$$

$$\frac{d(\Delta\phi_{ij})}{d\psi} = -d \cdot \sin(\psi) \tag{4-15}$$

Therefore, if a certain level of measurements bound counting the crossing points is considered, the bound as an angular domain on the Ambiguity Net Image is different according to the slope angle of asymptote. The relation between the measurement variation $\delta\left(\Delta\phi_{ij}\right)$ and angular variation $\delta\psi$ $\left(\equiv \psi_e - \psi_s\right)$ at the slope angle of ψ_s is described in Equation (4-16).

$$\left|\delta\left(\Delta\phi_{ij}\right)\right| = \left| d\int_{\psi_s}^{\psi_e} \left|\sin(\psi)\right| d\psi \right| \tag{4-16}$$

As the pixel size is defined in the angular domain, the bound size in the measurement domain is transferred to the angular domain utilizing Equation (4-16). Accordingly, the angular bound is scaled and ceiled to get the pixel bound using Equation (4-17), where $\delta\gamma$: *pixel step size* .

$$pixel\ bound = ceil\left[\frac{\delta\psi}{\delta\gamma}\right] \tag{4-17}$$

With the antenna baseline length of d = 67.3cm (<2.5λ), the bound of 7.8mm in the measurement domain ($2\sigma_{\Delta\phi}, where\ \ \sigma_{\phi} = 2.8mm$), and the pixel step size of 0.2°, the bound in pixels according to the slope angle of asymptote is described as Figure 4-10 when the principal axis of the antenna baseline is on the x-axis: α_k =0°.

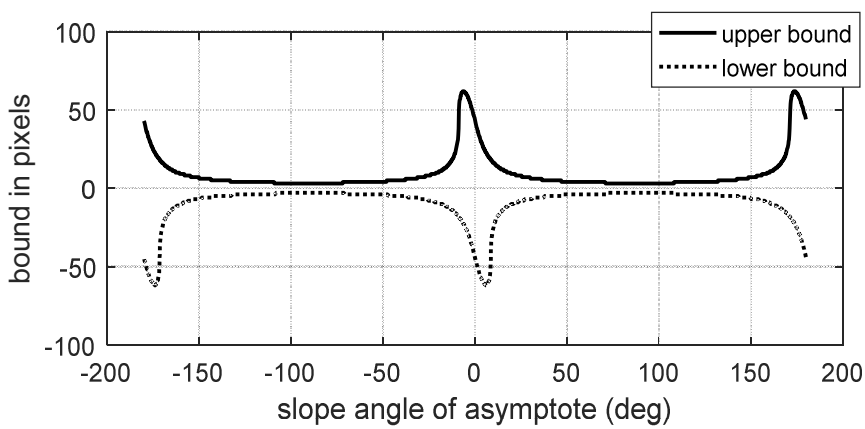

Figure 4-10 Pixel bound according to the slope angle of asymptote

When the slope angle of asymptote is 0°, the bound of 7.8mm in the measurement domain is 44 pixels for both upper and lower bounds in the pixel domain. In addition, ±3 pixel at +90° and -90° of slope angles have same bound size in the measurement domain with 44 pixels at 0°. Upper and lower bounds in Figure 4-10 is asymmetric, because they are calculated each directions; $\psi_e > \psi_s$ for upper and $\psi_e < \psi_s$ for lower bounds by

integrating the absolute value of sine function as in Equation (4-16).

The Upper Pixel Bound (UPB) and the Lower Pixel Bound (LPB) are utilized to find the crossing points on the Ambiguity Net Image, and they are defined as $UPB^k(s)$ and $LPB^k(s)$ according to the slope angle of asymptotes s, where k is an index of the antenna baselines. $UPB^k(s)$ and $LPB^k(s)$ have different values by slope angles of each antenna baseline, α_k from Figure 4-1. $UPB(s)$ and $LPB(s)$ in Figure 4-10 is the case that the slope angle of antenna baseline is zero: $\alpha_k = 0°$. Non-zero α_k makes an offset from $UPB(s)$ and $LPB(s)$ on the x-axis as in Equations (4-18) and (4-19).

$$UPB^k(s) = UPB(s - a_k / \delta\gamma) \tag{4-18}$$

$$LPB^k(s) = LPB(s - a_k / \delta\gamma) \tag{4-19}$$

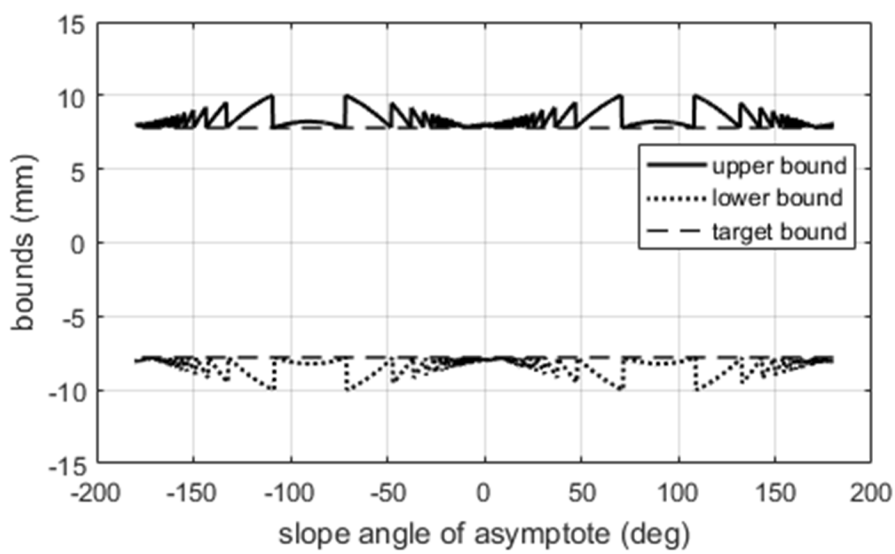

Figure 4-11 Bound residuals caused by the pixel resolution

As the unit of pixel is used for numbering the crossing points, its resolution makes a difference to the actual bound in the measurement unit. The difference caused by the resolution of pixel according to the settings of Figure 4-10 is described in Figure 4-11. Target bounds for upper and lower boundary is 7.8mm, but during the ceil process as in Equation (4-17), actual pixel bound is at least larger than the target bound: solid and dotted lines in Figure 4-11. In addition, the maximum size of residuals is depend on the pixel step size $\delta\gamma$. To minimize the effect by bound residuals, it is recommended to use smaller pixel step size, but the small step size increases the number of total pixels with computational load.

4.3.3. Ambiguity Net Technique

Ambiguity Net Technique considers the number of Crossing Points (CP) as an indicator to cycle ambiguity resolution performance. CP means that there is at least a dot within boundaries of UPB and LPB around a certain pixel for all layer of ANI^k. Boundary Check (BC) represents the existence of at least a dot inside of bounds for the k-th antenna baseline at pixel index of *(u, s)* as described in Equation (4-20), (4-21) and (4-22):

$$BC^k(u,s)=\begin{cases}1 & \textit{if there exists x and y satisfying } ANI^k\left(\{x\}_{u-1}^{u+1},\{y\}_{s-LPB^k(s)}^{s+UPB^k(s)}\right)=1\\ 0 & \textit{otherwise}\end{cases} \tag{4-20}$$

, where

$$\{x\}_{u-1}^{u+1}=\{x:u-1\le x\le u+1\} \tag{4-21}$$

$$\{y\}_{s-LPB^k(s)}^{s+UPB^k(s)} = \{y : s - LPB^k(s) \le y \le s + UPB^k(s)\} \tag{4-22}$$

For the rectangular boundaries of BC whose center is the pixel index of *(u, s)*, UPB and LPB are boundaries for y-axis. In addition, ±1 pixel bounds for x-axis are empirically considered to cover the gap between grid points which are the grids of the angle of user position.

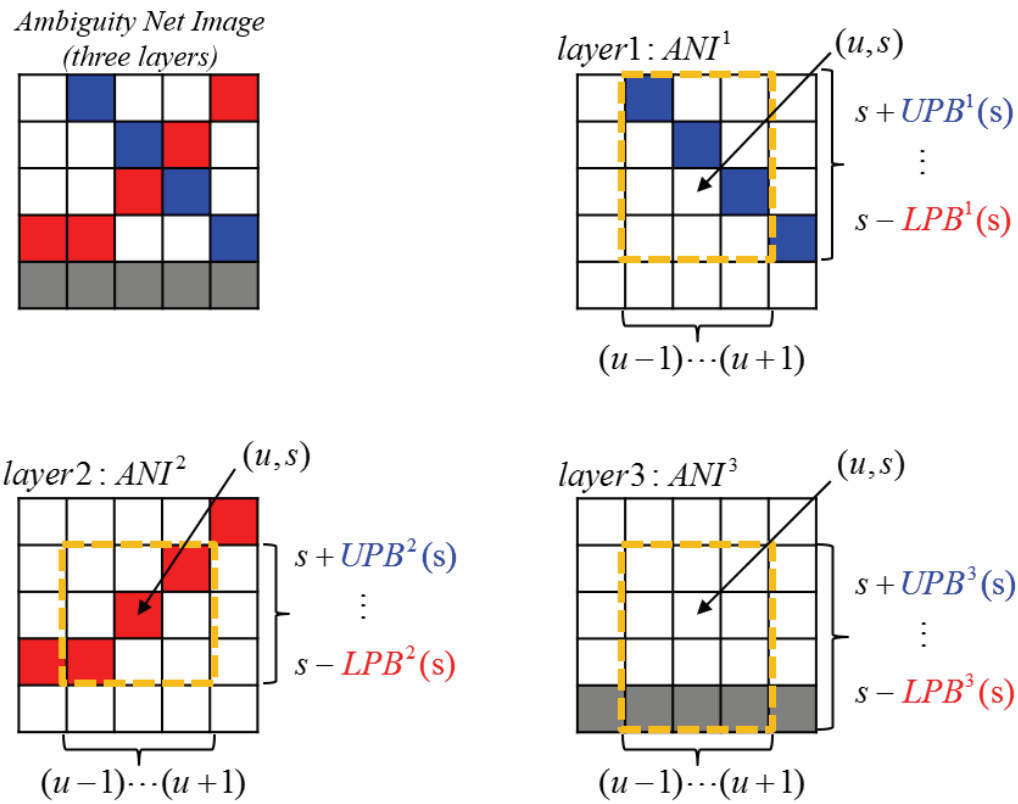

Figure 4-12 Ambiguity Net Image and boundary checks at each layer
(dashed rectangle is the boundary)

An example of simple Ambiguity Net Image and BC^k on each layer of ANI^k with three antenna baselines from four pseudolite antennas are described in Figure 4-12. Figure 4-12 displays $BC^k(u,s)$ on the layer of ANI^k at the pixel index of (u, s), where $k=1,2,3$. $UPB^k(s)$ and $LPB^k(s)$ of Table 6-2 are applied for the example.

Table 4-1 Upper and lower pixel bounds in Figure 4-12

Antenna baseline (k)	$UPB^k(s)$	$LPB^k(s)$
1	2	1
2	1	1
3	1	2

In Figure 4-12, $BC^1(u,s)$, $BC^2(u,s)$, and $BC^3(u,s)$ are all *1*, as at least a dot is inside of the rectangular bound on all layers of ANI^k.

The CP at pixel index of (u, s) is described as in Equation (4-23), where k is the index of antenna baseline and K means the total number of antenna baseline.

$$CP(u,s) \equiv \prod_{k=1}^{K} BC^k(u,s) \tag{4-23}$$

The value of CP is 1 or 0, as BC^k is also defined 1 or 0 and CP is products of BCs. The value of $CP(u,s)$ is 1 when all $BC^k(u,s)$ are 1, where $k=1,2,\cdots,K$. Therefore, $CP(u,s)=1$ means that there is at least a dot within a certain boundaries around the pixel index of (u,s) for all layers of ANI^k. According to Figure 4-12, $CP(u,s)$ is *1*, because all BC^k $(k=1,2,3)$ are *1*.

Equation (4-23) represents the existence of CP at the pixel index of *(u,s)*, and the total number of CP over all pixels of *u* (*u=1,2,⋯,U*) and *s* (*s=1,2,⋯,S*) are divided by the total number of pixels of user angle *U* to represent the Average Number of CP (ANCP) as defined in Equation (4-24). ANCP is a representative indicator for the ambiguity resolution performance to be utilized for the antenna arrangement process.

$$ANCP \equiv \frac{1}{U}\sum_{u=1}^{U}\sum_{s=1}^{S} CP(u,s) \tag{4-24}$$

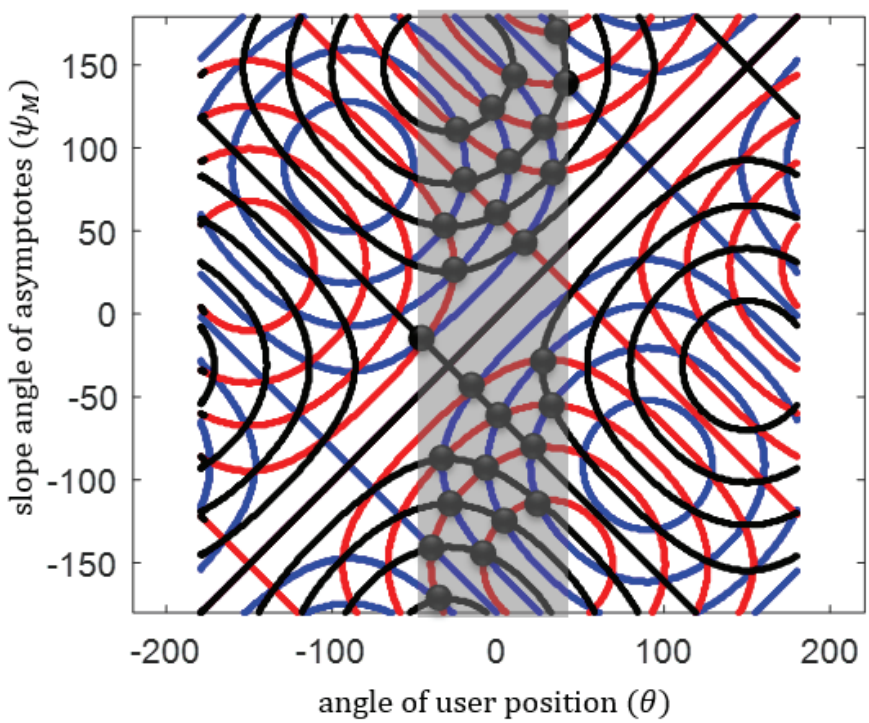

Figure 4-13 Ambiguity Net Image considering AOI of ±60°
(black filled circle: crossing points through all layers)

When AOI of the certain area is considered, counting the crossing points inside the AOI bounds of user angle, x-axis bounds on the Ambiguity Net Image, is enough. An example of the AOI bound of ±60° is displayed in Figure 4-13 as a shadowed area on x-axis bounds of ±60°. In addition, counting the crossing points only in the shadowed area, black filled circles of Figure 4-13, is necessary.

The ANCP considering the AOI can be expressed as in Equation (4-25). The pixel index of the angle of user position, *u,* only within the AOI is considered for the summation of *CP(u,s)*. In addition, U^{AOI} means the number of grid pixels of the user angle inside the AOI.

$$ANCP^{AOI} \equiv \frac{1}{U^{AOI}} \sum_{u}^{AOI} \sum_{s=1}^{S} CP(u,s) \tag{4-25}$$

For the antenna arrangement process, it is required to search the antenna formation with zero-number ANCP for fast and robust cycle ambiguity resolution. Zero-ANCP probabilistically assures the performance of cycle ambiguity. The meaning of zero-ANCP and ANCP>0 are as below:

- Zero-ANCP: all possible false cycle ambiguity candidates have at least one residual of measurements over the pre-defined statistical bound,
- ANCP > 0: more than one of false ambiguity candidates have that all residuals of measurements are within the pre-defined statistical bound.

The bound could be 2σ (<95.4%), 3σ (<99.7%) of errors of measurements, or any required criteria. Therefore, the antenna arrangement with zero-ANCP is the antenna formation that the non-existence of false cycle ambiguity candidate with small residuals is probabilistically ensured. The probabilistic relation between the zero-ANCP and the

chi-square distribution by the square sum of residuals is analyzed in Appendix B.

When pixel bounds of Figure 4-10 and Figure 4-11 are applied in the case of antenna configuration of Figure 4-2 with pixel step size of 0.2°, ANCP with AOI of ±30° and ±60° according to ranges of α_2 of 0°~180° and α_3 of 180°~270° are described in Figure 4-14 and Figure 4-15 respectively. There are sharply increased lines following 90° of α_2, 270° of α_3 and '$\alpha_3 = \alpha_2 + 180°$' lines. The cases of α_2=90° and α_3=270° are because that α_2 and α_3 are aligned to α_1 referring Figure 4-1. The case of '$\alpha_3 = \alpha_2 + 180°$' line is that α_2 and α_3 have aligned direction. Except the area of increased lines, ANCP meshes in Figure 4-14 and Figure 4-15 are not smoothed curves but almost randomly fluctuated.

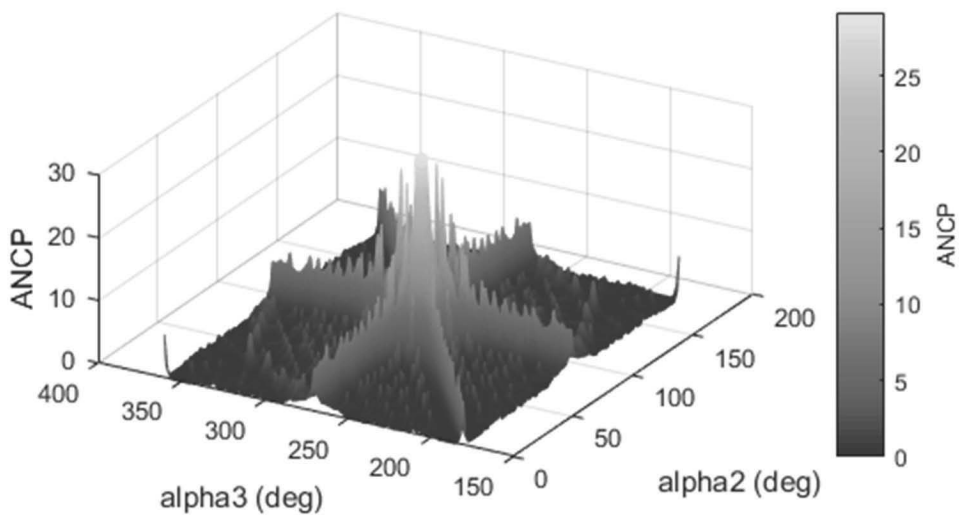

Figure 4-14 Average number of crossing points (AOI of ±30°)

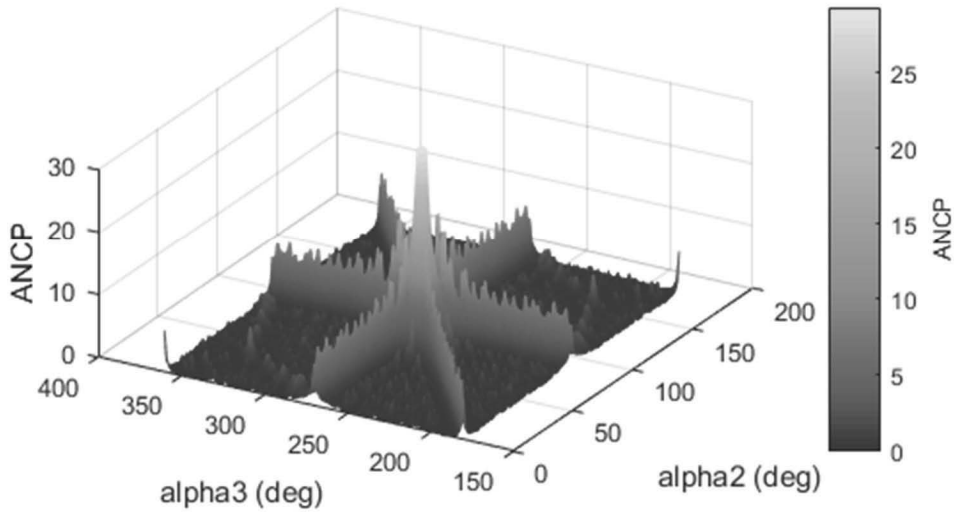

Figure 4-15 Average number of crossing points (AOI of ±60°)

4.3.4. Tendency Simulation

The relation between the ANCP and the ambiguity resolution performance is verified relying on Monte-Carlo simulations. The verification process is performed making a variation of α_2 baseline angle in Figure 4-1, and two baseline angles are fixed: $\alpha_1=90°$ and $\alpha_3=330°$.

Simulation settings are as below: antenna baseline length, *d,* is 67.3cm (<2.5λ), only noise is considered for the error of measurement where σ_ϕ=2.8mm and σ_{DME},=34m, the size of pixel step is 0.5°, the bound for BC in a measurement domain is 7.8mm ($2\sigma_{\Delta\phi}$), AOI is ±180° for all area, and ±1 pixel bounds for x-axis are considered.

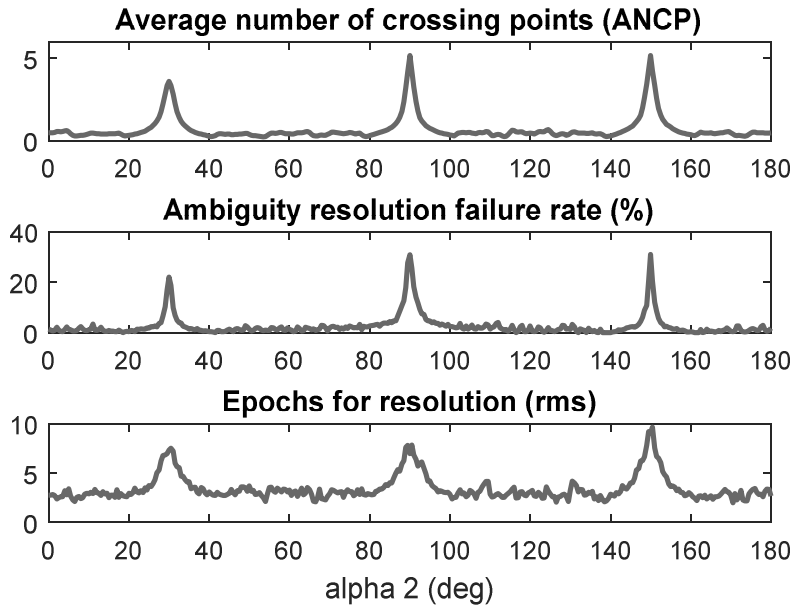

Figure 4-16 Simulation results about the relation between ANCP and the ambiguity resolution performance

Monte-Carlo simulations are conducted 1000 times for each antenna arrangement considering the static user whose positions are randomly distributed on the arc of the radius of 10km. In addition, the 99.9999% of chi-square distribution for residual threshold test and 99% f-distribution for ratio test are applied during the simulations.

The Monte-Carlo simulation results describe the correlated tendency between the ANCP and the performance of ambiguity resolution as in Figure 4-16. The failure rate of ambiguity resolution is the rate of cases that the cycle ambiguity is not solved within 30 epochs. In addition, root mean squares of the number of required epochs for ambiguity resolutions are also compared with ANCP.

4.4 Antenna Arrangement considering Positioning Accuracy and Cycle Ambiguity Resolution Performance

4.4.1. Antenna Arrangement Method

Two aspects for antenna arrangement, the positioning accuracy and the cycle ambiguity resolution performance, are described in previous sections. Accordingly, the antenna arrangement method considering both terms is needed to be derived. The antenna arrangement process described in this section is to find the optimized antenna formation which has a minimum DOP with zero-ANCP when the number of antennas and baseline lengths are fixed. The general strategy to search the antenna arrangement even considering the number of pseudolite antennas and the length of antenna baselines will be described in Chapter 5.

The first step is to find the antenna arrangement to satisfy the Equation (4-5). This is a general optimization problem. Hence, the Genetic Algorithm (GA) is utilized to solve this, as GA has been widely applied for the optimization problem of antenna arrangements [52-58]. Genetic Algorithm in MATLAB Toolbox is utilized for the optimization process. Consequently, the number of crossing points using Ambiguity Net Technique at this antenna formation is surveyed. When ANCP is zero, then the antenna formation is an optimized solution. If it is not, calculate the DOP values of neighbor antenna formation and makes a list of antenna arrangement with its DOP value. In the list, select the antenna arrangement with the best DOP, and calculate the ANCP. If it is not zero, calculate the DOP of neighbor grids of antenna arrangement, and add these results to the list. This process is performed repeatedly until zero-ANCP is found. Accordingly, the searched antenna arrangement has the best DOP with zero-ANCP.

This antenna arrangement approach is one of method to find the definite solution which has the minimum DOP with zero-ANCP, but it takes time until the zero-ANCP is found, because the ANCP is not considered at all for the grid search during optimization process. The search method considering the ANCP will be described in Chapter 5.

There are two grids for the antenna arrangement process. One is for Ambiguity Net Technique: the pixel grid. The other is the grid for the search of antenna formation formed by α_2 and α_3 as in Figure 4-17. It is recommended to have the same step size between two grids to minimize the loss by resolution gap.

The antenna arrangement process is performed in two cases of AOI ±30° and ±60°. The settings for process are as below; range from station to user is 10 km, baseline length between antennas is 67.3cm (<2.5λ), only noise is considered for the error of measurement (σ_ϕ=2.8mm and σ_{DME},=34m), the pixel step size is 0.2°, the bound for BC is 7.8mm ($2\sigma_{\Delta\phi}$), and ±1 pixel bounds for x-axis is considered. In addition, only α_2 and α_3 are considered for the antenna arrangement where α_1 is fixed at 90° as in Figure 4-1.

The results of antenna arrangement processes are in Figure 4-17 and Figure 4-18 for AOI of ±30° and ±60° respectively. Contours in two figures represent ANDOP levels, and red areas are zero-ANCP. Grey area means the calculated points until the zero-ANCP is appeared. Aa black doughnut is the start point of the antenna arrangement process, and a yellow doughnut is the end point: the searched antenna formation.

Monte-Carlo simulations are conducted to verify the performance of the searched antenna formation. The settings for simulations are same as described in the section 4.3.4. Table 4-2 describes the performance of cycle ambiguity resolution of the searched antenna arrangements.

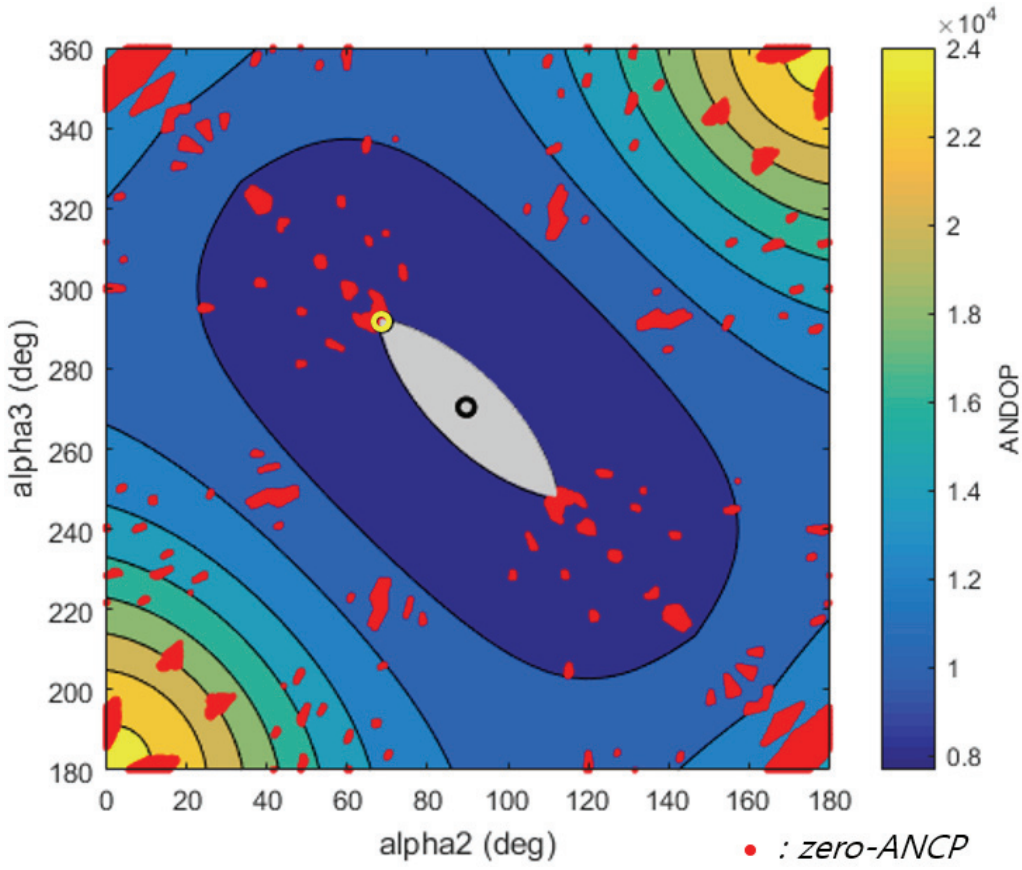

Figure 4-17 Search process using optimization method when AOI is ±30°

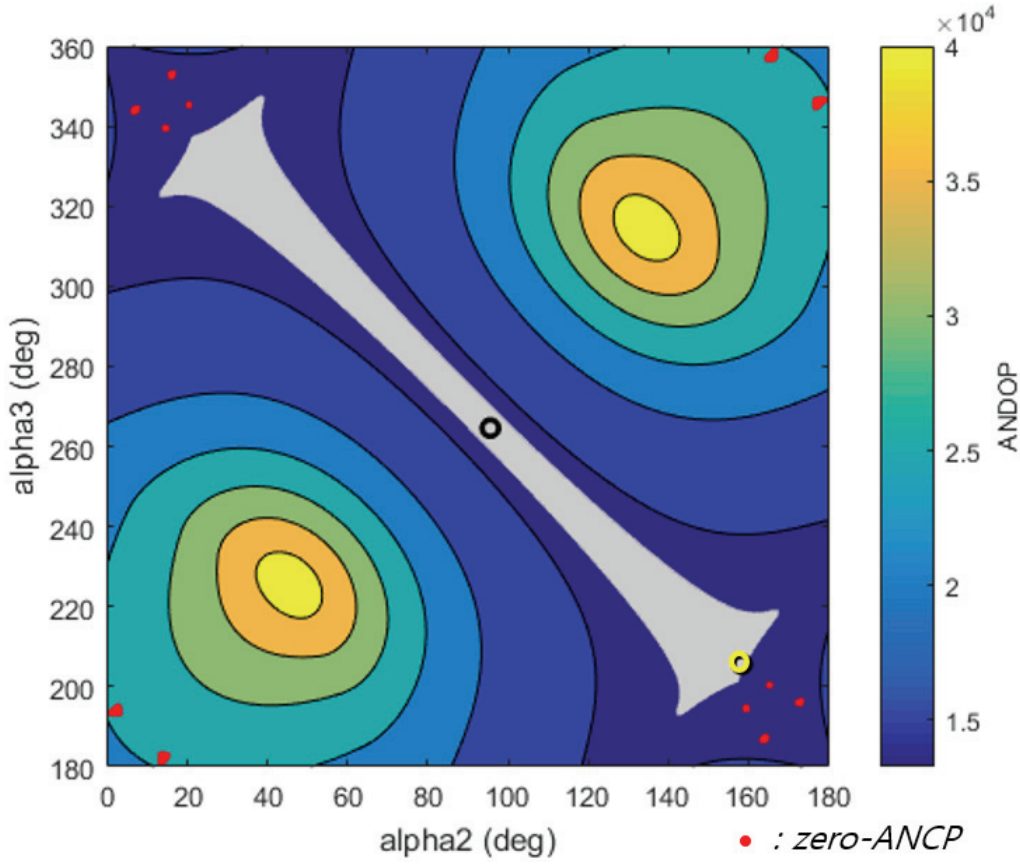

Figure 4-18 Search process using optimization method when AOI is ±60°

Table 4-2 Ambiguity resolution performance of searched antenna arrangement

Case	AOI	α_1	α_2	α_3	Success rate	Epochs for resolution (rms)
1	±30°	90°	68.8°	291.6°	100 %	2.41
2	±60°	90°	158.4°	205.6°	100 %	1.48

The meaning of success rate is the rate that cycle ambiguity is solved within 30 epochs. The results in Table 4-2 describes that the searched antenna arrangements have 100% success rate of ambiguity resolution within a few epochs.

4.4.2. Robust Antenna Arrangement to Antenna Position Error

Antenna position error, such as an unexpected displacement, can cause the degradation of ambiguity resolution performance. To address this issue, it is recommended to select the antenna formation on the center of the zero-ANCP area which is the red area in Figure 4-17 and Figure 4-18.

In case of Figure 4-17, the antenna arrangements of the red area including a yellow doughnut are good for both DOP and ambiguity resolution. The zero-ANCP area is displayed together with ANCP contours in Figure 4-19.

The zero-ANCP area with good DOP value is indicated by a white-rectangle in Figure 4-19. The size of white-rectangle is 62° ~ 69.8° for α_2 and 289.8° ~ 299° for α_3. If the antenna arrangement of $(\alpha_2, \alpha_3) = (67.4°, 292.4°)$ is selected, the cycle ambiguity resolution performance can endure a few degrees of antenna arrangement errors. It still probabilistically ensures the cycle ambiguity resolution performance as long as it is zero-ANCP.

The ambiguity resolution performance of four cases of antenna arrangement near the white-rectangle in Figure 4-19 are compared conducting Monte-Carlo simulations of 1000 samples. Each cases are described in Figure 4-20. Case 1 and 2 are the antenna arrangements with zero-ANCP, but only case 1 is robust to antenna position error because

the case 2 is near the boundary of zero-ANCP area. Case 3 is the antenna arrangement with non-zero ANCP but low ANCP, and case 4 has a high ANCP value.

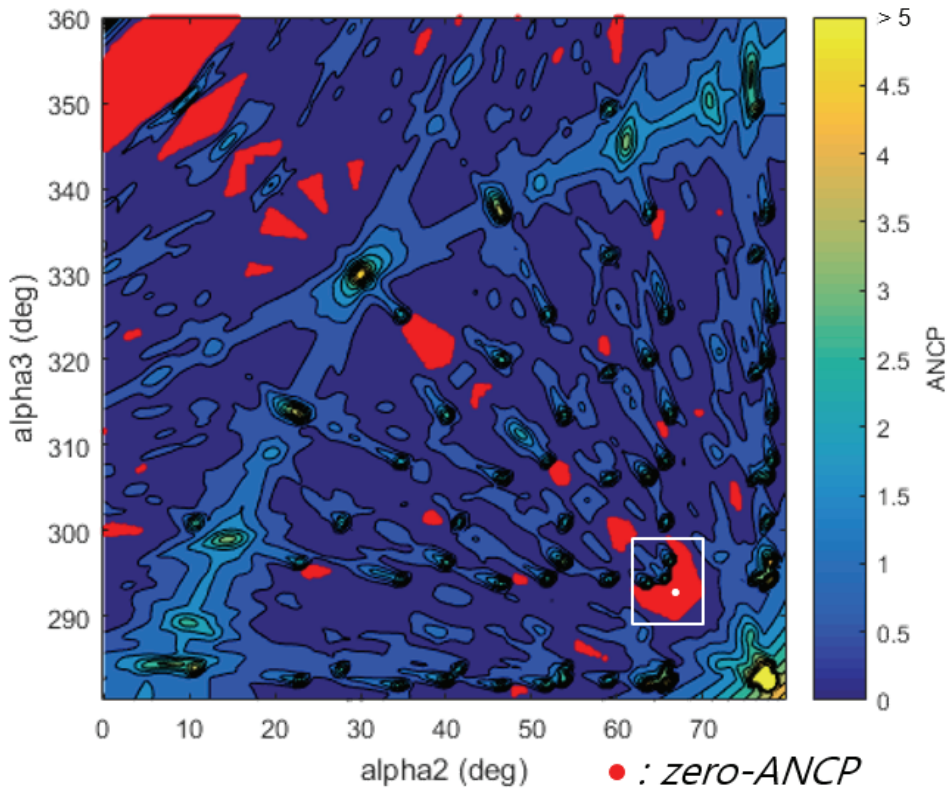

Figure 4-19 ANCP contours according to α_2 and α_3

Same simulation settings are applied for Figure 4-17. Simulation results are described in Table 4-3.

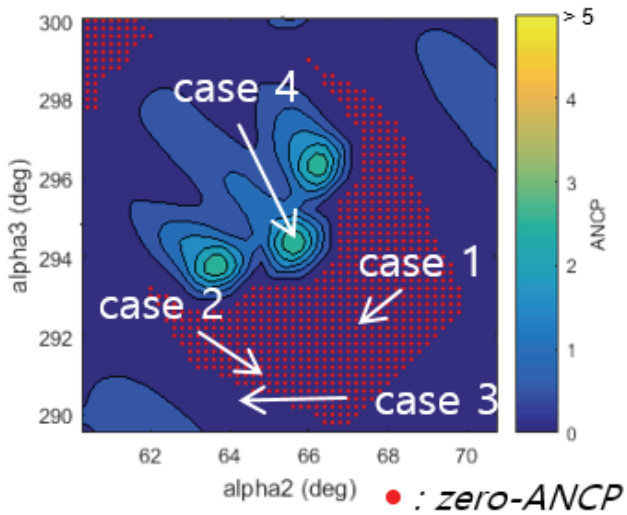

Figure 4-20 Enlarged ANCP contours around white-rectangle of Figure 4-19

Table 4-3 Ambiguity resolution performance of four cases of Figure 4-20

Case	α_1	α_2	α_3	ANCP	Success rate	Epochs for resolution (rms)
1	90°	67.4°	292.4°	0	100 %	2.01
2	90°	64.8°	290.6°	0	100 %	2.01
3	90°	64.4°	290.2°	0.05	100 %	2.21
4	90°	65.6°	294.4°	3.01	82.5%	7.93

Case 2 and 3 with zero-ANCP have similar ambiguity resolution performance with the success rate of 100% and around 2 epochs for the ambiguity resolution. With the increase of ANCP, the ambiguity resolution performance is decreased. Required epochs for the resolution of case 3 is slightly larger than case 1 and 2 with non-zero but low ANCP.

However, case 4 with high ANCP value has very poor performance even the success rate is not 100%.

In this situation, the antenna arrangement of case 1 is the solution with zero-ANCP with good DOP and robustness to the antenna position error.

Unlike the influence of ambiguity resolution performance by antenna displacement, the antenna position error directly affects the positioning accuracy. The influence of positioning accuracy by antenna displacement error is analyzed in [23].

4.4.3. Bound Size Analysis for Ambiguity Net Technique

The bound size of Ambiguity Net Technique applied for Figure 4-17, Figure 4-19 and Figure 4-20 is 7.8mm ($2\sigma_{\Delta\phi}$) of 95.4% in the measurement domain. If the bound size is extended from $2\sigma_{\Delta\phi}$ to $3\sigma_{\Delta\phi}$ of 99.7%, ANCP contours around white-rectangle of Figure 4-20 is as in Figure 4-21.

The area of zero-ANCP is decreased compared to the Figure 4-20, but the zero-ANCP in Figure 4-21 ensures the ambiguity resolution performance more tightly compared to the cases of Figure 4-20 relying on higher statistical bound.

Monte-Carlo simulations are conducted to compare the ambiguity performance with case 1 and case 5 in Figure 4-21. Case 1 is the same antenna arrangement of zero-ANCP in Figure 4-20 with $2\sigma_{\Delta\phi}$ bound, and case 5 is a new antenna arrangement with zero-ANCP with $3\sigma_{\Delta\phi}$ bound.

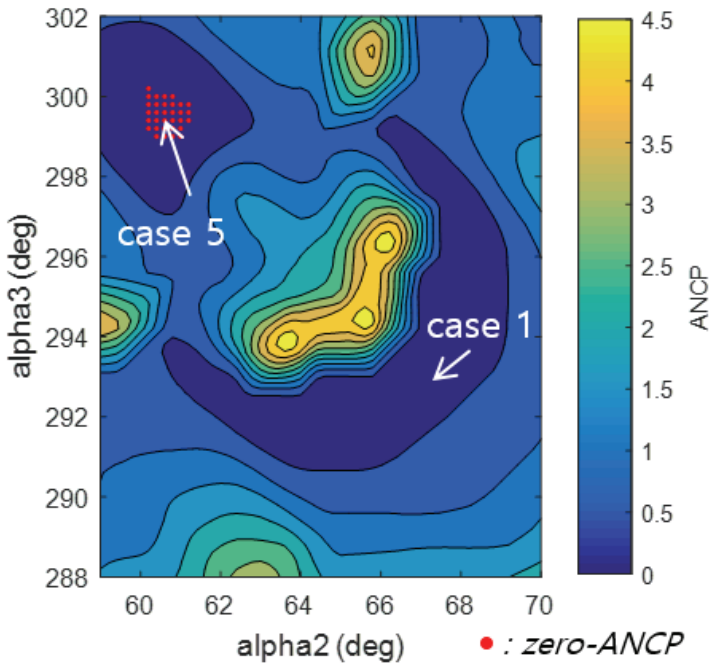

Figure 4-21 ANCP contour around white-rectangle of Figure 4-19 with $3\sigma_{\Delta\phi}$ bound

Simulation settings are same with Table 4-3 except that different bound sizes for Ambiguity Net Technique are applied for case 1 and 5. The simulation results are described in Table 4-4.

Table 4-4 Ambiguity resolution performance for case 1 and 5 of Figure 4-21

Case	α_1	α_2	α_3	ANCP	Success rate	ANDOP	Epochs for resolution (rms)
1	90°	67.4°	292.4°	0 ($2\sigma_{\Delta\phi}$)	100 %	7998	2.01
5	90°	60.6°	299.6°	0 ($3\sigma_{\Delta\phi}$)	100 %	8240	1.14

Both cases have zero-ANCP with success rate of 100%, but the required epochs for ambiguity resolution of case 5 is less than the epochs of case 1, considering that higher bound for zero-ANCP is applied for the case 5.

To find the antenna formation focusing on ambiguity resolution performance, it is an efficient approach to fine the zero-ANCP starting with a small bound and increasing the bound size gradually, i.e. from $2\sigma_{\Delta\phi}$ to $3\sigma_{\Delta\phi}$.

In the aspect of DOP, however, case 1 is better than case 5 as described in Figure 4-3, Figure 4-17 and Table 4-4. In addition, case 1 has a better robustness to the antenna position error, because the adjacent zero-ANCP area of case 1 is wide compared to the area of case 5 referring Figure 4-19.

In this situation, the cycle ambiguity performance is in a trade-off relationship with DOP and robustness to antenna position error. Therefore, the selection of antenna arrangement between case 1 and 5 is made according to which features are important for the system operation.

Chapter 5. Strategy of Multi-Antenna Arrangement

5.1 Strategy Background

For a strategy of multi-antenna arrangement, two factors of the positioning accuracy and the cycle ambiguity resolution performance are considered. In terms of the positioning accuracy, the performance index of DOP is the main concern. To derive the strategy for the ambiguity resolution, some special features are needed to be examined.

There are common facts for favorable integer ambiguity resolution;

- False candidates with large residuals make the cycle ambiguity resolution fast
- Small number of ambiguity candidates can contribute to the quick ambiguity resolution
- Large number of measurements makes easy cycle ambiguity resolution
- Quick change of relative position between station and user is favorable for the ambiguity resolution.

The first description is utilized for the Ambiguity Net Technique. The second means that short antenna baselines are good for ambiguity resolution with small number of ambiguity candidates referring to the Mosaic concept as in Equation (3-7). However, shoat antenna baselines make poor DOP in terms of the positioning accuracy. Hence, proper antenna baseline lengths should be considered during the antenna arrangement process. In the third description, a large number of measurements is good for both positioning accuracy and ambiguity resolution performance. The last description means

high-speed users are favorable for cycle ambiguity resolution. This feature is utilized for verification process of the antenna arrangement that the ambiguity resolution performances of static users, in adverse conditions, are mainly investigated.

There are assumptions to work out the strategy;

- All antenna baseline lengths are equal to apply the Mosaic concept equally
- The distance from station to user is far enough to abbreviate the effects caused by two terms: 1) it is assumed that the centers of all antenna baseline are on the center of coordinate system. 2) the direction to user on hyperbolic curve is simplified as its asymptotic line
- Small number of pseudolite antennas makes the system configuration simple.

This chapter only includes the results that all antenna baseline lengths are equal. The results and their analyses from non-equal antenna baselines are remained for future works. As the main application of this dissertation is an air-transport, the distance from station to user is generally far at least a few kilometers (or nautical miles). Hence, the second assumption is reasonable, and the analysis about the assumption 2) is described in Appendix A. The third description includes the term of cost-effectiveness to minimize the number of pseudolites.

A strategy for the antenna arrangement meeting the requirement is based on above descriptions. The most solid strategy finding an optimized solution is to calculate all possible antenna arrangements and to find the formation with zero-ANCP and best DOP. However, if the number of pseudolite antenna is large, a computational load cannot be disregarded, because the increase of the number of antenna increases the calculating load exponentially.

The strategy considering the computation load is described in this chapter. Some values are needed to set for the strategy:

- Performance index for the positioning accuracy: ANDOP, Horizontal DOP or Position DOP, etc.
- Accuracy requirement: APNT requirement or other requirements
- Settings for the Ambiguity Net Technique : grid step size, measurement bound for Average Number of Crossing Points (ANCP)
- Area of Interest (AOI)

If other constraints, such as the maximum number of pseudolite antennas or the maximum baseline length between antennas, are existed, they are needed to be considered for the strategy properly.

5.2 Antenna Arrangement Strategy

The purpose of an antenna arrangement strategy in this chapter is to find the antenna arrangement guaranteeing the ambiguity resolution performance, meeting the accuracy requirement and minimizing the number of pseudolite antennas. The strategy should satisfy two requirements, the positioning accuracy and the ambiguity resolution performance. Methods to search the optimized antenna arrangements for each aspect are described in sections of 4.2 and 4.3 separately. However, the strategy in this chapter should not only consider these two terms simultaneously but to provide results fast and efficiently.

Two strategies are presented as in Figure 5-1 and Figure 5-2. There are common factors

between them. An outermost loop is to increase the number of pseudolite antennas, considering that the increment of the system complexity remains to the last. An initial antenna arrangement, only optimized for the positioning accuracy in the AOI, is calculated relying on Genetic Algorithm-based process. If the accuracy of the initial antenna formation ($\bar{\alpha}_{int}$) or $\bar{\alpha}_i$ during the process is insufficient, the strategy increases the length of antenna baselines for better DOP. Subsequently, the process is conducted until the antenna arrangement with zero-ANCP meeting the positioning accuracy is searched.

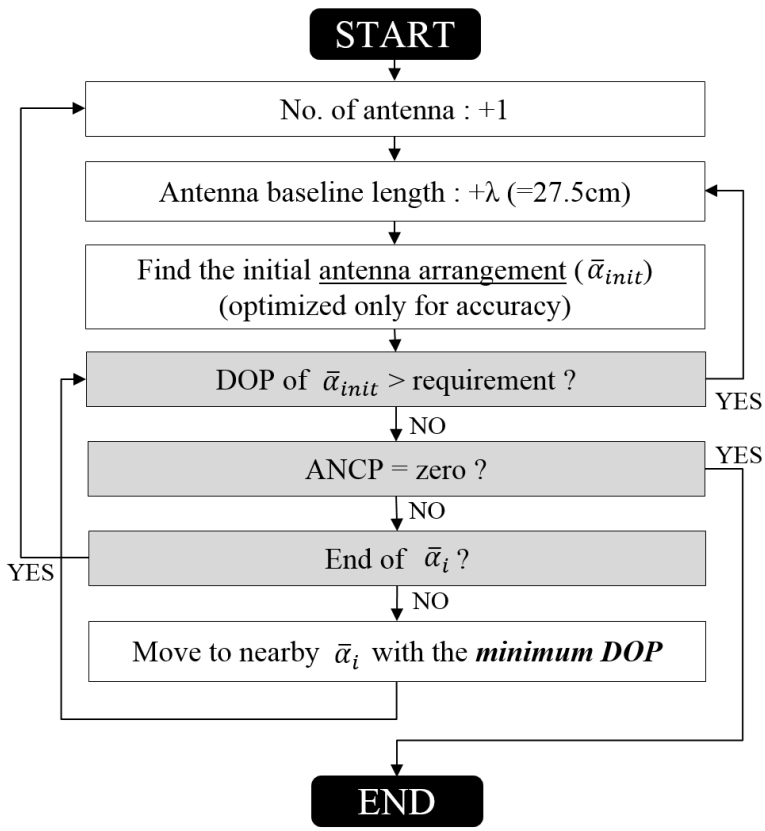

Figure 5-1 Antenna arrangement strategy (method A)

The antenna arrangement process is conducted based on grid searches of the angles of antenna arrangement $\bar{\alpha}_i$ where i is an index of the gird point of antenna arrangement with a grid step size $\delta\gamma$. In addition, an antenna arrangement table is utilized to add and remove of grid points during the search process.

There are two options when one grid point of antenna arrangement is moved to next one. In method A of Figure 5-1, the performance index of positioning accuracy in an aspect of DOP is the main concern to find the optimal solution.

After the assessment of ANCP at $\bar{\alpha}_i$, if ANCP is not zero, the index of this antenna arrangement is removed in the table. In addition, DOP values around $\bar{\alpha}_i$, a set of $\{DOP(\bar{\alpha}_i)\}_{\pm\delta\gamma}$ as in Equation (5-1), are surveyed, and elements in $\{DOP(\bar{\alpha}_i)\}_{\pm\delta\gamma}$ which are not on the antenna arrangement table are added to the list of the table.

$$\begin{aligned}\left\{DOP\left(\bar{\alpha}_i\right)\right\}_{\pm\delta\gamma} \equiv \Big\{ & DOP\left(\alpha_{i,1}+\delta\gamma,\alpha_{i,2},\cdots,\alpha_{i,k}\right), DOP\left(\alpha_{i,1}-\delta\gamma,\alpha_{i,2},\cdots,\alpha_{i,k}\right), \\ & DOP\left(\alpha_{i,1},\alpha_{i,2}+\delta\gamma,\cdots,\alpha_{i,k}\right), DOP\left(\alpha_{i,1},\alpha_{i,2}-\delta\gamma,\cdots,\alpha_{i,k}\right), \\ & \cdots, DOP\left(\alpha_{i,1},\alpha_{i,2},\cdots,\alpha_{i,k}+\delta\gamma\right), DOP\left(\alpha_{i,1},\alpha_{i,2},\cdots,\alpha_{i,k}-\delta\gamma\right)\Big\}\end{aligned} \tag{5-1}$$

A grid point with the lowest DOP in the table is selected as a next antenna arrangement grid, and this process is repeated until the antenna formation with zero-ANCP is appeared. If there is no $\bar{\alpha}_i$ with zero-ANCP, the number of pseudolite antenna is increased, and the antenna arrangement process performs again with the initial value of antenna baseline length.

The results and analyses in a section of 4.4 are conducted based on this method. This method can provide the antenna formation with the minimum DOP and zero-ANCP. However, it needs to assess a huge amount of antenna arrangement grid points, because

only DOP values are considered for the search process.

One of the requirements of the strategy in this chapter is efficiency, i.e. a computational time. Hence, a method B which is relatively fast is described in Figure 5-2. In method B, only ANCP is considered to find the next antenna arrangement decreasing the number of crossing points. An antenna arrangement table is also utilized for method B, but $\{ANCP(\bar{\alpha}_i)\}_{\pm\delta\gamma}$ is applied instead of $\{DOP(\bar{\alpha}_i)\}_{\pm\delta\gamma}$.

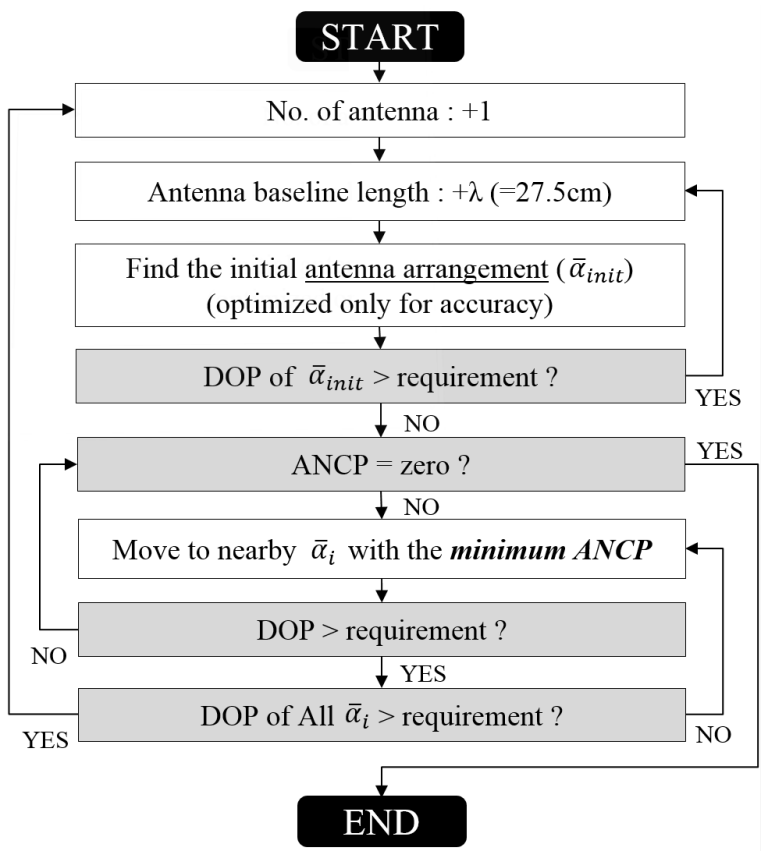

Figure 5-2 Antenna arrangement strategy (method B)

In the aspect of the positioning accuracy, the method B only assess whether or not the required performance is satisfied. If the accuracy of a certain antenna arrangement does not satisfy the requirement, the next grid point, which has the minimum ANCP values on the table list, is selected for a next assessment. In addition, the strategy increases the number of antenna when DOPs of all remained antenna arrangements in the table are not meet DOP requirement.

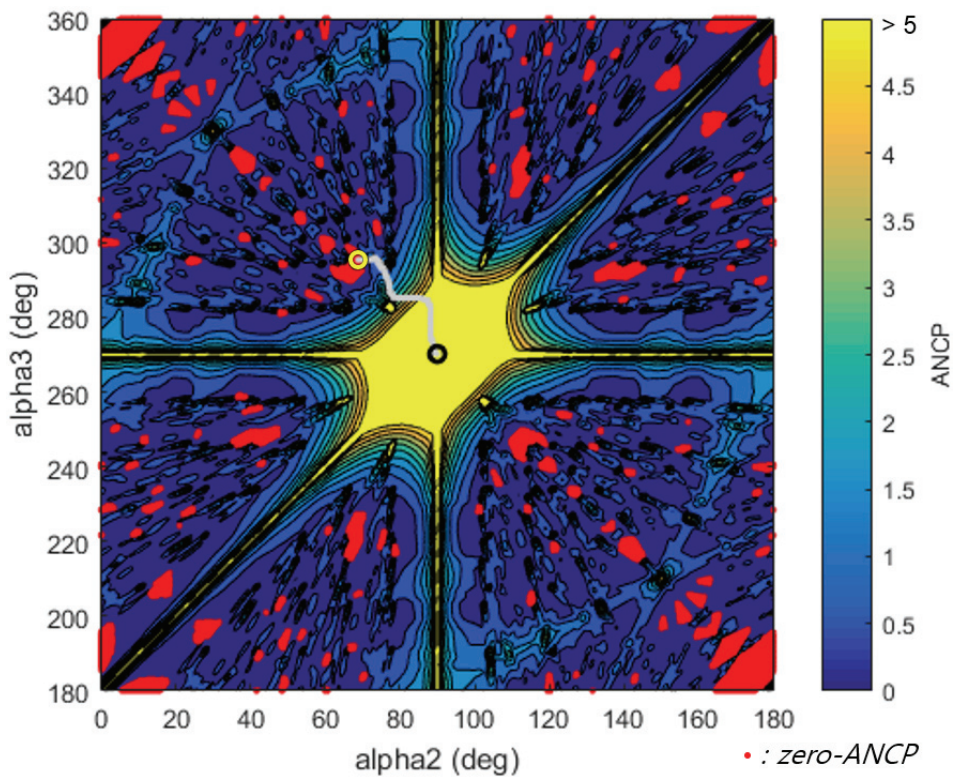

Figure 5-3 Method B-based searching process when AOI is ±30° (contours: ANCP)

The search process of method B, minimizing ANCP values, is described in Figure 5-3. Simulation settings of Figure 5-3 are same with Figure 4-17 except the kinds of search processes. A black doughnut is the start point of the antenna arrangement process, and a yellow doughnut is the end point. A grey trajectory presents the calculated grid points until zero-ANCP is appeared.

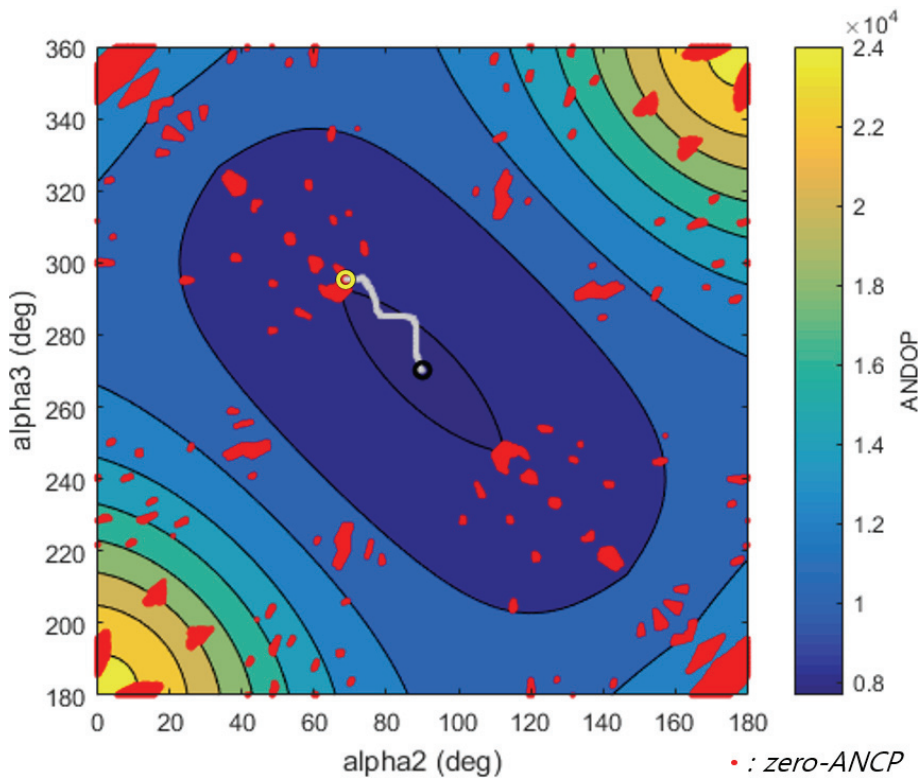

Figure 5-4 Method B-based searching process when AOI is ±30° (contours: ANDOP)

The computational loads of methods A and B can be compared using Figure 4-17 and

Figure 5-4. Figure 5-4 depicts the search process of Figure 5-3 with DOP contours. As the number of grey points, or grey area, represents the assessed grid points of antenna arrangements until the solution is searched, it is definite that method B-based search process of Figure 5-4 is much efficient.

In the aspect of the positioning accuracy, method A finds the optimal solution which is a yellow doughnut of Figure 4-17 with minimum DOP and zero-ANCP. In Figure 5-4, a DOP value at a yellow doughnut is slightly larger than the value of Figure 4-17.

The result of method B is a sub-optimal even though it has zero-ANCP meeting the positioning requirement, as the antenna arrangement which has a better DOP with zero-ANCP is still exists. In this chapter, however, the method B is mainly concerned relying on computating time.

5.3 Simulation Results for 2-D environment

Simulations to verify the strategy of the antenna arrangement considering the APNT accuracy requirement is conducted in this section. The strategy of method B is considered to get the results.

The performance index for positioning accuracy is Weighted Horizontal DOP (WHDOP) as defined in Equation (3-21), given that APNT has a requirement of horizontal positioning accuracy. When flight detector of flight technical error is considered, the required positioning accuracy in Airspace Class B is 307.1m (95%) as in Table 2-1. During the measurement generation processes for the simulations in this section, only

noise is considered as an error source. Hence, the performance index, the worst WHDOP in AOI, should be smaller than a half of 307.1 (≈153.6).

Simulation settings are as below: only noise is considered for the error of measurement (σ_{ϕ} =2.8mm, σ_{DME} =34 m), pixel step size is 0.2° and the grid step size to find the angle of antenna baseline is also 0.2°. For the Ambiguity Net Technique, a bound in a measurement domain is 7.8mm ($2\sigma_{\Delta\phi}$), and ±1 pixel bounds for x-axis are considered. The length of antenna baseline is smaller than a certain integer M and p $(0 \leq p < 0.5)$ as in Equation (3-4). p of 0.44 is applied considering the error size of $4\sigma_{\Delta\phi}$. Hence, the antenna baseline lengths are 0.44λ, 1.44λ, 2.44λ, ··· according to the integer M.

The strategy searches solutions considering three AOI: ±30°, ±60° and ±180° (all area). The solutions are compared with other antenna arrangements, such as regular polygon formation (square or pentagon) and the antenna arrangements only optimized for the positioning accuracy.

Monte-Carlo Simulations are conducted 1000 samples for each antenna arrangement considering the static user whose positions are randomly distributed on the arc of AOI with the radius of 55.56km (30nmi), the boundary of Mode C-veil of Airspace Class B. In addition, 99.9999% of chi-square distribution for residual threshold test and 99% f-distribution for ratio test are applied for the ambiguity resolution processes.

5.3.1. AOI: ±30° bound

The process searching the antenna arrangement meeting the APNT accuracy requirement with zero-ANCP has been performed in AOI of ±30°. Steps following the strategy of

method B is described in Table 5-1.

Table 5-1 Strategy process for the AOI of ±30°

Ant. No.	Ant. baseline length	WHDOP	Notes
4	1.44λ	201.7	(Optimized only for positioning accuracy) insufficient accuracy (WHDOP > 153.6)
4	2.44λ	122.3	(Optimized only for positioning accuracy) ANCP : 112.4
: (search process using method B) :			
4	2.44λ	149.8	ANCP : 0

The first step is to find the antenna arrangement optimized only for the positioning accuracy using genetic algorithm with four antenna and the baseline of 1.44λ. However, the WHDOP at the worst location is not sufficient for the required accuracy. Hence, the antenna baseline is extended to 2.44λ which satisfies the requirements. Subsequently, search process using method B is conducted until the antenna arrangement which has zero-ANCP satisfying the APNT requirement is found.

The antenna arrangement searched by the strategy is compared with other cases: square formation and the arrangement optimized only for the positioning accuracy. The slope angles of baselines to be compared are as in Table 5-2. These antenna arrangements have a form of Figure 5-5 base on Figure 4-1. Case 1 has the worst WHDOP in the AOI and case 2 has the best WHDOP.

Table 5-2 Cases of antenna arrangements to be compared (AOI of ±30°)

Case	α_1	α_2	α_3	WHDOP	Notes
1	90°	180°	180°	229.9	regular polygon (square)
2	90°	90°	270°	122.3	optimized only for positioning accuracy
3	81.2°	103.4°	312°	149.8	the result by strategy

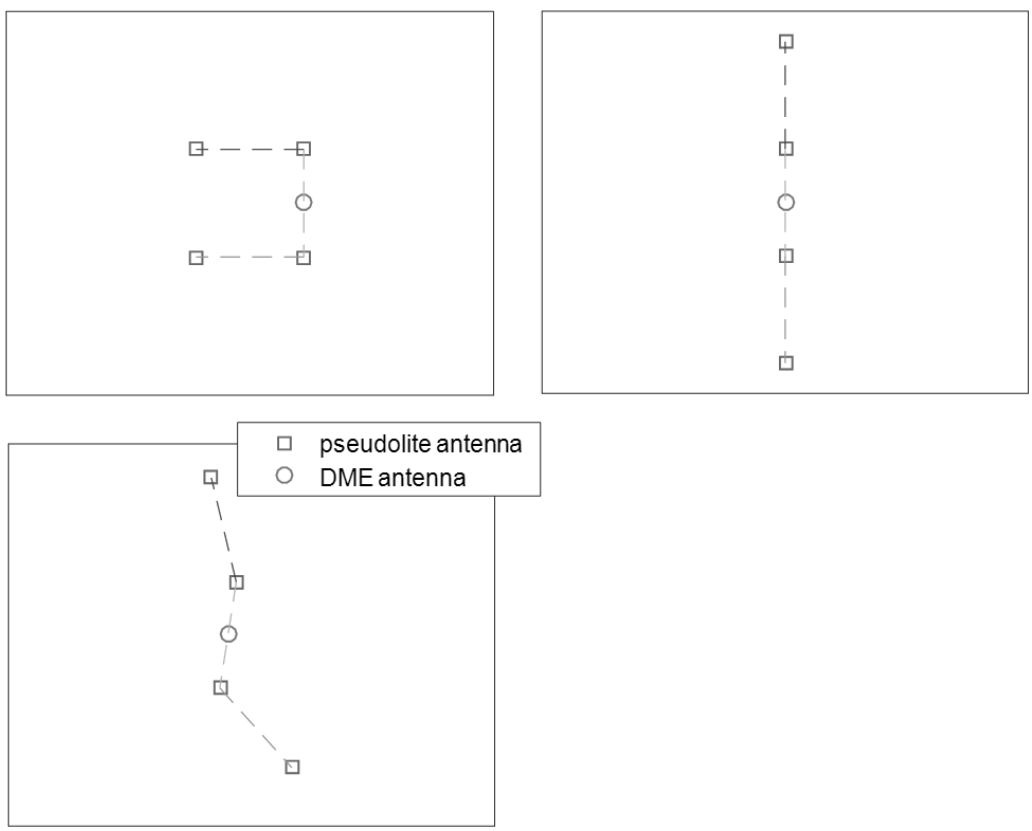

Figure 5-5 Antenna arrangement cases for AOI of ±30°
(top-left: case 1, top-right: case 2, bottom-left: case 3)

Monte-Carlo simulations are conducted to compare the cycle ambiguity resolution performance, and the results are described in Table 5-3. The success rate is defined as that the cycle ambiguity is resolved within 30 epochs. Epochs for resolution means the root-mean-square value of the required number of epochs among the cases that the cycle ambiguities are successfully solved.

Table 5-3 Monte-Carlo results of ambiguity resolution (AOI of ±30°)

Case	Success rate	Epochs for resolution (rms)	ANCP	Notes
1	71.4%	9.0	6.9	regular polygon (square)
2	0%	-	112.4	optimized only for positioning accuracy
3	100%	1.2	0	the result by strategy

The first case has a poor ambiguity resolution performance that even success rate is not 100%. A histogram of required epochs for the case 1 is displayed in Figure 5-6. The second case displays the 0% success rate, as all antenna baselines are in one line. In the aspect of Ambiguity Net Technique, all layers of Ambiguity Net Image are overlapped with a large number of crossing points for case 2. The third case which has zero-ANCP displays the 100% success rate and instantaneous cycle ambiguity resolution. It requires 1.15 epochs in root-mean-square (rms), and at most four epochs are required as depicted in Figure 5-7. In addition, WHDOP value of case 3 is 65% of case 1 according to Table 5-2.

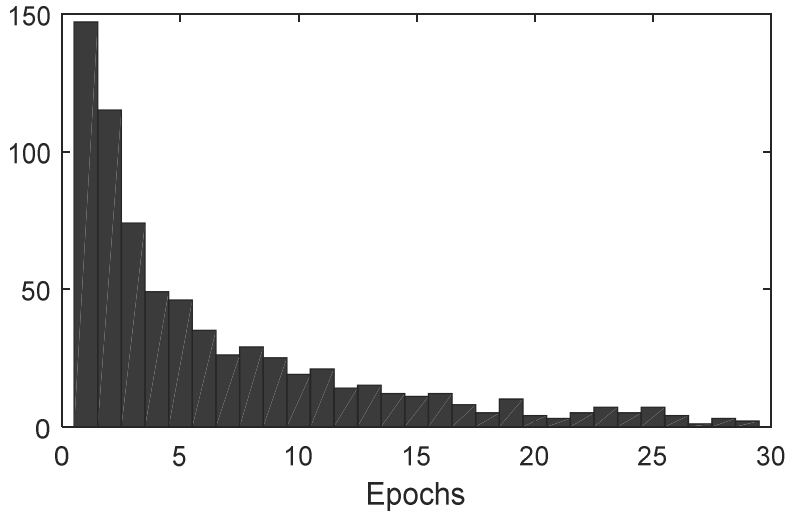

Figure 5-6 Histogram of required epochs for ambiguity resolution (AOI ±30°: case 1)

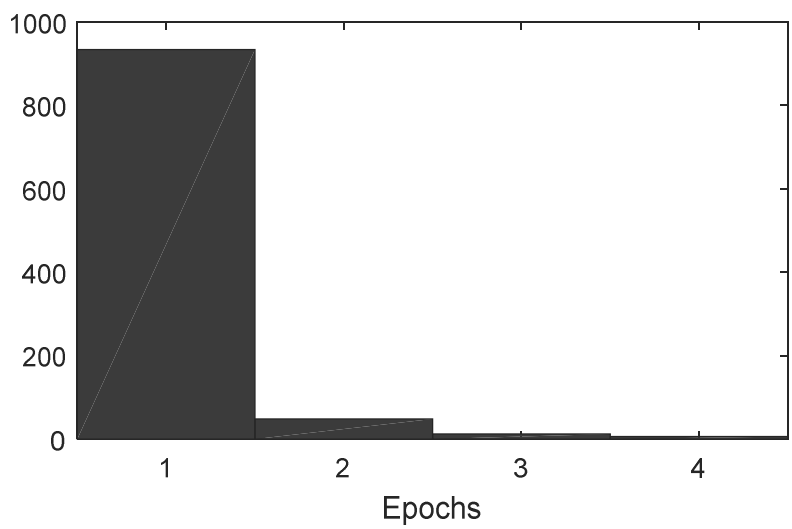

Figure 5-7 Histogram of required epochs for ambiguity resolution (AOI ±30°: case 3)

5.3.2. AOI: ±60° bound

The antenna arrangement process is described in Table 5-4. It begins with the settings of four pseudolite antennas and the baseline lengths of 2.44λ. The length of antenna baseline is extended to 3.44λ, as the accuracy performance is not met with APNT requirement. During the search process, it is found that there is no zero-ANCP antenna arrangement meeting the requirement. Therefore, the number of antenna is increased, and the search process begins again from the antenna baseline of 2.44λ. It continues until finding the antenna formation with zero-ANCP meeting the requirement.

Table 5-4 Strategy process for the AOI of ±60°

Ant. No.	Ant. baseline length	WHDOP	Notes
4	2.44λ	206.7	(Optimized only for positioning accuracy) insufficient accuracy (WHDOP > 153.6)
4	3.44λ	148.3	(Optimized only for positioning accuracy)
:			
(search process using method B, but no zero-ANCP satisfying WHDOP < 153.6)			
:			
5	2.44λ	147.8	(Optimized only for positioning accuracy) ANCP : 12.5
:			
(search process using method B)			
:			
5	2.44λ	149.8	ANCP : 0

A searched antenna formation and other cases for comparisons are described in Table 5-5 and Figure 5-8.

Table 5-5 Cases of antenna arrangements to be compared (AOI of ±60°)

Case	α_1	α_2	α_3	α_4	WHDOP	Notes
1	54°	-54°	-18°	18°	172.4	regular polygon (hexagon)
2	91.2°	-91.2°	93.6°	-93.6°	147.8	optimized only for positioning accuracy
3	274°	86°	293.2°	70.4°	149.8	the result by strategy

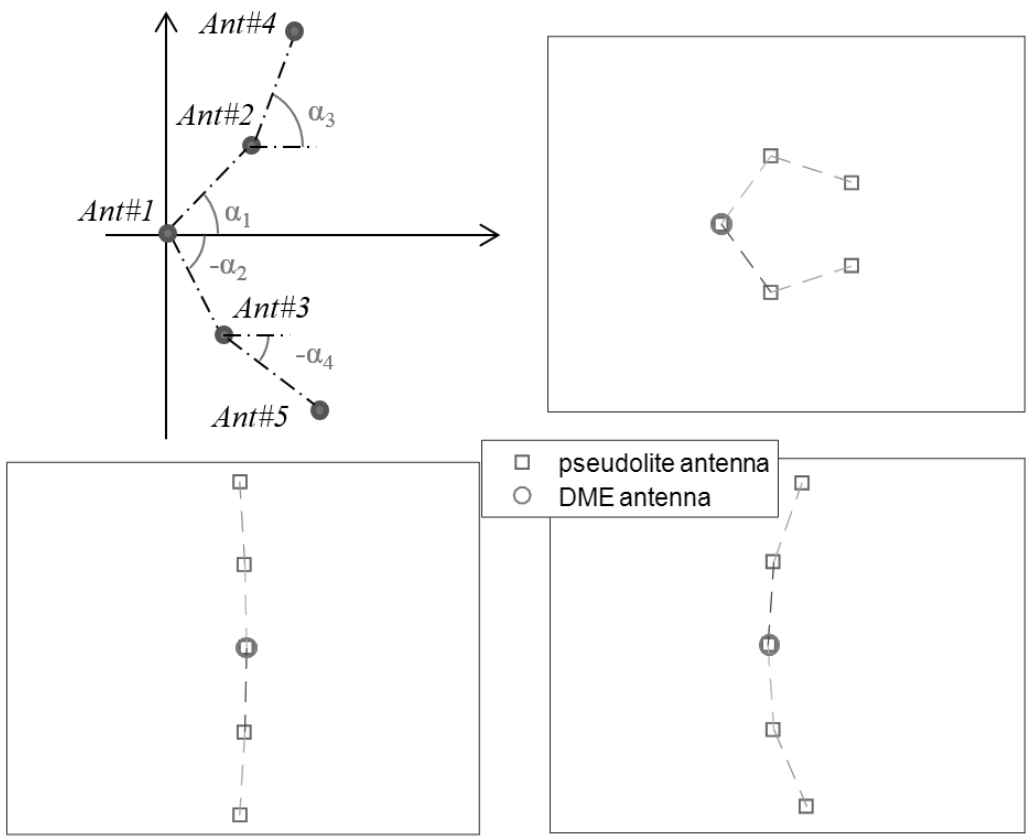

Figure 5-8 Antenna arrangement cases for AOI of ±60° (top-left: the form of antenna arrangement, top-right: case 1, top-left: case 2, bottom-right: case 3)

Monte-Carlo simulation results about the ambiguity resolution performances are in Table 5-6. The result of pentagon formation, case 1, describes all cycle ambiguities are resolved within an epoch with zero-ANCP. However, the case 1 does not have enough positioning accuracy. The case 2 has the best positioning accuracy, but the success rate of its ambiguity resolution performance is low less than 40%. The histogram of the epochs for resolution of case 2 is displayed in Figure 5-9. The case 3 is the recommended antenna arrangement satisfying both WHDOP requirement and zero-ANCP with good ambiguity resolution performance as described in Table 5-6 and Figure 5-10.

Table 5-6 Monte-Carlo results of ambiguity resolution (AOI of ±60°)

Case	Success rate	Epochs for resolution (rms)	ANCP	Notes
1	100%	1	0	regular polygon (hexagon)
2	36.9%	13.0	12.5	optimized only for positioning accuracy
3	100%	1.3	0	the result by strategy

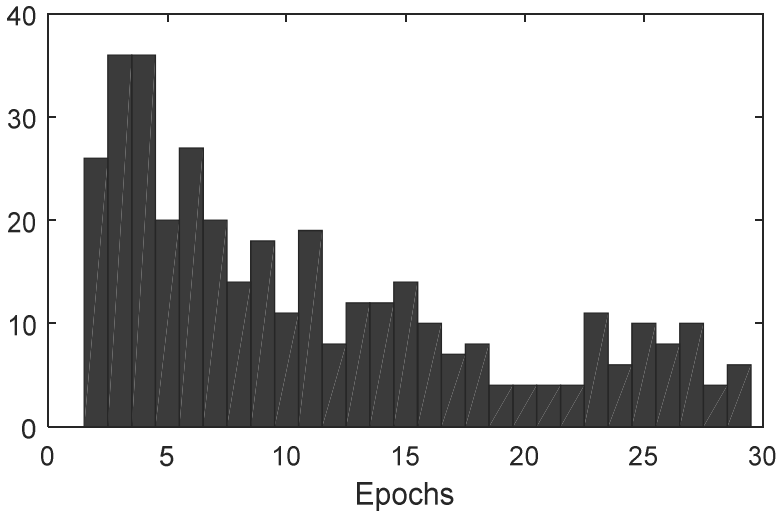

Figure 5-9 Histogram of required epochs for ambiguity resolution (AOI ±60°: case 2)

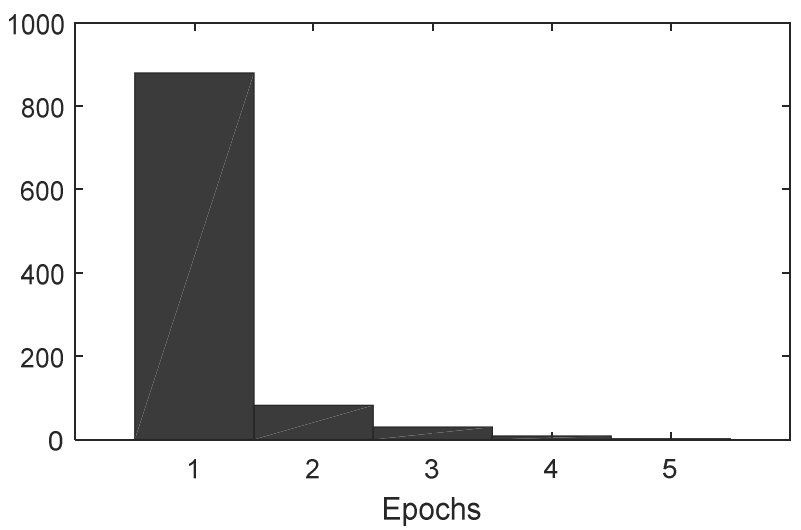

Figure 5-10 Histogram of required epochs for ambiguity resolution (AOI ±60°: case 3)

5.3.3. AOI: all area (-180° ~ 180°)

This section considers the AOI of all around the station. For the antenna arrangement process the slope angle of the first antenna baseline between antenna #1 and #2 is fixed at 90°. As the AOI for the antenna arrangement process includes all directions, the variation of the first baseline angle makes no effect.

The process for the antenna arrangement strategy is as in Table 5-7. As the antenna baseline length of 2.44λ is insufficient for the requirement, it is extended to 3.44λ. It continues to search until the antenna arrangement of zero-ANCP is found.

Table 5-7 Strategy process without bound (all area)

Ant. No.	Ant. baseline length	WHDOP	Notes
5	2.44λ	155.7	(Optimized only for positioning accuracy) insufficient accuracy (WHDOP > 153.6)
5	3.44λ	113.0	(Optimized only for positioning accuracy) ANCP : 0.64
:			
(search process using method B)			
:			
5	3.44λ	113.1	ANCP : 0

The searched antenna arrangement is the third case described in Table 5-8 and Figure 5-11, and it is compared with the formation of regular polygon and the case which is only optimized for the positioning accuracy which are case 1 and 2, respectively. As described in Table 5-8 and Figure 5-11, the shapes of antenna formations of case 2 and 3 are similar, hence the WHDOP values are also similar. However, the ANCP values are different with

different ambiguity resolution performances as described in Table 5-9 and two histograms of Figure 5-13 and Figure 5-14.

Table 5-8 Cases of antenna arrangements to be compared (all area)

Case	α_1	α_2	α_3	α_4	WHDOP	Notes
1	54°	-54°	-18°	18°	124.7	regular polygon (hexagon)
2	90°	18°	71°	37°	113.0	optimized only for positioning accuracy
3	90°	20°	73.4°	36.4°	113.1	the result by strategy

According to Table 5-9, the case 1 is near zero-ANCP with an outstanding ambiguity resolution performance. Required epochs for ambiguity resolution of case 1 are almost same with the one of case 3. With regards to Figure 5-12 and Figure 5-14, two histograms also describe similar results. In the aspect of the positioning accuracy, on the other hand, case 3, the result searched by the strategy, has better WHDOP than case 1. WHDOP of case 3 is 91% of case 1 according to Table 5-8.

Table 5-9 Monte-Carlo results of ambiguity resolution (all area)

Case	Success rate	Epochs for resolution (rms)	ANCP	Notes
1	100%	1.0	0.002	regular polygon (hexagon)
2	98.9%	2.5	0.67	optimized only for positioning accuracy
3	100%	1.0	0	the result by strategy

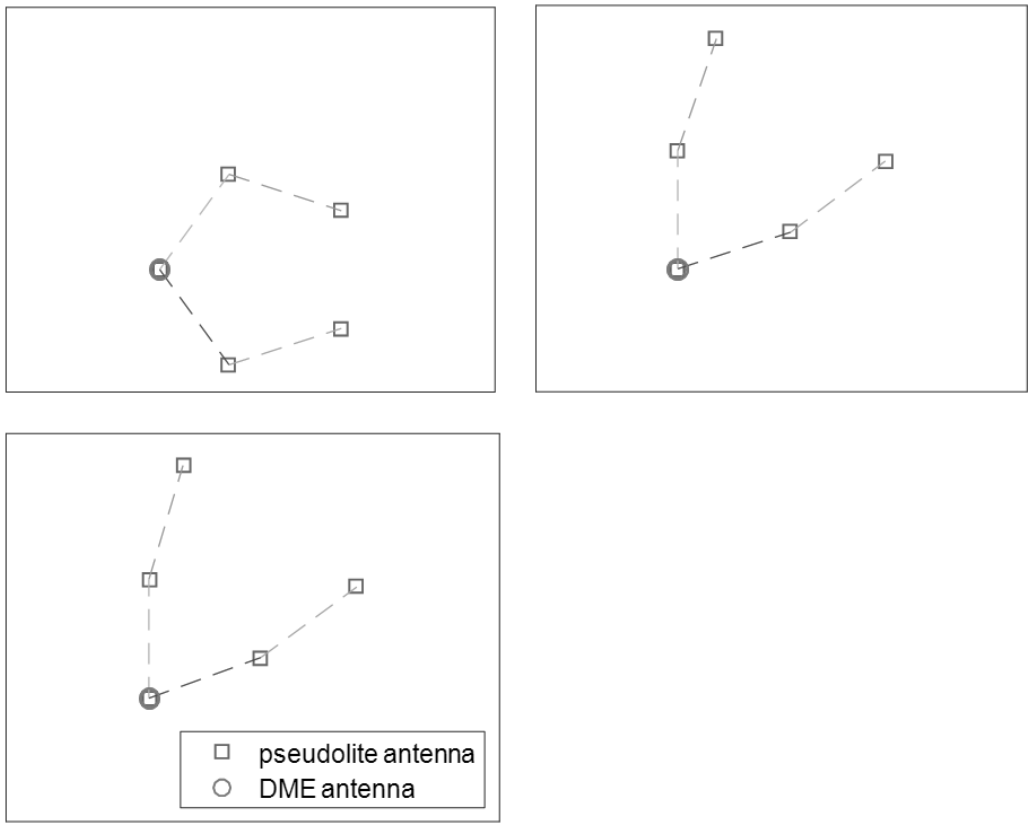

Figure 5-11 Antenna arrangement cases for all area
(top-left: case 1, top-right: case 2, bottom-left: case 3)

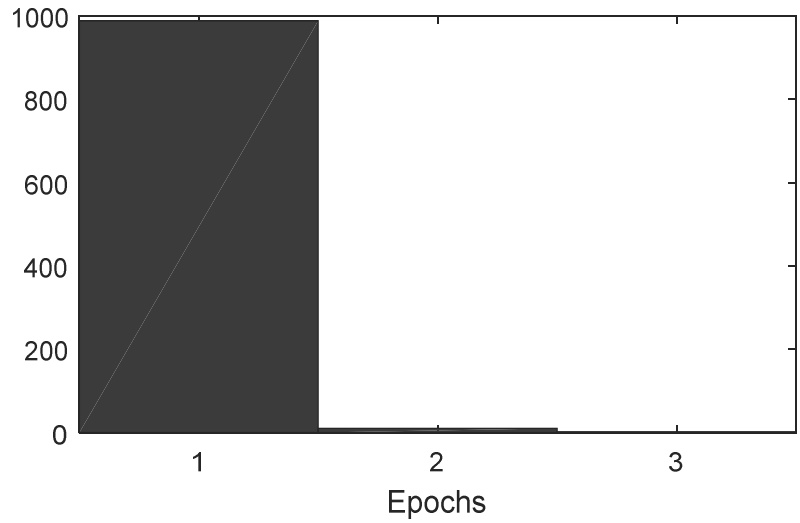

Figure 5-12 Histogram of required epochs for ambiguity resolution (AOI ±180°: case 1)

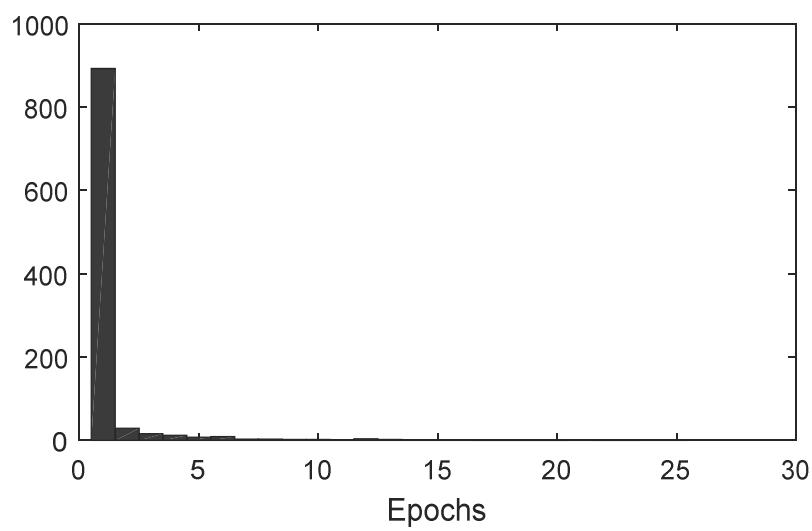

Figure 5-13 Histogram of required epochs for ambiguity resolution (AOI ±180°: case 2)

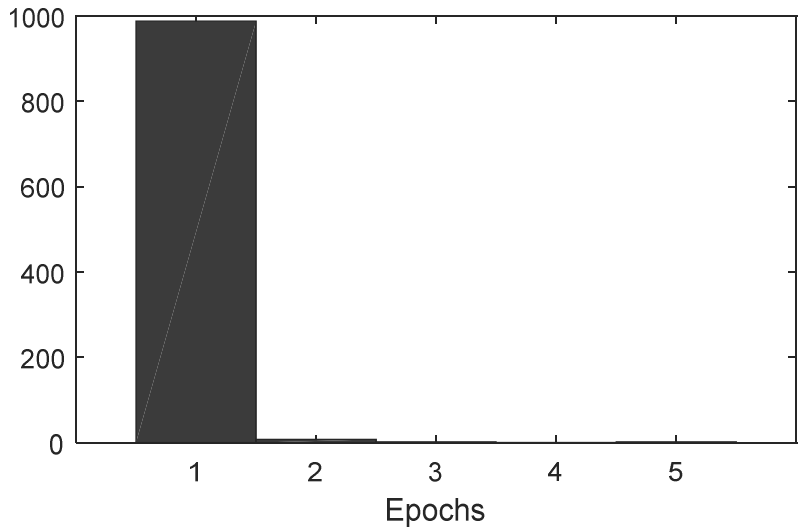

Figure 5-14 Histogram of required epochs for ambiguity resolution (AOI ±180°: case 3)

Chapter 6. Multi-Antenna Arrangement for 3D Environment

The antenna arrangement methods and its strategy for a 2D environment described in Chapter 3 and Chapter 4 are extended to a 3D environment in this chapter. In 2D cases, only one angle (azimuth angle) of each antenna baseline is needed to be decided, if the lengths of all antenna baselines are fixed. In a 3D environment, however, two angles, azimuth and elevation angles, are needed to be considered for the antenna arrangement process when antenna baseline lengths are fixed. An example of an antenna formation of a regular rectangular pyramid is displayed in Figure 6-1 with four antenna baselines which are solid lines. Azimuth and elevation angles of four antenna baselines to form the pyramid are in Table 6-1

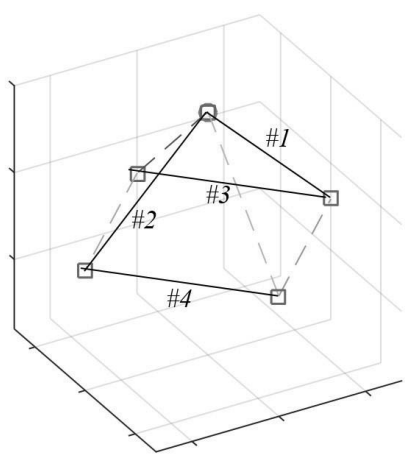

Figure 6-1 Antenna formation of regular rectangular pyramid

Table 6-1 Azimuth and elevation angles for regular rectangular pyramid

(az : azimuth, el: elevation)

Antenna formation	az_1/el_1	az_2/el_2	az_3/el_3	az_4/el_4
regular rectangular pyramid	90° / -45°	-90° / -45°	-45° / 0°	135° / 0°

The antenna arrangement process in a 3D environment is to find azimuth and elevation angles of each antenna baseline considering two terms, the positioning accuracy and the cycle ambiguity resolution performance. In addition, the AOI is also considered, but it is redefined to eliminate the unnecessary area.

6.1 Area of Interest (AOI)

For the antenna arrangement process in a 3D environment, AOI, Non-Interested Area (NIA) and Discarded Area (DIA) are introduced and considered. AOI is the main air routes which are mainly considered for the antenna arrangement process. The DIA is the area where the user cannot exist, such as undergrounds with negative altitude or mountains. During the Ambiguity Net Technique, Crossing Points (CP) in DIA are neglected, and the user also does not consider the possibility that the user is in DIA. The NIA is the area except AOI and DIA. It is disregarded during the antenna arrangement optimization process, but the user considers that they can be located in NIA.

As in a 2-D case, the AOI is defined using the angular directions which are azimuth and elevation bounds on the polar coordinated system where the station is located at the origin.

6.2 Antenna Arrangement for Positioning Accuracy

The performance index for the optimization process in an aspect of the positioning accuracy for a 3D environment is also the worst DOP over the AOI. Some kinds of DOP can be a performance index, such as Weighted Horizontal DOP (WHDOP) as in Equation (3-21) or Weighted Position DOP (WPDOP) as in Equation (3-22). In order to meet the APNT requirement, WHDOP is considered, as the horizontal accuracy is the main concern for APNT.

An optimization problem for the positioning accuracy is described as Equation (6-1), a generalized form from Equation (4-5), where $\overline{az} = (az_1, az_2, \ldots, az_i, \ldots, az_k)$ and $\overline{el} = (el_1, el_2, \ldots, el_i, \ldots, el_k)$ are vectors consisting of azimuth and elevation angles of each antenna baseline. i is an index of antenna baselines and k is a total number of antenna baselines.

$$\left\{\overline{az}, \overline{el}\right\} = \underset{0<az_i, el_i<2\pi}{\arg\min}\left[\max_{AOI}\left(DOP(\overline{az}, \overline{el})\right)\right] \tag{6-1}$$

The purpose is to maximize the accuracy at the worst location over the AOI, in other words, minimize the DOP at the worst location.

6.3 Antenna Arrangement for Ambiguity Resolution

The principle of the Ambiguity Net Technique in a 3D environment is same with the 2-dimensional case. However, it is extended to a 3D environment increasing the complexity.

A hyperbola in a 2D environment is extended to a circular hyperboloid in a 3D

environment with the rotation on a principal axis. In addition, asymptotic lines in 2D are asymptotic circular cones in 3D as described on the right of Figure 6-2. If the distance from station to user is long enough, the hyperboloid can be regarded as cones which are asymptotic surfaces of hyperboloid.

In Figure 6-2, a principal axis of hyperboloid is on z-axis. Two square dots are focuses of hyperboloid, and it is assumed that the user is located at a circular dot on the surface of upper objects. When the DME measurement is considered, the distance from station to user is known. Hence, the trajectory of possible solutions has a shape of circle on the surface of the asymptotic cone as described in both sides of Figure 6-2. This circular trajectory is termed as an asymptotic circle in this dissertation.

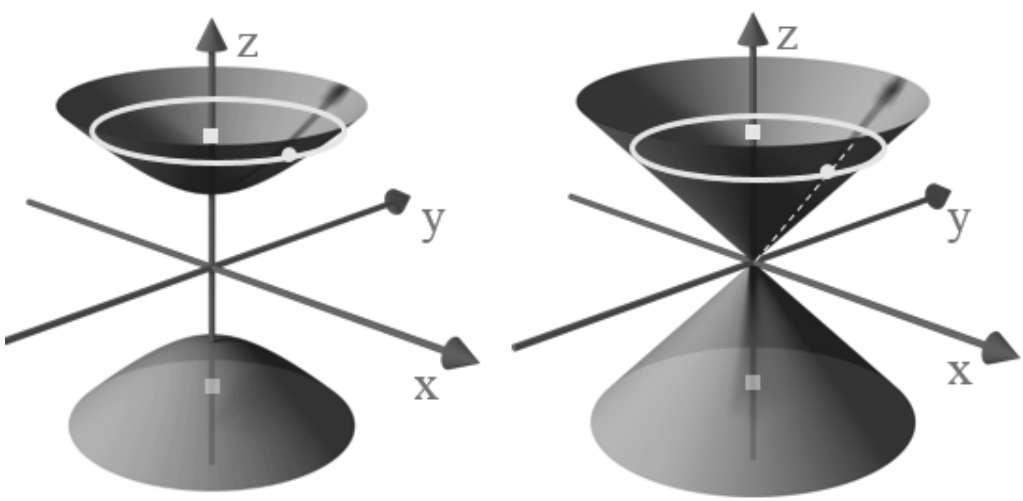

Figure 6-2 Circular hyperboloid (left), asymptotic circular cones (right) and asymptotic circles on the surfaces (yellow rings) [59, 60]

Ambiguity Net Image for a 2D environment is a 2-dimensional image, where the x-axis means the angle of user position and y-axis represents the angle of slope by each cycle ambiguity candidates. In a 3D environment, the dimension of Ambiguity Net Image is four. There are two dimensions for azimuth and elevation angles of user position and other two dimensions for the azimuth and elevation angles of asymptotic circles generated by each cycle ambiguity candidate. Asymptotic circles when azimuth and elevation angles of user position are 30° and 10° respectively, are described in Figure 6-3, where three antenna baselines of $\{(\overline{az}, \overline{el})\} = \{(0°, 90°), (0°, 45°), (90°, 0°)\}$ are considered with the antenna baseline length of 1.5λ. Three different trajectories are crossed at the user position (circle). Accordingly, the crossing point except the user position, the square in Figure 6-3, is a hazardous false candidate which is difficult to discriminate the true ambiguity. Figure 6-3 is the 3D version of Figure 4-7.

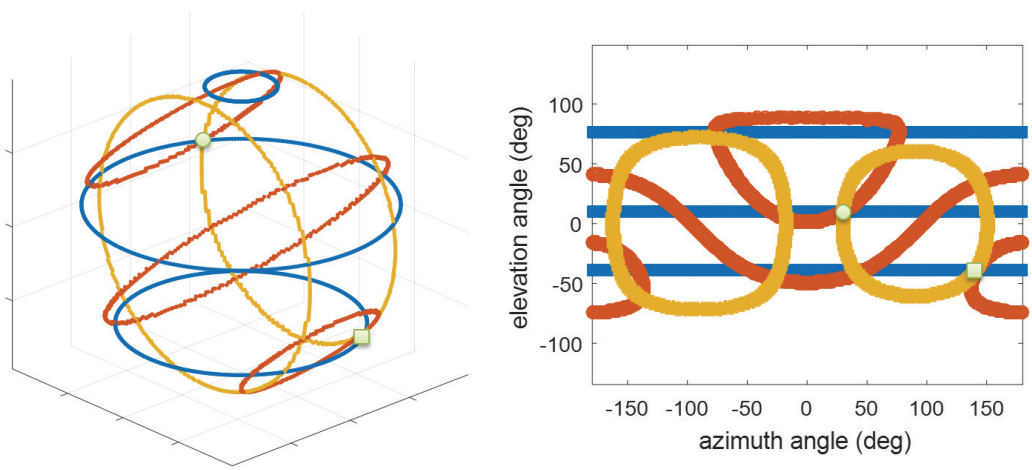

Figure 6-3 Asymptotic circles by each cycle ambiguity candidates when user position (circle) is on the azimuth of 30° and elevation of 10°
(left: position domain, right: azimuth-elevation angles domain)

As the dimension of Ambiguity Net Image is four, the image can be displayed when at least one of elements is fixed. Figure 6-4 and Figure 6-5 are examples of Ambiguity Net Image for a 3D environment if one of elements is fixed. To visualize two images, a coarse grid step size of 5° is considered.

The Ambiguity Net Technique counts the number of CP on the image. The assessment process of CP in a 3D environment is similar with the 2-dimensional case as in Equation (6-2), where u_{az} and u_{el} are pixel indexes representing the azimuth and elevation angles of user positions, s_{az} and s_{el} are pixel indexes representing the slope angles of asymptotic circles, and k is the index of antenna baseline and K means the total number of antenna baseline.

$$CP\left(u_{az},u_{el},s_{az},s_{el}\right)\equiv\prod_{k=1}^{K}BC^{k}\left(u_{az},u_{el},s_{az},s_{el}\right) \tag{6-2}$$

Boundary Check (BC) in a 3D environment utilizes the characteristic of asymptotic circles. Asymptotic circles are axisymmetric about the principal axis of hyperboloid. Hence, only the elevation angle can define each asymptotic circle with the azimuth and elevation angles of antenna baselines, as all azimuth angles of -π~+π are always applied around the principal axis. Utilizing the elevation angles without azimuth information is enough for the counting the number of CPs.

At each pixel grid, elevation angles of each layer, k, in the spherical coordinate system whose z-axis is on the principal axis of hyperboloid are utilized to decide whether or not the elevation angles of asymptotic circles are within the bound. If all elevation angles of asymptotic circles of all layers are in the bound, this gird point is CP with the CP value of 1.

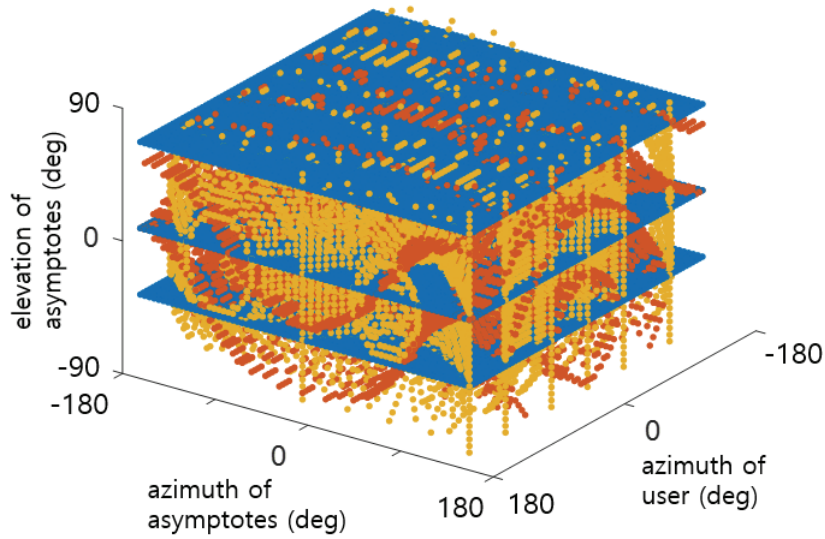

Figure 6-4 Ambiguity Net Image when the elevation angle of user is fixed

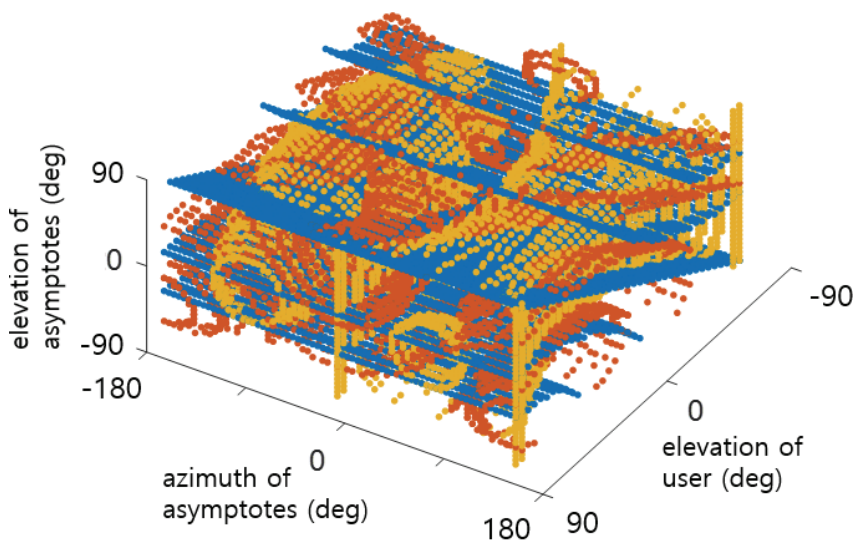

Figure 6-5 Ambiguity Net Image when the azimuth angle of user is fixed

In a 2D environment, ±1 pixel bounds for x-axis of Ambiguity Net Image, angular direction in positioning domain, are considered to cover the gap between user grid points. In a 3D environment, ±1 pixel bounds for both user azimuth and elevation grids are considered during the BC process.

Average Number of Crossing Point (ANCP) at a certain antenna arrangement can be calculated as Equation (6-3) considering AOI, NIA and DIA, where $U_{az,el}^{AOI}$ means the total number of grid pixels of the user azimuth and elevation angles inside the AOI.

$$ANCP^{AOI} \equiv \frac{1}{U_{az,el}^{AOI}} \sum_{u_{az}}^{AOI} \sum_{u_{el}}^{AOI} \sum_{s_{az}}^{AOI \cup NIA} \sum_{s_{el}}^{AOI \cup NIA} CP\left(u_{az}, u_{el}, s_{az}, s_{el}\right) \tag{6-3}$$

The pixel bound for elevation is calculated based on the same method as described in section 4.3.2. Considering only elevation bound is enough for assessing the CP. An example of the calculated pixel bound and its limitation by pixel resolution are in Figure 6-6 and Figure 6-7 respectively, where d = 1.21m (<4.5λ), the bound of 16.7mm considering $2\sigma_{\Delta\phi}$ with various error sources according to Table 3-3, and the pixel step size of 0.2° are considered.

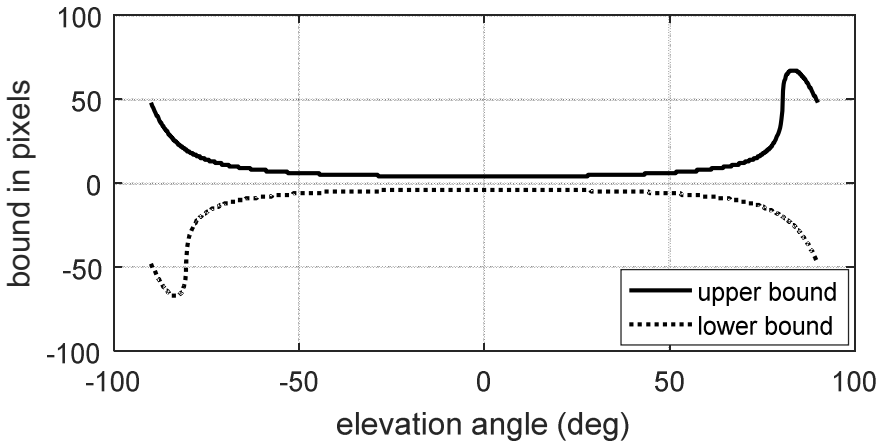

Figure 6-6 Pixel bounds according to elevation angle when antenna baseline is on z-axis

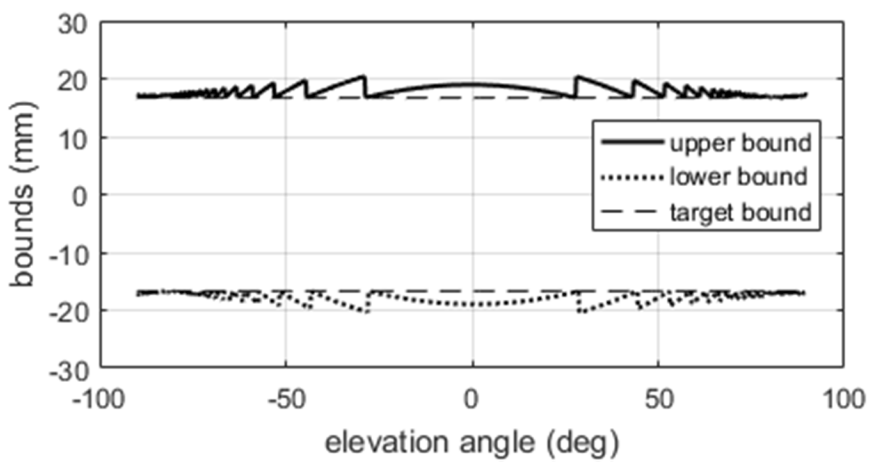

Figure 6-7 Bound residuals caused by pixel resolution when antenna baseline is on z-axis

6.4 Simulation Results

6.4.1. Simulation Settings

The strategy of method B in section 5.2 for the antenna arrangement process is also applied for 3D simulations. Searching the antenna arrangement is performed manually until the sub-optimal solution which has the local minimum-ANCP is found. The antenna arrangement process in a 3-D environment is difficult to find the zero-ANCP, because of its huge amount of computational load. In a 3-D environment, two angles of both azimuth and elevation of each antenna baselines are needed to be decided. Hence, the searching area is considerably increased compared to the 2-D case, and the dimension of Ambiguity Net Image is also increased from 2-D to 4-D as from Equation (4-25) to Equation (6-3).

Proper grid is required for the Ambiguity Net Technique. In a 3-D environment, regular spacing for both azimuth and elevation angles in the spherical coordinate system is not recommended, as the densities of grids in high and low elevations are different; grid points in high elevations are denser than lower elevation cases. Accordingly, the grid points which have same azimuthal arc lengths at each elevation with equal elevation step are applied for simulations. Regular elevation step angle is highly recommended as the CP assessment process is based on only elevation angles. Figure 6-8 describes the grid in both Cartesian and spherical coordinate systems with elevation step angle of 5° for visualization.

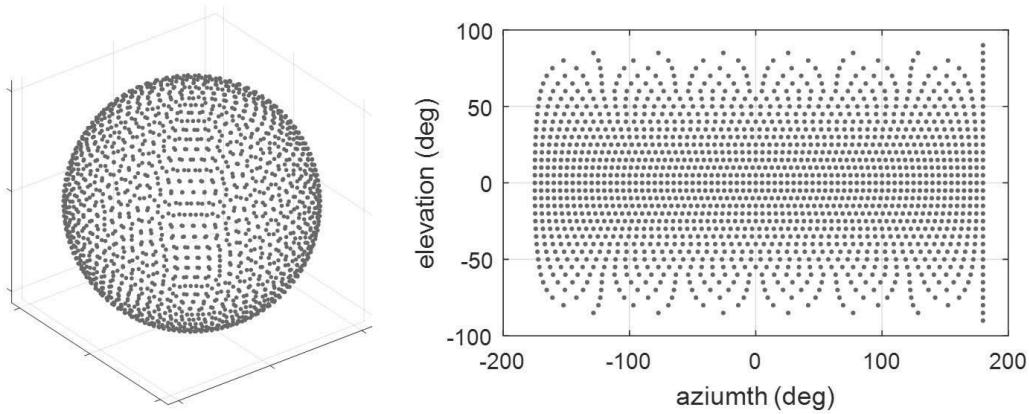

Figure 6-8 Grid for 3-D Ambiguity Net Technique with elevation step angle of 5°
(left: Cartesian coordinate system, right: spherical coordinate system)

The grid size for searching the antenna arrangement is 0.2°. In addition, Ambiguity Net Technique is also applied with the pixel size of 0.2°. Five antennas with the antenna baseline length of 4.5λ are mainly considered in simulations of various cases. The first case of antenna formation has a shape of regular rectangular pyramid as already described in Figure 6-1. The second case is to optimize only for the positioning accuracy based on Genetic Algorithm. In addition, a few cases during the method B process of strategy decreasing the ANCP are also considered. The last case is the antenna arrangement with local minimum-ANCP. During the antenna optimization process, azimuth and elevation angles of a pair of opposite antenna baselines, (az_1, el_1) with (az_2, el_2) and (az_3, el_3) with (az_4, el_4), are varied symmetrically to maximize the positioning accuracy and search the formation efficiently reducing the elements to be decided. The antenna baseline length is smaller than a certain integer M and p $(0 \leq p < 0.5)$ as in Equation (3-4). p of 0.38 is applied considering the error size of $4\sigma_{\Delta\phi}$. Antenna formation cases for simulations are described

in Table 6-3 and Figure 6-9. Total 16 cases are considered and compared.

Table 6-2 Antenna arrangement cases (No. of antenna: 5, baseline length: 4.38λ)

Case	az_1/el_1	az_2/el_2	az_3/el_3	az_4/el_4	Notes
1	90.0°/ -45.0°	-90.0°/ -45.0°	-45.0°/ 0°	135.0°/ 0°	regular pyramid
2	8.4°/ -20.0°	171.6°/ -20.0°	21.0°/ -36.0°	159.0°/ -36.0°	optimized only for positioning accuracy
3	8.4°/ -20.0°	171.6°/ -20.0°	21.0°/ -35.0°	159.0°/ -35.0°	(in ANCP decreasing process)
4	8.4°/ -20.0°	171.6°/ -20.0°	21.0°/ -33.6°	159.0°/ -33.6°	(in ANCP decreasing process)
5	8.4°/ -19.6°	171.6°/ -19.6°	21.0°/ -33.6°	159.0°/ -33.6°	(in ANCP decreasing process)
6	8.4°/ -19.6°	171.6°/ -19.6°	21.0°/ -33.2°	159.0°/ -33.2°	(in ANCP decreasing process)
7	8.4°/ -19.4°	171.6°/ -19.4°	21.0°/ -33.2°	159.0°/ -33.2°	(in ANCP decreasing process)
8	8.4°/ -19.4°	171.6°/ -19.4°	21.0°/ -33.0°	159.0°/ -33.0°	(in ANCP decreasing process)
9	8.4°/ -19.2°	171.6°/ -19.2°	21.0°/ -33.0°	159.0°/ -33.0°	(in ANCP decreasing process)
10	8.4°/ -19.2°	171.6°/ -19.2°	21.0°/ -32.8°	159.0°/ -32.8°	(in ANCP decreasing process)
11	8.4°/ -19.2°	171.6°/ -19.2°	21.6°/ -32.8°	158.4°/ -32.8°	(in ANCP decreasing process)
12	8.4°/ -19.2°	171.6°/ -19.2°	21.6°/ -32.6°	158.4°/ -32.6°	(in ANCP decreasing process)
13	8.2°/ -19.2°	171.8°/ -19.2°	21.6°/ -32.6°	158.4°/ -32.6°	(in ANCP decreasing process)
14	8.2°/ -19.4°	171.8°/ -19.4°	21.6°/ -32.6°	158.4°/ -32.6°	(in ANCP decreasing process)
15	8.2°/ -19.4°	171.8°/ -19.4°	21.6°/ -32.8°	158.4°/ -32.8°	(in ANCP decreasing process)
16	8.2°/ -19.6°	171.8°/ -19.6°	21.6°/ -32.8°	158.4°/ -32.8°	local minimum ANCP

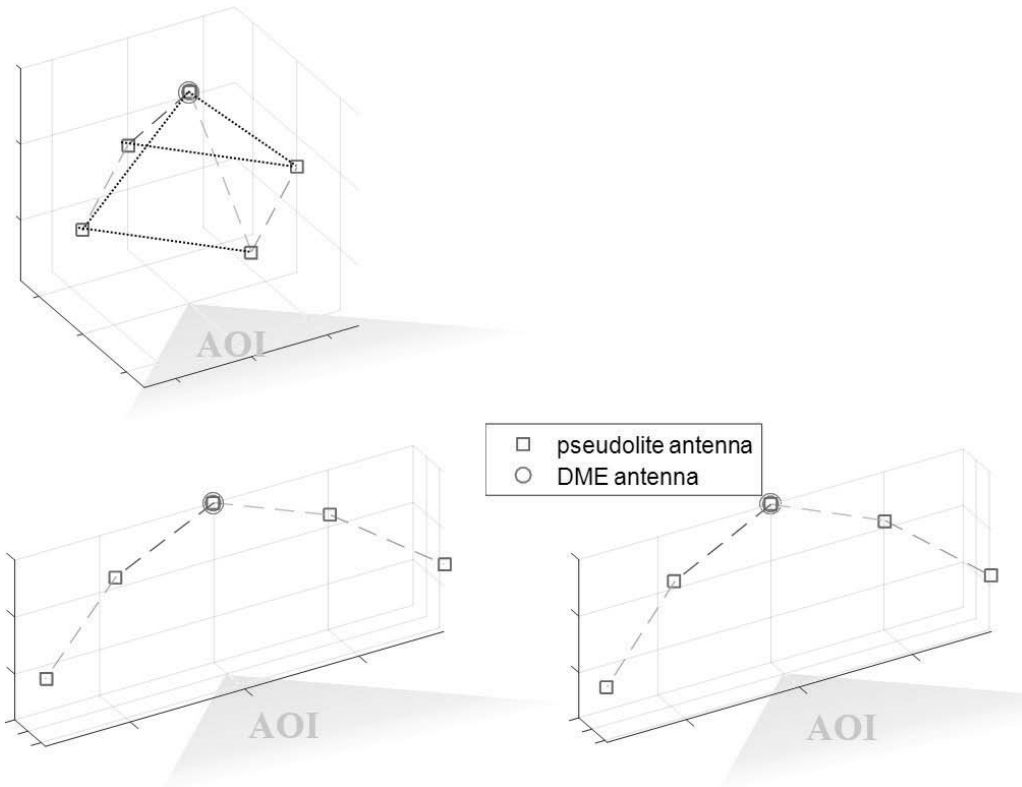

Figure 6-9 Antenna arrangement cases (3-D simulation)
(top-left: case 1, bottom-left: case 2, bottom-right: case 16)

For simulations, one AOI is considered. The AOI has the elevation range of 2~12° and the azimuth range of 60~150° from the station. The maximum distance is 55.64km to cover the Mode C-veil of Airspace Class B with the radius of 30nmi (55.56km) and the altitude of 10,000ft (3.05km). The AOI for simulations is described as in Figure 6-10. A target positing accuracy is as in Table 2-1: horizontal accuracy of 307.1m (<95%) for RNAV/RNP 0.3 considering Flight Detector.

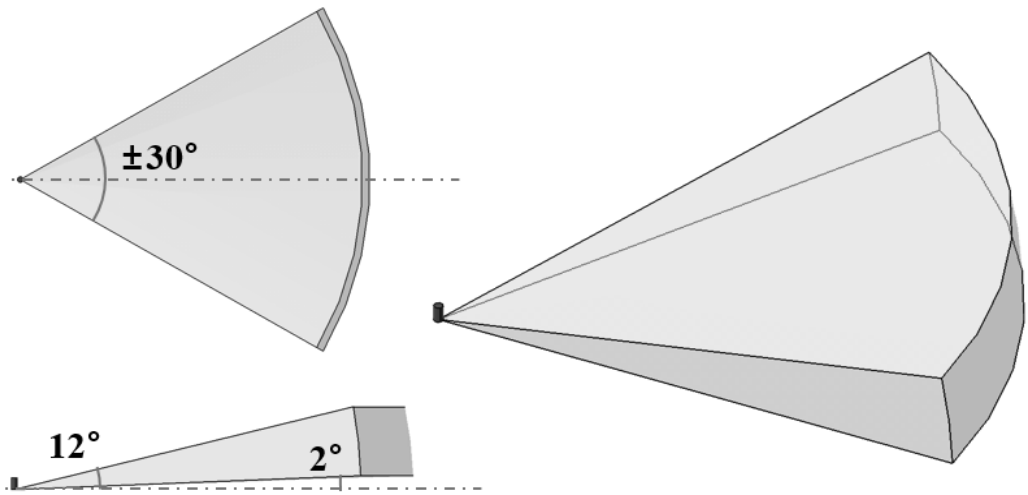

Figure 6-10 AOI for 3-D simulations
(left-top: top view, left-bottom: front view, right: isometric view)

Two kinds of Monte-Carlo simulations are conducted. The first is to investigate the performance of cycle ambiguity resolution. The second is the simulation verifying the positioning accuracy.

For both simulations, measurement errors of Table 3-3 are applied. For DME errors, white Gaussian noise including all error sources is used. Tropospheric error, multipath error, thermal noise and other error sources are considered separately for the generation of carrier-phase measurements. Only static user cases, which have the worst performance of cycle ambiguity resolution, are considered for simulations.

The WDOP values at the worst location in AOI and calculated ANCP using Ambiguity Net Technique for each case are described in Table 6-3.

Table 6-3 WDOP and ANCP for each case (3-D simulation)

Case	worst WHDOP	ANCP	Notes
1	287.5	1343.6	regular pyramid
2	138.3	397.5	optimized only for positioning accuracy
3	138.5	187.6	(in ANCP decreasing process)
4	138.8	102.5	(in ANCP decreasing process)
5	138.8	93.4	(in ANCP decreasing process)
6	138.9	87.2	(in ANCP decreasing process)
7	138.9	84.6	(in ANCP decreasing process)
8	139.0	83.7	(in ANCP decreasing process)
9	139.0	82.4	(in ANCP decreasing process)
10	139.1	82.4	(in ANCP decreasing process)
11	139.1	68.4	(in ANCP decreasing process)
12	139.1	67.9	(in ANCP decreasing process)
13	139.1	67.6	(in ANCP decreasing process)
14	139.1	65.4	(in ANCP decreasing process)
15	139.0	65.3	(in ANCP decreasing process)
16	139.0	63.5	local minimum ANCP

6.4.2. Ambiguity Resolution Results

Two thousand samples for each antenna arrangement are conducted for the Monte-Carlo simulations of cycle ambiguity resolutions, and the positions of user are randomly distributed on the arc of the AOI with the distance from station is fixed at 55.64km. In addition, 99.9999% of chi-square distribution for residual threshold test and 99% f-

distribution for ratio test are applied.

The results for the performance of cycle ambiguity resolution are depicted in Table 6-4. The tendency between ANCP and required epochs for resolution is described in Figure 6-11.

Table 6-4 Monte-Carlo results of ambiguity resolution (3-D simulation)

Case	Success rate	Epochs for resolution (rms)	ANCP	Notes
1	11.5 %	20.25	1343.6	regular rectangular pyramid
2	95.9 %	10.65	397.5	optimized only for positioning accuracy
3	100 %	4.17	187.6	(in ANCP decreasing process)
4		3.15	102.5	(in ANCP decreasing process)
5		2.90	93.4	(in ANCP decreasing process)
6		3.29	87.2	(in ANCP decreasing process)
7		3.15	84.6	(in ANCP decreasing process)
8		3.48	83.7	(in ANCP decreasing process)
9		3.29	82.4	(in ANCP decreasing process)
10		3.63	82.4	(in ANCP decreasing process)
11		2.93	68.4	(in ANCP decreasing process)
12		3.14	67.9	(in ANCP decreasing process)
13		3.08	67.6	(in ANCP decreasing process)
14		3.25	65.4	(in ANCP decreasing process)
15		3.00	65.3	(in ANCP decreasing process)
16		3.10	63.5	local minimum ANCP

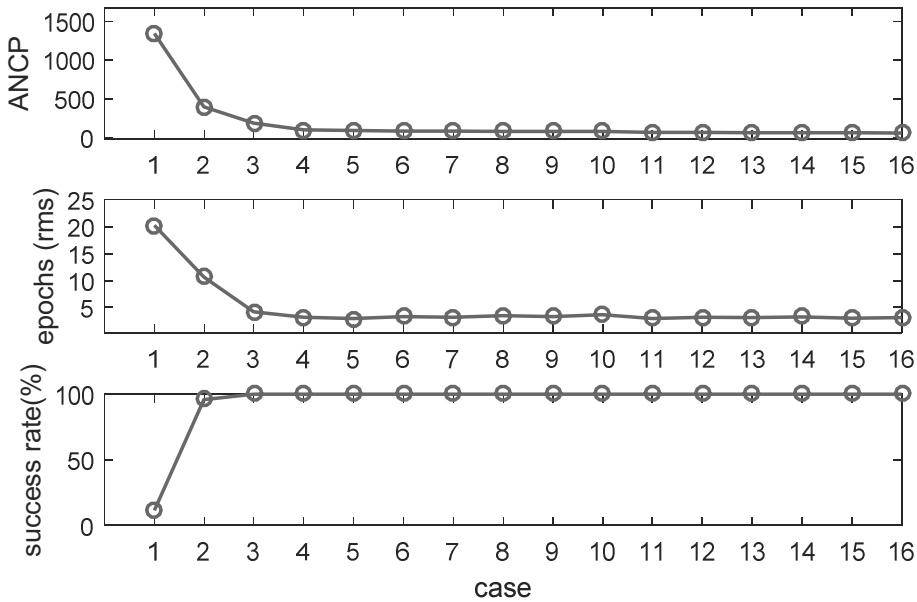

Figure 6-11 Tendency between ANCP and cycle ambiguity resolution performances

The first and second cases don't have the success rate of 100% with poor performances. On the other hand, antenna formations with low ANCP, cases 3~16, have better cycle ambiguity resolution performances with success rates of 100%. The antenna formation with local minimum ANCP, case 16, has required epochs for resolution compared to 15.3% of case 1 and 29.1% of case 2.

Figure 6-11 describes the tendency between ANCP and the performance of cycle ambiguity resolution. It is roughly depicted that decreasing ANCP causes to faster cycle ambiguity resolution. However, this tendency is not fit definitely, as cases of 6, 8, 10, 12, 14 and 16 are slightly larger than previous cases. As the cycle ambiguity resolution performance is probabilistically guaranteed only with zero-ANCP and there are still

bound residuals as in Figure 6-7, the tendency in Figure 6-11 can be regarded for reference only.

Histograms of required epochs for ambiguity resolution of case 1, case 2 and case 16 are described in Figure 6-12, Figure 6-13 and Figure 6-14. In Figure 6-12 and Figure 6-13, histograms of only samples whose ambiguity resolutions are solved within 30 epochs are depicted. The antenna arrangement with local minimum ANCP of case 16 describes the result that 98.0% of samples are resolved within 5 epochs.

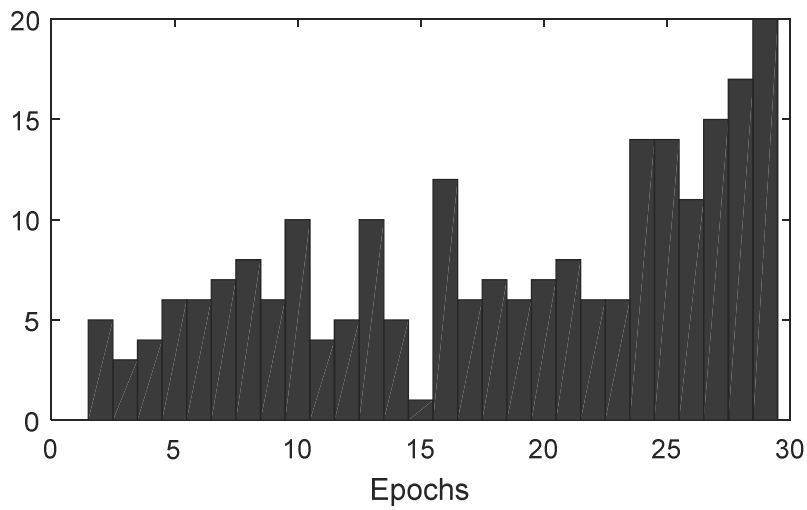

Figure 6-12 Histogram of required epochs for ambiguity resolution (3-D: case 1)

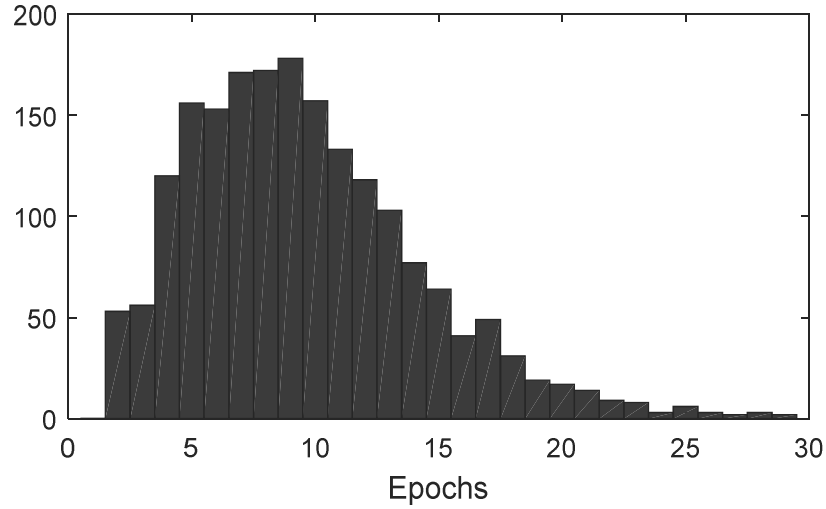

Figure 6-13 Histogram of required epochs for ambiguity resolution (3-D: case 2)

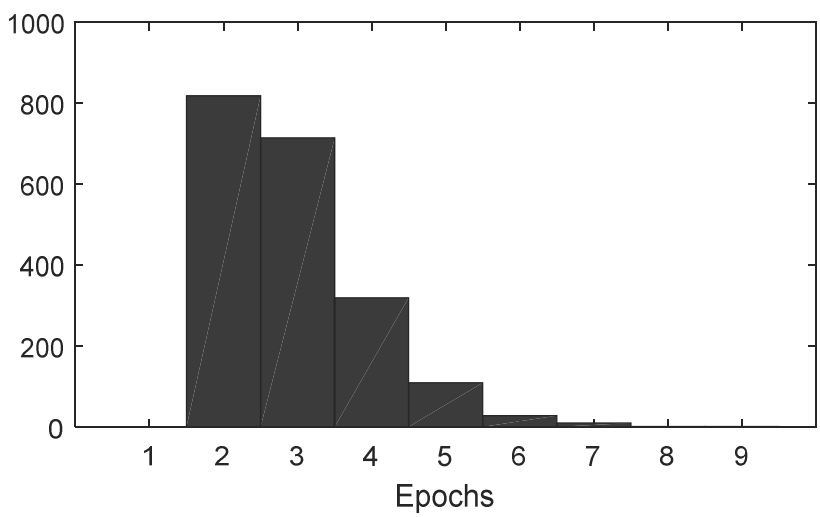

Figure 6-14 Histogram of required epochs for ambiguity resolution (3-D: case 16)

The scale of ANCP values in Table 6-4 are different from the case of 2-D environments. It is difficult to compare 2-D and 3-D cases directly, as the dimensions of ANCP are different.

The goal of Ambiguity Net Technique is to find the antenna formation with zero-ANCP which ensures fast and robust ambiguity resolutions, but this dissertation describes the results until to find the local minimum ANCP, because of its computation load. Searching the antenna arrangement with zero-ANCP is remained for future works. Or increasing the number of pseudolite antennas would be an alternate approach to find the zero-ANCP with low computation load, but the system complexity would be increased.

6.4.3. Positioning Accuracy Results

Monte-Carlo simulations for the positioning accuracy are conducted 5000 samples to verify whether or not the positioning accuracy of each antenna formation satisfies the required performance. As the error sources such as tropospheric delay and multipath are considered, the positioning accuracy is not directly derived from WHDOP.

Total three cases, regular rectangular pyramid, optimized only for the positioning accuracy and the local minimum ANCP are analyzed and compared. For the accuracy simulations, it is assumed that cycle ambiguity problems are solved.

The user locations for simulations are spread with the grid size of 2° on the outer surface of AOI: azimuth range of 2°~12° and elevation range of 60°~120° as in Figure 6-15.

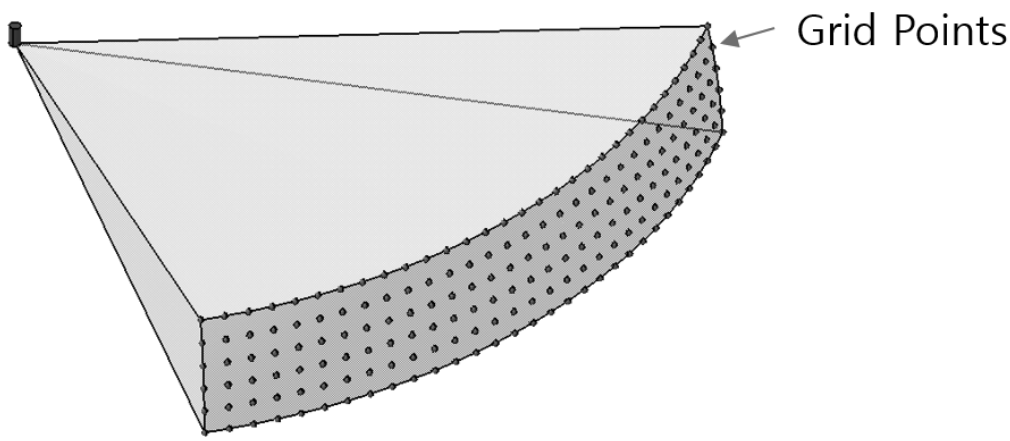

Figure 6-15 Grid points for positioning accuracy simulations

Table 6-5 Monte-Carlo results of positioning accuracy (3-D simulation)

Case	Horizontal Error (<95%)		worst WHDOP	Notes
	worst	average		
1	583.2 m	559.1 m	287.5	regular rectangular pyramid
2	276.7 m	236.9 m	138.3	optimized only for positioning accuracy
16	278.2 m	236.1 m	139.0	local minimum ANCP

The simulation results are described in Table 6-5. Horizontal positioning errors at the worst location and averaged horizontal errors in grids are calculated. The second has the best accuracy as expected, but the case 16 also good positioning accuracy compared to the case 1: 47.7 % in the worst positioning error and 42.2 % in the averaged error.

In addition, even considering the worst positioning error, case 2 and case 16 satisfy the required horizontal APNT accuracy, 307.1m.

Chapter 7. Conclusions

7.1 Conclusions

A single station-based precise positioning system for air transport, termed as Mosaic/DME introduced in this dissertation. Mosaic/DME is an independent positioning system for air transport that considers an environment in which satellite-based navigation systems are unavailable.

Mosaic/DME uses a conventional DME with multiple pseudolite transmitters, which are inherently time-synchronized. Consequently, the most significant characteristic is that it can provide three-dimensional positioning, which includes the altitude of the aircraft, using only a single station. This can be achieved when carrier-phase measurements from pseudolites are used. The issue of integer cycle ambiguity is handled using the Mosaic concept, which bounds the range of the cycle ambiguity candidates geometrically.

In this dissertation, researches to find the optimized antenna arrangement considering both positioning accuracy and the ambiguity resolution performance while targeting the Area of Interest (AOI) are presented. For the performance index of positioning accuracy, Dilution of Precision (DOP), such as the angular DOP or weighted horizontal DOP are the main concerns. The Ambiguity Net Technique is used to investigate the Average Number of Crossing Points (ANCP) to determine whether or not a certain antenna arrangement is favorable for fast and robust cycle ambiguity resolutions. A strategy to find proper antenna arrangements considering both the positioning accuracy and the ambiguity resolution performance is also presented.

Monte-Carlo simulations are performed to verify the performance of the system considering various error sources. Simulations are conducted in both 2-D and 3-D environments, and the results indicate that the Ambiguity Net Technique performs effectively when used to find an antenna arrangement capable of solving the cycle ambiguity problem robustly, designing the target measurements boundary, and working rapidly in only a few epochs. The strategy also helps to find antenna arrangements which satisfy the two requirements of positioning accuracy and zero-ANCP.

7.2 Suggestions for Future Work

In this dissertation, a single station-based positioning system, termed the Mosaic/DME system, and a strategy for an antenna arrangement which considers both the positioning accuracy and the cycle ambiguity resolution performance is presented. As the concept of this system is new, numerous works can be done in the future.

The first suggestion for future research is the implementation of the system to verify its operation. Experiments should be performed to assess the operation of the single station-based positioning system and to analyze its performance. Afterward, the results of an optimized antenna arrangement should be verified through experiments.

For the implementation of this system, the key issue is time-synchronization between pseudolites to broadcast time-synchronized signals. Even if this time-sync between pseudolites is conducted, clock bias between pseudolites may still exist, and it may drift very slowly. However, this bias can easily be handled if the reference receiver estimates the value and transmits it to the user, or if the signals from pseudolites can contain correction data to eliminate the time-sync bias between pseudolites.

The integrity of Mosaic system should also be carefully considered. As the cycle ambiguity resolution is used for positioning, coverage of the integrity includes assessing the correctness of the ambiguity resolution. As Mosaic is an independent navigation system, external equipment such as an Inertial Navigation System (INS), an attitude and heading reference System or even an altimeter can serve to improve the integrity of this system.

Integration with INS is also a valuable research topic. In the case of Mosaic/DME, this system can be used to prevent an increase in the cumulative INS error, similar to a GPS for a GPS/INS system.

As noted in the introduction of this dissertation, the Mosaic concept for Multilateration (MLAT) is also worthy of study. For MLAT, station with multiple antennas receives the signal from the target, and this single station can calculate the target's position. The advantage using a single station can also be realized for both local area MLAT and wide area MLAT. With regard to air traffic surveillance, a system using the Mosaic concept can be utilized for the verification of an Automatic Dependent Surveillance-Broadcast (ADS-B) signal, given that ADS-B is vulnerable to security.

Another good application of a single station-based positioning system is indoor navigation, as GNSS signals are too weak to use in indoor environments. The best scenario is to implement the Mosaic concept integrated with the tele-communication access point for both communication and positioning simultaneously.

The mosaic concept can also be utilized for positioning in a marine application. In this case, analyses for two-dimensions as described in Chapter 4 would be useful.

Chapter 8. Reference

[1] Kee, C., and Lee, T., "Positioning System and Method based on Radio Communication Apparatus Comprising Multiple Antenna (KR),"1009796230000, Patents (Registered), Republic of Korea, 2009.

[2] Kim, C., Kim, O.-J., Lee, T., and Kee, C., "Indoor Positioning System using Single Pseudolites with Multiple Antenna," Proceedings of the 2012 International Technical Meeting of The Institute of Navigation, The Institute of Navigation (ION), Newport Beach, CA, 2012.

[3] Eldredge, L., Enge, P., Harrison, M., Kenagy, R., Lo, S., Loh, R., Lilly, R., Narins, M., and Niles, R., "Alternative Positioning, Navigation & Timing (PNT) Study," Working Group Meetings of International Civil Aviation Organisation Navigation Systems Panel (NSP), Working Group Meetings, Montreal, Canada, May 2010, Citeseer.

[4] Kee, C., and Lee, T., "Positioning System and Method based on Radio Communication Apparatus Comprising Multiple Antenna (PCT),"WO 2010/137790 Al, Patents (PCT), World Intellectual Property Organization, 2010.

[5] Kim, O.-J., Kim, C., Song, J., Kim, Y., and Kee, C., "Instantaneous Ambiguity Resolution of MOSAIC/DME: A Single Station Based 3D Positioning System for Alternative PNT," Proceedings of ION GNSS+ 2013, The Institute of Navigation (ION), Nashville, TN, 2013, pp. pp. 521-528.

[6] Kim, O.-J., Kim, C., Song, J., Yun, H., Kim, D., Kee, C., and Lee, T., "A New Concept of APNT: MOSAIC/DME 3D-Positioning with a Single DME Station," Proceedings of the 2012 International Technical Meeting of The Institute of Navigation, The Institute of Navigation (ION), Newport Beach, CA, 2012, pp. pp. 142-150.

[7] Kim, O.-J., "3D-Positining System with a Single DME Station for the Next Generation Air Transport," Master Thesis, Seoul National University, 2013.

[8] Federal Aviation Administration (FAA), "Concept of Operations for NextGen Alternative Positioning Navigation and Timing (APNT)," APNT CONOPS, March 2012.

[9] Lo, S., and Enge, P., "Preliminary assessment of alternative navigation means for civil aviation," Proceedings of the International Technical Meetings 2010 of the Institute of NavigationSan Diego, CA, January 2010.

[10] Kim, E., "Investigation of APNT optimized DME/DME network using current state-of-the-art DMEs: Ground station network, accuracy, and capacity," Proceedings of Position Location and Navigation Symposium (PLANS), 2012 IEEE/ION, IEEE, Myrtle Beach, South Carolina, 2012, pp. 146-157.

[11] Lo, S. C., and Enge, P., "Assessing the capability of distance measuring equipment (DME) to support future air traffic capacity," Navigation, 2012, 59(4), pp. 249-261.

[12] Li, K., and Pelgrum, W., "Enhanced DME Carrier Phase: Concepts, Implementation, and Flight-test Results," Navigation, 2013, 60(3), pp. 209-220.

[13] Pelgrum, W., Li, K., Smearcheck, M., and van Graas, F., "eDME architecture development and flight-test evaluation," Proceedings of IEEE/AIAA 31st Digital Avionics Systems Conference (DASC), IEEE, Williamsburg, VA, USA, 2012, pp. 1-37.

[14] Chen, Y. H., Lo, S., Enge, P., and Jan, S. S., "Evaluation & Comparison of Ranging Using Universal Access Transceiver (UAT) and 1090 MHz Mode S Extended Squitter (Mode S ES)," Position, Location and Navigation Symposium-PLANS 2014, 2014 IEEE/ION, IEEE, Monterey, California, pp. 915-925.

[15] Lo, S., Peterson, B., Akos, D., Narins, M., Loh, R., and Enge, P., "Alternative Position Navigation & Timing (APNT) Based on Existing DME and UAT Ground Signals," Proceedings of the ION GNSS 2011 of the Institute of Navigation, Citeseer, Portland, OR, September 2011, pp. 1-9.

[16] Kim, E., "A coverage analysis methodology for APNT pseudolite ground network," Proceedings of the ION GNSS 2011 of the Institute of NavigationPortland, OR, September 2011.

[17] Lo, S. C., and Enge, P., "Capacity study of multilateration (MLAT) based Navigation for alternative position navigation and timing (APNT) services for aviation," Navigation, 2012, 59(4), pp. 263-279.

[18] Lombardi, M. A., Narins, M., Enge, P., Peterson, B., Lo, S., Chen, Y.-H., and Akos, D., "The Need for a Robust, Precise Time and Frequency Alternative to GNSS," GPS World, 2012, 23(GPS World).

[19] Helwig, A., Offermans, G., Stout, C., and Schue, C., "Design and performance of a low frequency time and frequency dissemination service," Proceedings of the 2012 International Technical Meeting of The Institute of Navigation (ION GNSS 2012)Nashville, TN, September 2012, pp. 462-471.

[20] Kee, C., and Lee, T., "Positioning System and Method based on Radio Communication Apparatus Comprising Multiple Antenna (US),"US8928529B2, Patent (Registered), United States, 2015.

[21] Kee, C., and Lee, T., "Positioning System and Method based on Radio Communication Apparatus Comprising Multiple Antenna (CN),"CN.102460202.B, Patent (Registered), China, 2015.

[22] Kee, C., and Lee, T., "Positioning System and Method based on Radio Communication Apparatus Comprising Multiple Antenna (EUR),"EP.2438456.A4, Patent (pending), Europe, 2015.

[23] Kim, O.-J., Kim, C., Song, J., Kim, Y., and Kee, C., "The study of error sources for

MOSAIC/DME system: A single station based positioning system for APNT," Position, Location and Navigation Symposium-PLANS 2014, 2014 IEEE/ION, IEEE, Monterey, CA, May 2014, pp. 855-863.

[24] Kim, O. J., Kim, C., Song, J., Lee, T., Park, B., and Kee, C., "A Single Distance Measuring Equipment (DME) Station-Based Positioning System for Alternative Position Navigation and Timing (APNT)," Navigation: Journal of The Institute of Navigation, 2015, 62(4), pp. 313-327.

[25] Eckert, K., "DME-Based system for enroute/terminal navigation, all-weather landing and air traffic control," Technical report of NASA foreign Exchange Program, 1976.

[26] Evans, J. E., Johnson, J. R., and Sun, D., "Application of advanced signal processing techniques to angle of arrival estimation in ATC navigation and surveillance systems," Technical Report 582 of Lincoln Laboratory of Massachusetts Institute of Technology, MA, June 1982.

[27] Federal Aviation Administraion, M., "NextGen Implementation Plan," Washington, DC, 2010, Available: http://www.faa.gov/nextgen/media/ng2011implementationplan.pdf (accessed March 18, 2011).

[28] RTCA Special Committee-159, "Minimum Operational Performance Standards for Airborne Supplemental Navigation Equipment Using Global Positioning System (GPS)," 1991.

[29] Fried, W. R., and Kayton, M., Avionics navigation systems, John Wiley & Sons, Inc., 1997.

[30] U.S. Department of Transportation and Federal Aviation Administration, "Performance Specification: Distance Measuring Equipment (DME)," FAA-E-2996, April 2008.

[31] Li, K., and Pelgrum, W., "Flight test evaluation of enhanced dme (edme) performance enhancements," Proceedings of the ION GNSS 2012 of the Institute of NavigationNashville, TN, September 2012, pp. 803-811.

[32] Lo, S., Chen, Y. H., Enge, P., Peterson, B., Erikson, R., and Lilley, R., "Distance measuring equipment accuracy performance today and for future alternative position navigation and timing (APNT)," Proceedings of the ION GNSS+ 2013 of the Institute of NavigationNashville, TN, September 2013, pp. 711-721.

[33] Department of Defense, Department of Homeland Security and Department of Transportation, 2017 Federal Radionavigation Plan, Springfield, Virginia, 2017.

[34] Ministry of Land Infrastructure Transport and Tourism (JAPAN), "VOR / DME, VORTAC Facilities," http://www.mlit.go.jp/koku/15_hf_000075.html.

[35] Hanish, O., "Figure of Class B Airspace," http://oliverhanisch.com/groundschool/document_library/Airspace/LessonPlanUS-Airspaces.html, ed.

[36] Kim, E., "Hybrid APNT architecture using DME/DME and multilateration," 2012

IEEE/AIAA 31st Digital Avionics Systems Conference (DASC), IEEE, Williamsburg, VA, USA, October 2012, pp. 5A5-1-5A5-10.

[37] Niles, F. A., Conker, R. S., El-Arini, M. B., O'Laighlin, D. G., and Baraban, D. V., "Wide Area Multilateration for Alternate Position, Navigation, and Timing (APNT)," MITRE-CAASD, Tech. Rep, 2012.

[38] Jan, S.-S., Jheng, S.-L., Chen, Y.-H., and Lo, S., "Evaluation of Positioning Algorithms for Wide Area Multilateration Based Alternative Positioning Navigation and Timing (APNT) Using 1090 MHz ADS-B Signals," Proc. 27th Int'l. Tech. Meeting Satellite Division of the Institute of Navigation (ION GNSS+ 2014), Tampa, Florida, USA.

[39] Misra, P., and Enge, P., "Global positioning system: Signals, measurements and performance second edition," Massachusetts: Ganga-Jamuna Press, 2006.

[40] Hatch, R., "Instantaneous ambiguity resolution," Kinematic systems in geodesy, surveying, and remote sensing, Springer, 1991, pp. 299-308.

[41] Parkinson, B. W., Enge, P., Axelrad, P., and Jr., J. J. S., "Global Positioning System: Theory and Applications, Volume II," Progress in Astronautics and Aeronautics, 1996.

[42] Cohen, C. E., "Attitude determination using GPS: Development of an all solid state guidance, navigation, and control sensor for air and space vehicles based on the global positioning system," Ph. D. Dissertation, Stanford University, December 1992.

[43] Cohen, C. E., and Parkinson, B. W., "Expanding the performance envelope of GPS-based attitude determination," ION GPS-91; Proceedings of the 4th International Technical Meeting of the Satellite Division of the Institute of NavigationAlbuquerque, NM, September 1991, pp. 1001-1011.

[44] Lau, L., and Cross, P., "Development and testing of a new ray-tracing approach to GNSS carrier-phase multipath modelling," Journal of Geodesy, 2007, 81(11), pp. 713-732.

[45] Georgiadou, Y., and Kleusberg, A., "On carrier signal multipath effects in relative GPS positioning," Manuscripta geodaetica, 1988, 13(3), pp. 172-179.

[46] RTCA Special Committee-159, "Minimum Operational Performance Standards for Global Positioning System / Wide Area Augmentation System Airborne Equipment," RTCA/DO-229D, 2006.

[47] Parkinson, B. W., Enge, P., Axelrad, P., and Jr., J. J. S., "Global Positioning System: Theory and Applications, Volume I," Progress in Astronautics and Aeronautics, 1996.

[48] Sairo, H., Akopian, D., and Takala, J., "Weighted dilution of precision as quality measure in satellite positioning," IEE Proceedings-Radar, Sonar and Navigation, 2003, 150(6), pp. 430-436.

[49] Li, J., and Wu, M., "The improvement of positioning accuracy with weighted least square based on SNR," Proceedings of the 5th International Conference on Wireless Communications, Networking and Mobile Computing, IEEE, Beijing, China, September 2009, pp. 5178-5181.

[50] Won, D. H., Ahn, J., Lee, S.-W., Lee, J., Sung, S., Park, H.-W., Park, J.-P., and Lee, Y. J., "Weighted DOP with consideration on elevation-dependent range errors of GNSS satellites," IEEE Transactions on Instrumentation and Measurement, 2012, 61(12), pp. 3241-3250.

[51] Kee, C., Kim, D., and Jang, J., "Efficient ambiguity search technique using separated decision variables," The Journal of Navigation, 2007, 60(1), pp. 147-157.

[52] Hornby, G., Globus, A., Linden, D., and Lohn, J., "Automated antenna design with evolutionary algorithms," Space 2006 San Jose, California, September 2006, p. 7242.

[53] Panduro, M. A., Brizuela, C. A., Balderas, L. I., and Acosta, D. A., "A comparison of genetic algorithms, particle swarm optimization and the differential evolution method for the design of scannable circular antenna arrays," Progress In Electromagnetics Research, 2009, 13, pp. 171-186.

[54] Rahmat-Samii, Y., and Michielssen, E., Electromagnetic optimization by genetic algorithms, John Wiley & Sons, Inc., 1999.

[55] Weile, D. S., and Michielssen, E., "Genetic algorithm optimization applied to electromagnetics: A review," IEEE Transactions on Antennas and Propagation, 1997, 45(3), pp. 343-353.

[56] Ares-Pena, F. J., Rodriguez-Gonzalez, J. A., Villanueva-Lopez, E., and Rengarajan, S., "Genetic algorithms in the design and optimization of antenna array patterns," IEEE Transactions on Antennas and Propagation, 1999, 47(3), pp. 506-510.

[57] Tennant, A., Dawoud, M., and Anderson, A., "Array pattern nulling by element position perturbations using a genetic algorithm," Electronics letters, 1994, 30(3), pp. 174-176.

[58] Xu, Z., Li, H., Liu, Q.-Z., and Li, J.-Y., "Pattern synthesis of conformal antenna array by the hybrid genetic algorithm," Progress In Electromagnetics Research, 2008, 79, pp. 75-90.

[59] Rohwedder, L. H., "Hyperboloid of two sheet," https://en.wikipedia.org/wiki/Hyperboloid#/media/File:Hyperboloid2.png, ed.

[60] Rohwedder, L. H., "double cone," https://en.wikipedia.org/wiki/Hyperboloid#/media/File:DoubleCone.png, ed.

Appendix A: Analysis about Linear Assumption of Hyperbolic Asymptotes

During the derivation of Ambiguity Net Technique in the section of 4.3, it is assumed that asymptotes represent directions by single-differenced carrier phase measurement with additions and subtractions of cycle ambiguity instead of hyperbolic curve. However, there is the difference between user angle by hyperbola and asymptotes angles, and it becomes larger if the distance from station to user is getting closer.

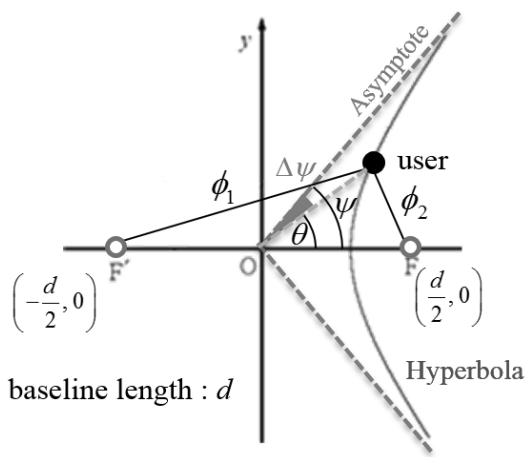

Figure A-1 Angular difference between Hyperbola and asymptote

An angular difference between hyperbolic curve and asymptote is defined as $\Delta\psi$ in Figure A-1, where θ is the user angle on hyperbola, ψ is the slope angle of asymptote, d is the

antenna baseline length, and the antenna baseline is on the x-axis with the slope angle of 0°. In general, two asymptotes are existed for each hyperbola, but only an asymptote near the user angle is considered here.

From Equation (4-6), Equation (A-1) can be derived;

$$\cos\psi = \frac{\Delta\phi}{d}. \tag{A-1}$$

If user positon is defined as ($r \cdot cos\theta$, $r \cdot sin\theta$), where r is the range from station to user, then the user angle θ can be expressed as Equation (A-2) by means of a hyperbola equation.

$$\cos^2\theta = \frac{\Delta\phi^2}{d^2}\left(1 + \frac{d^2 - \Delta\phi^2}{4r^2}\right) \tag{A-2}$$

Equation (A-2) can be expressed as Equation (A-3) combining with Equation (A-1). In addition, Equation (A-4) and (A-5) can be derived from Equation (A-3), where $k \equiv 1/\sqrt{1 + \left(d^2 - \Delta\phi^2\right)/4r^2}$.

$$\cos^2\theta = \cos^2\psi\left(1 + \frac{d^2 - \Delta\phi^2}{4r^2}\right) \tag{A-3}$$

$$\psi = \arccos\left(\cos\theta / \sqrt{1 + \frac{d^2 - \Delta\phi^2}{4r^2}}\right) \tag{A-4}$$

$$\psi = \arccos\left(k \cdot \cos\theta\right) \tag{A-5}$$

As a result, the angular difference between hyperbolic curve and asymptote, $\Delta\psi$, can be expressed as below;

$$\Delta\psi \equiv \psi - \theta = \arccos\left(k \cdot \cos\theta\right) - \theta\,, \tag{A-6}$$

where k has a range of $(0 < k \leq 1)$ and k is 1 only when $d^2 = \Delta\phi^2$ which happens when $\psi = \theta = \pm 0.5\pi$. The range from station to user, r, also affects the k that large r allows k to approach 1, meaning that $\Delta\psi$ is approaching to 0.

When the antenna baseline is 1 meter, $\Delta\psi$ according to θ with different ranges from station to user are described in Figure A-2.

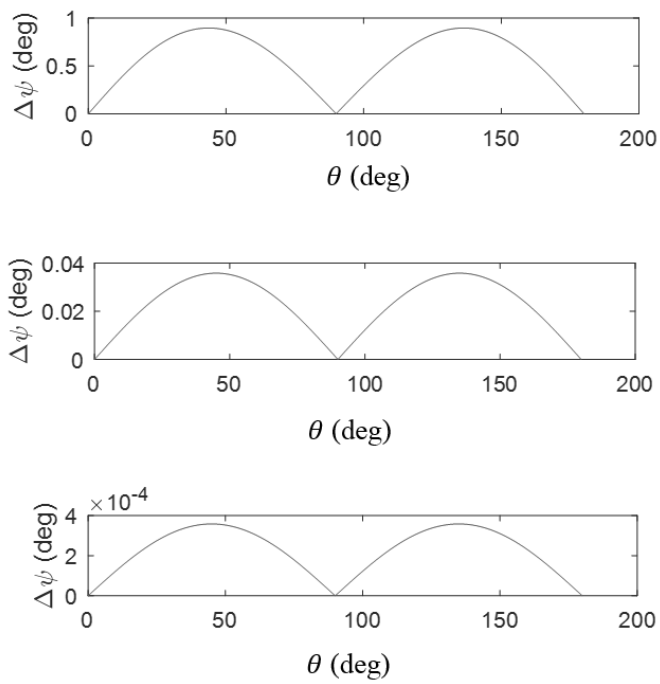

Figure A-2 Angular difference between hyperbolic curve and asymptote
(top: range = 2m, middle: range = 10m, bottom: range=100m)

Maximum $\Delta\psi$ according to different ranges are as in Table A-1. The maximum $\Delta\psi$ values decrease as the ranges increase. The results describe that even 10m of range makes the negligible angular difference smaller than 0.1°. The angular difference in the position domain is described in Figure A-3 where $\Delta\psi$ is maximum at θ=45°. Therefore, linear assumption of hyperbolic asymptote is reasonable particularly for air-transport application.

In addition, this analysis is also valid for the angular difference between hyperboloid and asymptotic cone in a 3D environment, as hyperboloids and asymptotic cones are results of rotations of hyperbola and asymptotic line around the principal axis respectively.

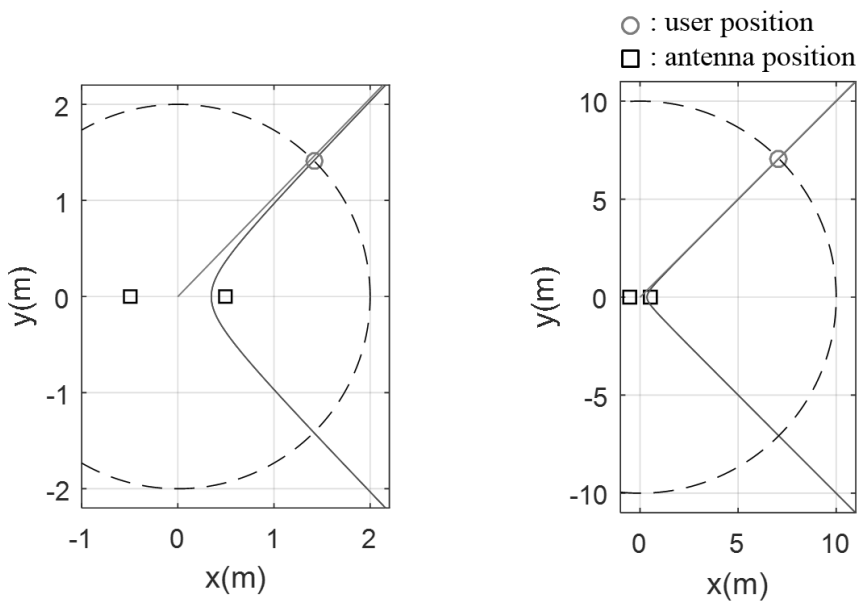

Figure A-3 Angular difference between hyperbolic curve and asymptote
(left: range = 2m, right: range = 10m)

Table A-1 Maximum $\Delta\psi$ with different ranges

Range	Maximum $\Delta\psi$
2 meter	0.9°
10 meter	0.036°
100 meter	3.6e-4°

Appendix B: Probabilistic Analysis of Zero-ANCP

The meaning of zero-ANCP of the Ambiguity Net Technique is as below;

- Zero-ANCP: all possible false cycle ambiguity candidates have at least one residual of measurements over the pre-defined statistical bound.

The relation between the statistical bound of the Ambiguity Net Technique and the chi-square distribution which is used for the ambiguity resolution process, is derived in this section.

If Z_i is an independent standard normal random variables, where $i=1,2,...,k$ and k is a Degree of Freedom (DOF), the sum of their squares Q_k has a chi-square distribution χ_k^2 as denoted in Equation (B-1).

$$Q_k = \sum_{i=1}^{k} Z_i^2 \sim \chi_k^2 \tag{B-1}$$

In this section, it is assumed that residuals of measurements of true cycle ambiguity candidate have zero-mean with same-level of errors. Accordingly, Z_i can be regarded as the residual of single-differenced carrier phase measurement divided by its standard deviation of error, and k is the number of single-difference measurements or antenna baselines. With regard to the meaning of zero-ANCP, if q-σ bound is applied for the Ambiguity Net Technique, the probability of Crossing Point (CP), P_{CP}, can be expressed as Equation (B-2).

$$P_{CP} = P\left(\bigcap_{i=1}^{k}\left(|Z_i| < q\right)\right) \tag{B-2}$$

One example, where k is 2 and q-σ bound for the Ambiguity Net Technique, is considered. The bound of the probability of CP, P_{CP}, and inner and outer bounds by chi-square distributions are visualized in Figure B-1 which can be regarded as x-y plane of two-dimensional probability density function. The inner area of white rectangle, white area, in Figure B-1 represents the area of Equation (B-2). The lower and upper bounds according to chi-square distributions are solid inner circle and dashed outer circle respectively.

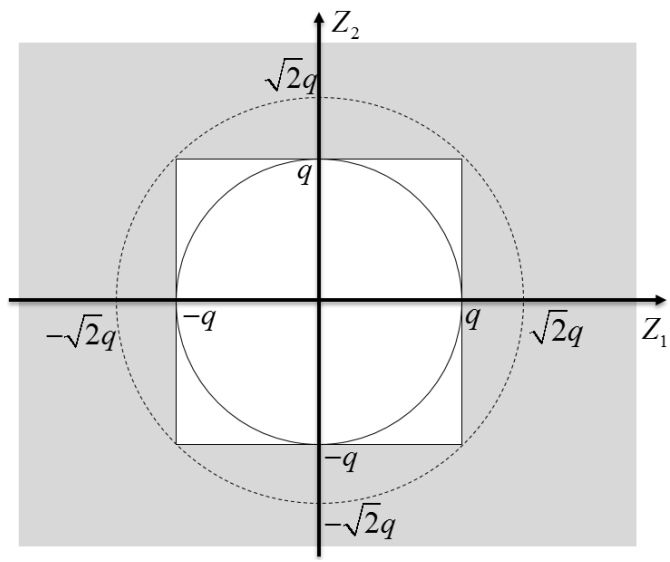

Figure B-1 Bounds of zero-ANCP and chi-squares in x-y plane of two-dimensional probability density function (two antenna baselines case)

If q is 2 for 2-σ (<95.4%) bound when k is *2*, Equation (B-3) can be derived. As Q_2 has a χ_2^2 -distribution, the Equation (B-3) has boundaries as in Equation (B-4). Hence, the probability P_{CP} has a range between two chi-square boundaries.

$$P(Q_2 < 4) \le P_{CP} \le P(Q_2 < 8) \tag{B-3}$$

$$0.87 \le P_{CP} \le 0.98 \tag{B-4}$$

According to the Equation (B-4), the range of probability that residuals from true ambiguity candidate has the CP is between 87% and 98%. ANCP counts the number of CPs which are assessed over all pixels, in other words, all area of the AOI. Hence, if a certain antenna arrangement has zero-ANCP with above conditions, there is no false candidates whose normalized square sum of residuals are smaller than at least 4 (87%) and at most 8 (98%).

A generalized version of Equation (B-3) is Equation (B-5).

$$P(Q_k < q^2) \le P_{CP} \le P(Q_k < k \cdot q^2) \tag{B-5}$$

Therefore, the representation of the probabilistic assurance of zero-ANCP in the aspect of chi-square distribution is as below:

- Zero-ANCP: there is no false cycle ambiguity candidates whose normalized square sum of residuals are smaller than a certain range of chi-square distributions which are derived from the pre-defined statistical bound.

If a pixel step size for the Ambiguity Net Technique is not small enough, actual probabilistic bounds can be larger than theoretical bounds of both sides of Equation (B-

3). Referring to Equation (4-17), Figure 4-11 and Figure 6-7, actual statistical bounds could be larger than their targets.

요 약

단일 스테이션 기반 위치결정시스템은 위성항법시스템을 사용할 수 없는 환경에서의 대체항법과 같은 백업시스템을 목적으로 한다. 본 논문에서는 기존의 DME(Distance Measuring Equipment)시스템에 단방향 연속신호를 방송하는 다수의 의사위성 안테나를 추가한 Mosaic/DME 시스템을 제안하였다. Mosaic/DME 시스템의 주요 특징은 하나의 스테이션에서 다수의 신호들을 동기화하여 방송할 수 있으며, 하나의 스테이션 만으로도 고도정보를 포함한 3 차원 위치결정이 가능해 진다는 점이다. 그리고 Mosaic/DME 의 DME 는 기존과 동일하게 동작하므로 기존 DME 스테이션과 호환되며, 양방향 신호와 단방향 신호를 둘 다 사용하므로 DME 스테이션의 항공기 수용능력 역시 증가하리라 기대할 수 있다.

Mosaic/DME 시스템은 하나의 스테이션에서 위치결정을 수행하므로 기하학적으로 배치가 좋지 않아 일반적인 방법으로는 높은 위치성능을 기대하기 어렵다. Mosaic/DME 스테이션은 이러한 문제점을 해결하기 위해서 반송파 위상 측정치를 사용하였다. 일반적으로 반송파 위상에는 파장길이에 대한 미지정수 항이 추가되어 위치계산을 위해서는 이 미지정수 값을 결정할 필요가 있다. 본 논문에서 제안하는 Mosaic 개념을 적용할 경우, 측정치의 미지정수 범위를 기하학적으로 제한하여 미지정수 결정을 효율적으로 수행할 수 있게 된다.

본 논문에서는 Mosaic/DME 에서 사용하는 다수의 의사위성 안테나를 어떻게 배치하는가에 대해 관심영역을 고려하여 위치정확도와 미지정수 결정성능 두 가지 관점에서 기술하였다. 미지정수 결정성능 관점에서 최적화된 안테나 배치를 도출하기 위해서 본 논문에서는 미지정수 그물(Ambiguity Net) 기법을 제안하였다. 미지정수 그물 기법을 적용하면 미지정수에 의해 그려지는 측정치 궤적의 교차점을 픽셀 단위로 판단하여 해당 안테나 배치가 미지정수 결정능력에 유리한 정도를 판단할 수 있다. 위치정확도 관점에서는 관심영역 내에서 가장 위치성능이 낮은 지점의 DOP(Dilution Of Precision)를 성능지수로 선정하여, 해당 성능지수가 가장 낮아지도록 안테나 배치의 최적화를 수행할 수 있다.

관심영역 내에서 앞서 언급한 미지정수 결정성능과 위치정확도 두 가지를 최적화할 수 있도록 안테나를 배치하는 전략에 대해서도 기술하였다. 목표 위치정확도를 만족하면서 동시에 미지정수 결정성능도 보장하는 안테나 배치에 대해 안테나 수, 안테나 간격 등을 최소화하는 전략을 단계적으로 기술하였다.

본 논문에서 제안되고 언급된 방법들과 전략에 대해 시뮬레이션으로 검증을 수행하였다. DOP 성능지수와 미지정수 그물 기법을 적용하여 결정된 안테나 배치에 대해, 시뮬레이션으로 위치정확도와 미지정수 결정능력을 확인하고, 다른 안테나 배치들과 비교/분석을 진행하였다.

주요어: 대체항법(APNT), 모자이크, 거리측정창치(DME), 미지정수 결정, 미지정수 그물, 안테나 배치

학번: 2013-30191